UNIVERSIDADE DO ALGARVE

“Role of insulin and insulin-like peptides in bone formation: Identification of bone-specific target genes and regulatory mechanisms, and characterization of the insulin-mimetic effect of vanadium”

Daniel António Martins Tiago

Doutoramento em Biologia

Especialidade em Biologia Molecular

2008

UNIVERSIDADE DO ALGARVE

"Role of insulin and insulin-like peptides in bone formation: Identification of bone-specific target genes and regulatory mechanisms, and characterization of the insulin-mimetic effect of vanadium"

Daniel António Martins Tiago

Doutoramento em Biologia

Especialidade em Biologia Molecular

Tese orientada por:

Profª. Drª. Maria Leonor Cancela,

Prof. Dr. Manuel Aureliano Alves e Dr. Vincent Laizé

2008

The content of this dissertation is of exclusive responsibility of the author

Daniel António Martins Tiago

Agradecimentos

À Prof. Dra. Leonor Cancela por me ter dado a oportunidade de trabalhar durante o doutoramento na sua equipa de investigação e por todo apoio que me tem dado desde então.

Ao Dr. Vincent Laizé pela orientação que me concedeu durante o doutoramento e por todas as discussões que tanto contribuíram para o desenvolvimento deste projecto e para a minha maturação científica.

Ao Prof. Dr. Manuel Aureliano Alves pela orientação e apoio durante o doutoramento.

Aos meus colegas de laboratório Ricardo Leite, Ricardo Afonso, Marta Rafael, Cátia Marques, Carla Viegas, Natércia Conceição, Dina Simes, Vanesa Robles, Sara Mira, Brigite Simões, Anabela Brito, Paulo Gavaia, Rita Ascenso, Vânia Roberto, Marta Valente, Sofia Cavaco (sem nenhuma ordem especial) pelos bons momentos que passámos durante os últimos anos e pelas saudáveis discussões científicas que tivemos durante as reuniões e que muito contribuíram para este projecto.

Aos meus colegas de curso pelo apoio que me deram durante essa fase do meu percurso académico.

Aos meus pais pela amizade, carinho e pela minha formação (não só pessoal como científica). A eles agradeço o apoio que me foi dado a todos os níveis durante os últimos 28 anos.

À minha irmã, Teresa, e ao marido Pedro, porque sempre estiveram comigo para me apoiar nos bons e maus momentos, e por todas as discussões científicas que partilhámos.

À minha mulher, Margarida, pelo apoio incansável nos bons e maus momentos. Tendo sido o meu ponto de equilíbrio durante este longo caminho, sem ela não teria sido possível realizar este projecto.

A realização deste trabalho teve o financiamento da Fundação para a Ciência e Tecnologia através da atribuição da bolsa de doutoramento SFRH/BD/12773/2003.

Abstract

Insulin and IGF-1 are small circulating peptides known to regulate bone mineral density and formation in vertebrates through the activation of intracellular PI-3K and MAPK signalling pathways. Vanadium/vanadate has recently been shown to regulate proliferation and differentiation of mammalian bone-derived cell lines also through the activation of both pathways. In this study, proliferative and mineralogenic effects of insulin, IGF-1 and vanadate have been investigated using fish bone-derived cell lines VSa13 (chondrocyte-like) and VSa16 (osteoblast-like). Short-term treatments of VSa13 cells with two different forms of vanadate in solution (meta- and decavanadate) reavealed that metavanadate (i) results in faster and higher accumulation of vanadate in the cell, and (ii) has a lower toxicity than decavanadate when administered *in vitro* to the cells. Chronic treatments with both solutions were found to partially mimic the effects of both factors, e.g. stimulated VSa13 cell proliferation, as IGF-1, and prevented ECM mineralization, as insulin. Treatments with wortmannin and PD98959 demonstrated the involvement of MAPK and PI-3K\Ras\ERK pathways in proliferative and mineralogenic effects, respectively. These data are consistent with recent observations in mammalian ATDC5 cells (chondrocytes) suggesting the conservation of mechanisms of action throughout evolution. Vanadate was also shown not only to interfere with regulatory pathways but also to inhibit alkaline phosphatase activity, a key enzyme in bone formation. In Vsa16 cells, similar effects have been observed on proliferation, using IGF-1 (*i.e.* stimulation), and ECM mineralization, using both IGF-1 and vanadate (*i.e.* inhibition), suggesting conservation of mechanisms across bone cell types. In parallel to this work, 3 spliced variants of seabream proIGF-1 (IGF-1a, 1b and 1c) were identified and associated to a different mode of action (local and systemic) in adult tissues and during development, as previously observed in mammals. Variants 1a

and 1b were also proposed to play a role in fish osmoregulation. Altogether, results presented here indicate a conservation of mechanisms between fish and mammals, further demonstrating the suitability of fish systems to study vertebrate insulin-like effects in bone.

Keywords

Insulin-like activity; vanadate; intracellular signalling; *in vitro* mineralization; bone-derived cell lines; vertebrate bone formation; teleost fish *Sparus aurata*; Pro-insulin-like growth factor 1 (proIGF-1); E domain; alternative splicing.

Resumo

Insulina e IGF-1 são pequenos péptidos circulantes conhecidos por regular a densidade mineral e formação óssea em vertebrados através da activação vias de sinalização celular PI-3K e MAPK. Por sua vez, demonstrou-se recentemente que o vanádio/vanadato regula a proliferação e diferenciação de linhas celulares derivadas do osso de mamíferos através mesmas vias. Neste estudo, os efeitos proliferativos e mineralogénicos da insulina, IGF-1 e vanadato foram investigados em linhas derivadas do osso de peixe: VSa13 (tipo condrócito) e VSa16 (tipo osteoblasto). Tratamentos agudos com metavanadato (espécies n-méricas 1 a 5) nas células VSa13 revelaram uma acumulação mais rápida e mais elevada de vanádio, bem como uma toxicidade mais baixa do que decavanadato (n = 1 ou 10). Tratamentos crónicos com ambas as soluções estimularam a proliferação das VSa13, tal como a IGF-1, e preveniram a mineralização, tal como a insulina. Tratamentos com wortmanina e PD98959 demonstraram o envolvimento das vias MAPK e PI-3K\Ras\ERK nos efeitos proliferativos e mineralogénicos, respectivamente. Os dados obtidos são consistentes com observações recentes nas células de mamífero ATDC5 (condrócitos) sugerindo uma conservação de mecanismos ao longo da evolução. Aparentemente o vanadato não só terá interferido com as vias de sinalização mas também com a actividade da fosfatase alcalina, uma enzima muito importante na formação óssea. Nas células VSa16 foram observados efeitos semelhantes na proliferação através de tratamentos com IGF-1 (estimulação), e na mineralização através de tratamentos com vanadato e IGF-1 (inibição), sugerindo uma conservação de mecanismos através dos tipos celulares de osso. Em paralelo, neste trabalho foram identificadas em seabream 3 variantes da proIGF-1 (IGF-1a, 1b e 1c) e associadas a diferentes modos de acção (local e sistémico) em tecidos de adultos e durante o desenvolvimento, tal como previamente demonstrado em mamíferos.

Propôs-se também que em peixes as variantes 1a e 1b estariam relacionadas com uma adaptação a diferentes salinidades. Em geral, os resultados aqui apresentados indicam uma conservação de mecanismos em vertebrados, demonstrando a importância dos sistemas derivados de peixes no estudo dos efeitos semelhantes à insulina no osso.

Palavras-chave

Actividade tipo insulina; vanadato; sinalização intracelular; mineralização *in vitro*; linhas celulares derivadas de osso; formação óssea em vertebrados; teleósteos (*Sparus aurata*); Pro-insulin-like growth factor 1 (proIGF-1); domínio E; "splicing" alternativo.

Abbreviations

ALP	Alkaline phosphatase
ANOVA	Analysis of variance
BSA	Bovine serum albumin
DAH	Days after hatching
DMEM	Dulbecco's modified Eagles medium
ECM	Extracellular matrix
ERK	Extracellular-regulated kinase
FGF	Fibroblast growth factor
GH	Growth hormone
GRB-2	Growth factor receptor-bound protein 2
HAF	Hours after fertilization
IGF	Insulin-like growth factor
IGF-1R	IGF-1 receptor
IGF-2R	IGF-2 receptor
IGFBP	IGF binding protein
IR	Insulin receptor
IRS	Insulin receptor substrate
LS	Laron syndrome
MAPK	Mitogen-activated protein kinase
MEK	MAPK/ERK kinase
MGP	Matrix Gla protein
MTS	3-(4,5-dimethylthiazol-2-yl)-5-(3-carboxy-methoxyphenyl)-2-(4-sulfophenyl)-2H-tetrazolium
NMR	Nuclear Magnetic Resonance

OC	Ostocalcin
PBS	Phosphate-buffered saline solution
PCR	Polymerase chain reaction
PDGF	Platelet-derived growth factor
PI-3K	Phosphatidylinositol-3 kinase
PKB	Protein kinase B
PKC	Protein kinase C
ProIGF	Insulin-like growth factor pro-peptide
PTK	Protein tyrosine kinase
PTPase	Protein tyrosine phosphatase
qPCR	Quantitative real-time PCR
RACE	Rapid amplification of cDNA ends
Ras	Rat sarcoma viral oncogene
RPL27a	Ribosomal protein L27a
Shc	SH2-containing collagen-related proteins
SSC	Standard saline citrate buffer
TKR	Tyrosine kinase receptor
TNAP	Tissue non-specific alkaline phosphatase

INDEX

Chapter I

1. Introduction

1.1. Insulin-like activity in mammals

In mammals, insulin and IGFs belong to a protein family composed of at least eight members, including relaxin and four insulin-like peptides [1]. Insulin is a small circulating peptide known for its metabolic effects and therapeutic properties in diabetes, through regulation of glucose levels in blood [2]. This peptide was first purified from bovine pancreas and injected in diabetic patients in 1922, but major advances in this therapy only arrived in 1978 when Genentech started to produce recombinant human insulin in E. *coli*. Insulin-like growth factors 1 and 2 (IGF-1 and IGF-2) are circulating peptides that share a high sequence similarity with insulin and that are known for its growth related and anti-apoptotic properties [3]. Like insulin but with more recent history, IGF-1 is currently being tested in clinical trials for the therapy of diabetes (type 1 and 2) and growth failure disorders. Companies are seeking United States of America Food and Drug Administration (FDA) approval for its commercialization.

1.1.1. Insulin and insulin-like growth factors

Insulin, IGF-1 and IGF-2 are synthesized as pre-pro-peptides. IGF-1 and IGF-2 pro-peptides (proIGFs) contain 5 domains (B, C, A, D and E) and are processed by the proteolytic removal of E domain [3]. Similarly, insulin pro-peptide (proinsulin) contains 3 domains (B, C and A) and is processed by the proteolytic removal of C domains [4]. ProIGFs and proinsulin are processed by SPC1 (furin) in the Golgi apparatus [5,6] forming mature peptides of approximately 70 and 51 residues (7.5 and 5.8 kDa), respectively. While B, C and A domains of proIGFs are structurally similar to those of

proinsulin in terms of amino acid composition, IGFs D domain has no equivalent domain in insulin (Figure 1.1) [3].

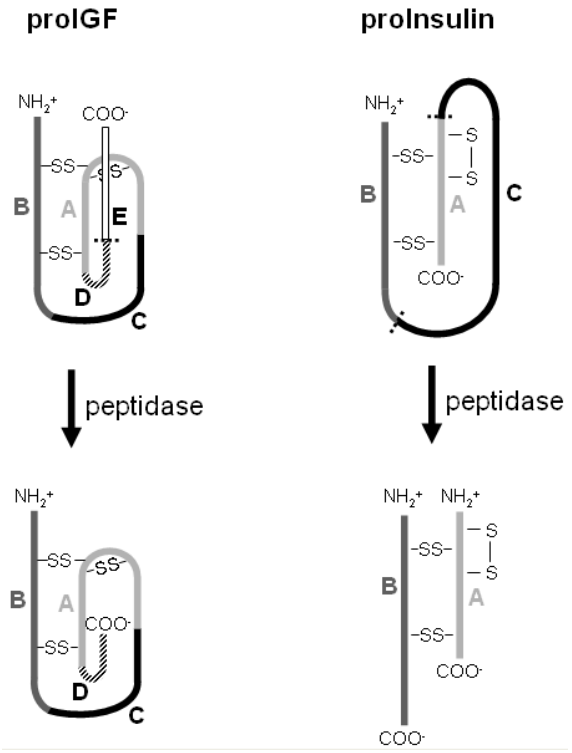

Figure 1.1 – Processing of IGF and insulin pro-peptides by intracellular peptidase and 2D structure of mature peptide. *Adapted from Berg et al, 2002, and http://dailymed.nlm.nih.gov/dailymed/fda/*.

1.1.2. Insulin and IGF biological effects

The physiological roles of insulin and IGFs are mainly associated in vertebrates to metabolism (glucose, amino acid and lipid), prenatal and postnatal growth, and regulation of tissue remodelling (bone) [2,3,8-10]. Insulin is mainly produced in β-cells of pancreatic islets of Langerhans under stimulation of circulating glucose and amino acids. After being released into bloodstream it readily decreases the circulating levels of glucose mainly through its action: (i) in liver, after stimulation of gluconeogenesis and glycogenolysis processes, and (ii) in muscle and adipose tissue, after stimulation of glucose uptake (mainly through glucose transporter-4, GLUT-4) and consumption [10]. Disorders associated to insulin deficiency or resistance, diabetes type I (incapacity to

produce insulin by pancreatic cells) and type II (both incapacity to produce insulin and tissue inability to respond to this hormone), are mainly characterized by the failure to regulate blood glucose levels [2,10]. Besides metabolic effects, insulin is also known to produce anabolic effects, such as lipid, protein and DNA synthesis, and to generally promote cell proliferation and differentiation during development [2]. Humans lacking active insulin receptors (IR), *i.e.* exhibiting Donohue syndrome, present severe growth retardations, adiposity, abnormal glycemia and β-cell failure to produce insulin [1].

IGF-1 and IGF-2 are both known to have important roles during development but also to act independently with a distinct spatio-temporal distribution [3]. IGF-1 is mainly produced in the liver under the stimulation of growth hormone (GH), which is secreted by the pituitary gland. In return, IGF-1 decreases GH secretion through its action in hypothalamus [3,9,11]. Although liver is responsible for most of circulating IGF-1 in vertebrates, approx. 260 ng/ml in mice [12], local production by specific tissues, through autocrine/paracrine processes, assumes an important role in organogenesis during postnatal growth [12]. IGF-2, which is highly expressed in various tissues (resulting in a 3-4 fold higher concentration in serum compared to IGF-1), has been shown to be particularly important during early embryogenesis but less determinant during postnatal growth [3,13]. Through its effects on either proliferation/differentiation of progenitor cells, metabolism or anabolism, several tissues/organs/systems have been shown to be regulated by IGFs: (i) central nervous system [14,15]; (ii) bone (this will be further discussed later in this chapter) [16-23]; (iii) skeletal muscle [24]; (iv) mammary gland; (v) adipose tissue [25,26]; (vi) pancreas (pancreatic β-cell proliferation and insulin release) [27-29]; and (vii) reproductive system [3]. Most of the tissues/organs/systems regulated by IGF-1 were shown to be affected in patients exhibiting Laron syndrome (LS), a disorder characterized by GH

resistance (due to GH receptor defects) and consequent reduced levels of circulating IGF-1. The main phenotype of patients with LS (Figure 1.2) [30] is: skeletal underdevelopment (patients also frequently develop osteoporosis at young age), sparse hair, obesity, muscle underdevelopment, hypoglycaemia and smaller/disproportioned bodies..

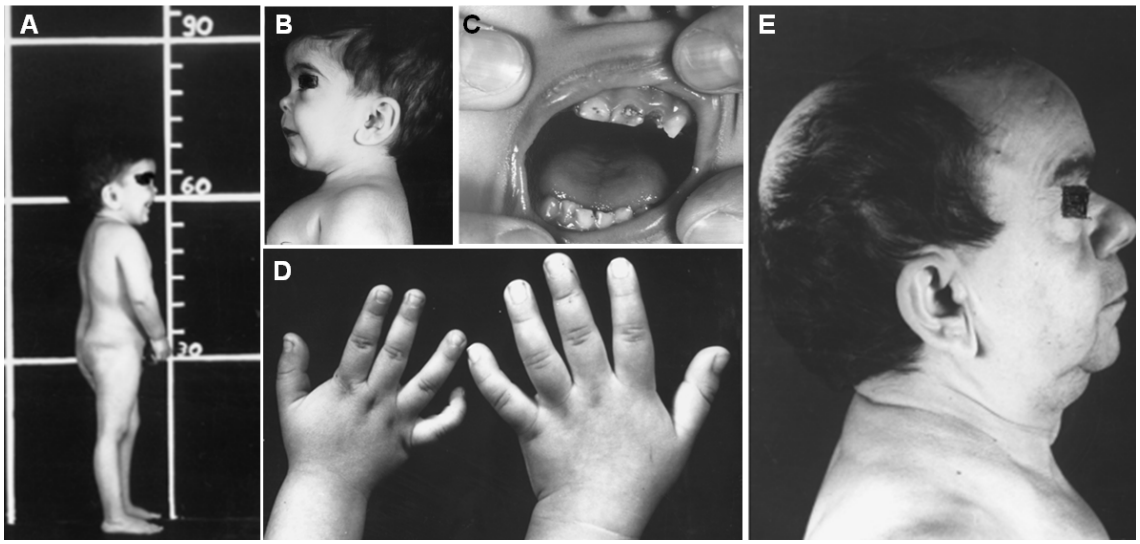

Figure 1.2 – Laron syndrome (LS) phenotype. **A** and **B**, lateral view of a 4-year-old male with LS: low height, slight obesity, small chin, saddle nose and protruding forehead. **C,** 5-year-old male exhibiting LS with defective teeth formation. **D**, hands of a 4-year-old male with LS (left) and 2-year-old male (right). **E**, lateral view of a 45-year-old male with LS exhibiting the same phenotype as in A-D and with sparse hair and occipital alopecia. *Adapted from Laron, 2002*.

The only effective known treatment for LS is the supplementation with exogenous IGF-1, which results in: (i) higher glucose (in young age) and lower cholesterol levels in blood; (ii) increased liver and bone alkaline phosphatase (ALP) activity; and (iii) reduced adipose tissue and increased muscle strength.

Finally, IGF-1 has been also shown to be related to lifespan and aging but this issue is still highly controversial. Nevertheless, IGF-1 receptor (IGF-1R) +/- mice knockout studies have suggested an interesting increase in oxidative stress tolerance associated to a higher lifespan [31].

1.1.3. Insulin, IGF-1 and IGF-2 receptors and IGF binding proteins

Biological effects associated with insulin and IGFs are promoted through their binding to specific membrane receptors, IR, IGF-1R and IGF-2R (Figure I.3). While IR and IGF-1R are both tyrosine kinase receptors (TKR), IGF-2R is a cation-independent mannose-6-phosphate receptor (CI-MPR). CI-MPRs are transmembrane glycoproteins with long extracellular domains that are implicated in lysosomal degradation [32]. In that sense, there has been some controversy concerning IGF-2R specific role in mediating IGF-2 effects, but evidences seem to indicate that this receptor is probably responsible for clearing circulating IGF-2 [3]. IGF-2 effects are thought to be promoted through its binding to a IR splicing variant (IR-A) and IGF-1R [33,34]. However, IGF-1, which may also bind to IR with a high affinity [1], can also bind to IGF-2R with a very low affinity (~100 times less than IGF-2), thus being cleared from circulation [33]. IR and IGF-1R are composed by 4 subunits: two α (extracellular) and two β (transmembrane) subunits linked by disulfide bridges [35,36]. β subunits exhibit intrinsic PTK activity resulting in auto-phosphorylation of tyrosine residues upon binding of specific peptides to the α subunits. Three of these residues are located near the PTK catalytic site of β subunit and are responsible for a conformational change and consequent activation: catalytic region becomes accessible to peptide substrates and MgATP [35,37-39].

IGF binding proteins (IGFBPs), which are also part of the IGF system, form a family of at least six members, and exhibit a high affinity for IGFs (higher than receptors) in circulation, but display a very low or inexistent affinity for insulin [40]. The main functions of IGFBPs are to: (i) carry IGF to cells/tissues; (ii) extend IGF half-life; (iii) modulate IGF availability; and (iv) modulate IGF binding to receptors and

its activities [40]. Additionally, there have been some evidences indicating additional IGFBPs effects on cell function (*e.g.* cell migration) through its interaction with specific receptors and independently of its binding to IGFs [40]. Although IGFBPs were originally thought to limit IGFs effects, recent studies have shown that, on the contrary, they are able to potentiate IGFs effects. It has been proposed that IGFBPs bind IGFs with high affinity in serum in order to transport them to the target tissues. This affinity would hypothetically be decreased by IGFBP/IGF complex interaction with ECM or IGFBPs proteolysis by specific proteases [40].

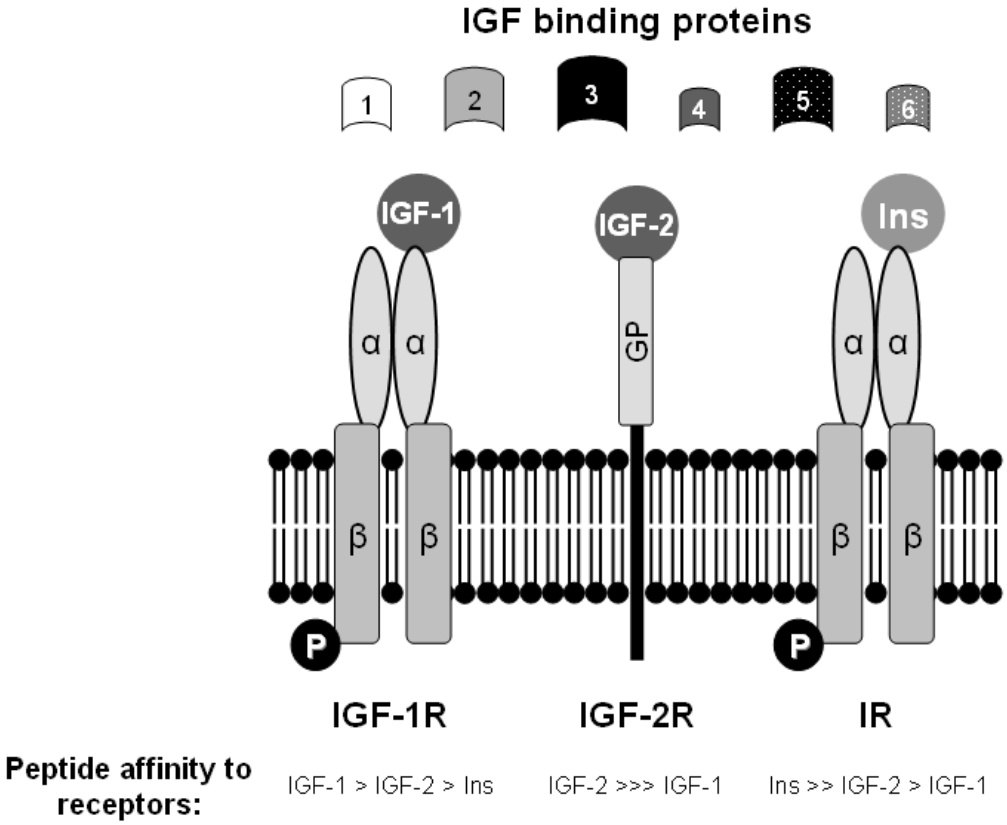

Figure 1.3 – Scheme illustrating insulin (Ins), IGF-1 and IGF-2, their specific receptors and binding proteins. **α** and **β** represent the subunits of insulin and IGF-1 receptors; **Circled P** represents phosphorylation of β subunit; **GP** indicates glycoprotein of IGF-2R. *Adapted from Florini et al., 1996*.

1.1.4. Insulin and IGF intracellular signalling

Binding of insulin and IGF to α subunits of IR and IGF-1R initiates intracellular signalling events that result in biological effects [2,41]. Two main signalling pathways can be activated through this mechanism: phosphatidylinositol-3 kinase (PI-3K) and mitogen-activated protein kinases (MAPK) [10,41] (Figure 1.4). Briefly, either insulin receptor substrates (IRS) or Shc (SH2-containing collagen-related) proteins bind to receptor's tyrosine kinases and become phosphorylated/activated (Figure 1.4). While activated Shc forms a complex with GRB-2 (growth factor receptor-bound protein 2) adapter and Sos (Son of sevenless), a guanidine nucleotide exchange protein, IRS forms a complex with GRB-2 and PI-3K. Consequently, either Shc/GRB-2/Sos complex consecutively activates Ras (rat sarcoma viral oncogene) and MAPK, or IRS/GRB-2/PI-3K complex activates protein kinase B or C (PKB or PKC) (Figure 1.4).

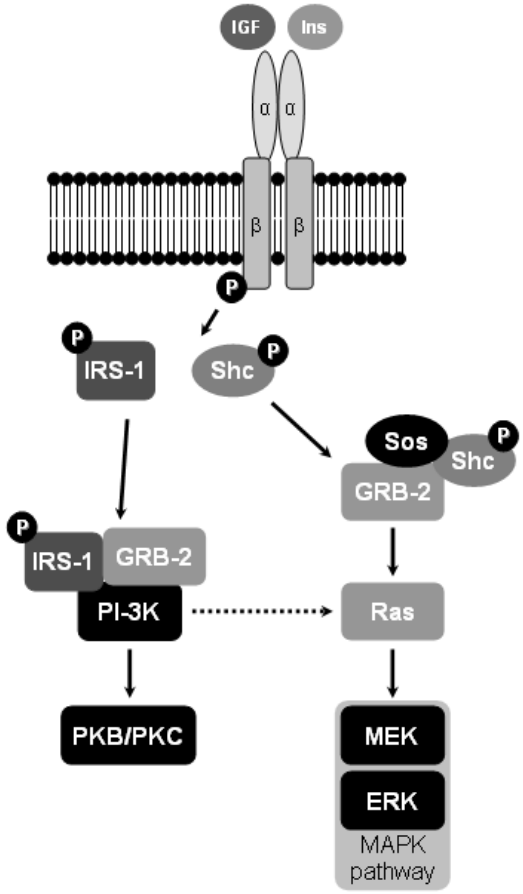

Figure 1.4 – Insulin (Ins) and insulin-like growth factor 1 and 2 (IGF) intracellular signalling pathways. **α** and **β** represent the subunits of insulin and IGF-1 receptors; **Circled P** represents phosphorylation of β subunit and signalling peptides. **Filled arrows** indicate activation by protein/complex; **dashed arrow** indicates PI-3K\Ras\ERK pathway. IRS-1, GRB-2, PKB and PKC indicate activated intermediates in PI-3K pathway. Shc, Sos, GRB-2 (also intermediate in PI-3K), Ras, MEK (MAPK/ERK kinase) and ERK (extracellular-regulated kinase) indicate intermediate proteins in MAPK pathway. *Adapted from Tiago et al. 2008*.

Until recently, it was widely accepted that MAPK and PI-3K pathways were responsible for proliferation/differentiation effects and metabolic/anti-apoptotic effects, respectively. However, recent data have revealed that each of these pathways can generate both responses [10,41,42]. In that sense, proliferative effects induced by MAPK were shown to result from downstream activation of transcription factors while the same effects are mediated by PI-3K through PKC activation. In both cases, growth responses start with activation of AP-1 family of transcription factors (including c-fos and c-jun) [2]. Alternatively, GRB-2/IRS/PI-3K complex was shown to be capable of activating MAPK through Ras, thus generating a PI-3K\Ras\ERK pathway (Figure 1.4) [2,41]. MAPK pathway was shown to mediate anti-apoptotic effects (usually associated to PI-3K action) in experiments using cell lines in which IRS (essential intermediate of PI-3K pathway) were absent [43].

Although IR and IGF-1R generate similar intracellular signalling events, insulin and IGFs promote in most cases distinct effects [1]. In general, studies using IR, IGF-1R and IGF-2R knock-out mice suggested that only IR can mediate insulin signal while IGF-1R absence can be compensated by IGFs binding to IR (in particular IGF-2). Thus, important questions have arisen concerning what features in each receptor trigger the distinct effects. Evidences obtained from studies in which specific residues of IGF-1R were mutated suggested that differential phosphorylation of tyrosine residues in receptor β subunit may be responsible for differences in signal transduction. Apparently, C-terminal tyrosines are specifically associated to mitogenic effects, while juxtamembrane tyrosines regulate both PI-3K and MAPK signalling activation [10,41]. In fact, a major difference between IR and IGF-1R is precisely located in the C-terminal region, in which a quartet of serines is present in IGF-1R and shown to be essential for maximal activation of MAPK pathway [44,45]. Finally, tyrosine kinase activity of IR is

apparently down-regulated after phosphorylation of serine/threonine in the β subunits. Following this idea, it has been suggested that activation of serine kinases (*e.g.* PKC) through either IGF-1 or other hormones and cytokines actions, could constitute a negative feedback regulatory mechanism of insulin signalling, or be associated to insulin resistance disorder (type II diabetes) [46].

1.1.5. Vanadium and its insulin-like activity

Vanadium, an essential element in organisms

Vanadium is a trace element that has been shown to be essential for biological activity in various organisms. In plants and algae, vanadium is directly involved in specific enzyme activities, acting as a cofactor in vanadium-nitrogenases and vanadate-dependent haloperoxidases [47-49]. In mammals, reduced doses of vanadium are associated with poorly developed animals, higher rates of spontaneous abortion or mortality and bone malformations [50]. Vanadium natural intake by human is approximately 10 μg V per day, mainly through vegetables, fruits, eggs, fish, beverages (beer and wine). Vanadium is absorbed in the upper gastrointestinal tract and it mainly accumulates in bones (ribs and carpal bones), kidney, spleen, ovary and uterus [50]. Biological effects of vanadium in vertebrates derive essentially from its capacity to interfere with several key enzymes, such as ATPases, phosphorylases, phosphatases (alkaline, acid and protein phosphatases) and ribonucleases [48]. This interference, in particular with phosphatases, has been attributed to vanadium oxidation states V^{V} and V^{IV} (vanadate and vanadyl, respectively), which exhibit some analogy with phosphate although to different extents (strong for vanadate and weak for vanadyl). Inhibition of phosphatases by vanadate was attributed to the formation of good transition state analogues during enzymatic catalysis [48,51] and a similar mechanism was proposed

for vanadyl although its geometry of coordination is somewhat different to that of phosphate [48].

An important feature of vanadate resides in its capacity to form different oligomeric species (monomeric to decameric species according to pH and concentration [52]; Figure 1.5), and to promote distinct effects depending on that oligomerization [53-57].

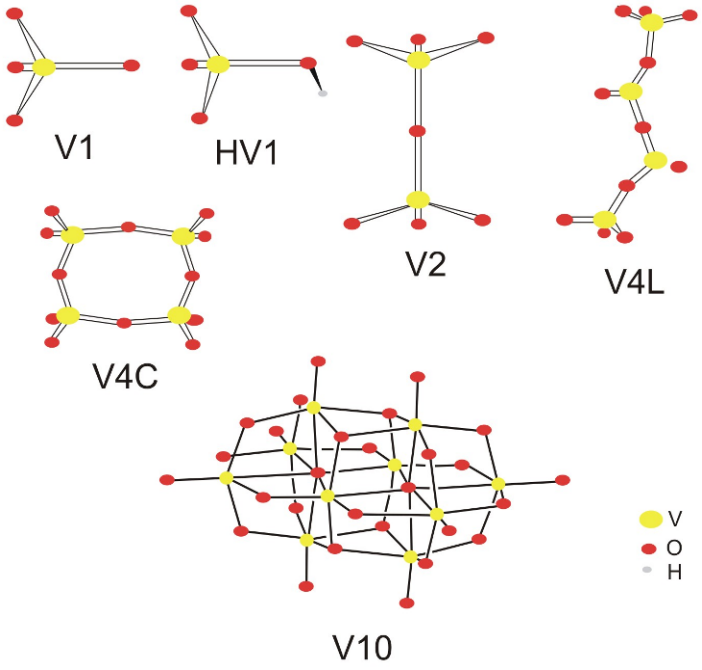

Figure 1.5 – Molecular structure of vanadate oligomers. V1, V2 and V10 indicate monomeric, dimeric and decameric vanadate species, respectively; HV1 indicates protonated monomeric vanadate (HVO_4^{2-}); V4L and V4C indicate linear and circularized tetrameric vanadate species, respectively; V, O and H indicate vanadium, oxygen and hydrogen atoms, respectively. *V1, V2 and V4 representations were adapted from Amado et al., 1993; V10 representation was adapted from Howarth and Jarrold, 1978.*

These distinct effects were demonstrated using *in vitro* and *in vivo* systems [53,59,60]. For example, decameric species were shown, in fish, to induce higher oxidative stress and haemoglobin oxidation, to stimulate antioxidant enzyme activities and to generate more tissue damages than other oligomeric species [54,61,62]. In contrast, monomeric species apparently accumulated at higher rates and doses in cardiac muscle, red blood cells and plasma [63]. Decameric species also revealed stronger

inhibition and affinity for ATPases, in particular myosin and sarcoplasmic reticulum Ca^{2+}-ATPase [53,55,64,65].

Vanadium insulin-mimetic properties

The most important biological effect of vanadium is probably insulin mimicking. It was first demonstrated in the early 80's, when vanadate and vanadyl treatments applied to isolated rat adipocytes [66,67] were shown to stimulate hexose transport, glucose oxidation and lipogenesis, as insulin [68]. Additional *in vivo* studies showed that vanadate oral administration to streptozocin-treated diabetic rats resulted in the reduction of blood glucose to normal levels [69,70], confirming its ability to mimic insulin. Vanadate was consequently proposed as a powerful therapeutic agent for diabetes mellitus (insulin-dependent). However, the therapeutic use of vanadate has been seriously hampered by its relatively high toxicity at administered doses [71,72]. Recent efforts have therefore focused on the discovery of chelating agents, which would reduce vanadyl and vanadate toxicity while preserving its insulin-like properties [73].

Insulin- and IGF-like properties of vanadium have been associated to specific inhibition of protein tyrosine phosphatases (PTPases) and consequent activation of receptor-associated PTK, including that of IR (Figure 1.6) [72,74-76]. Alternatively, non-receptor PTKs, *e.g.* IRS-1 or cytosolic PTK, are also putative targets in this mechanism [77].

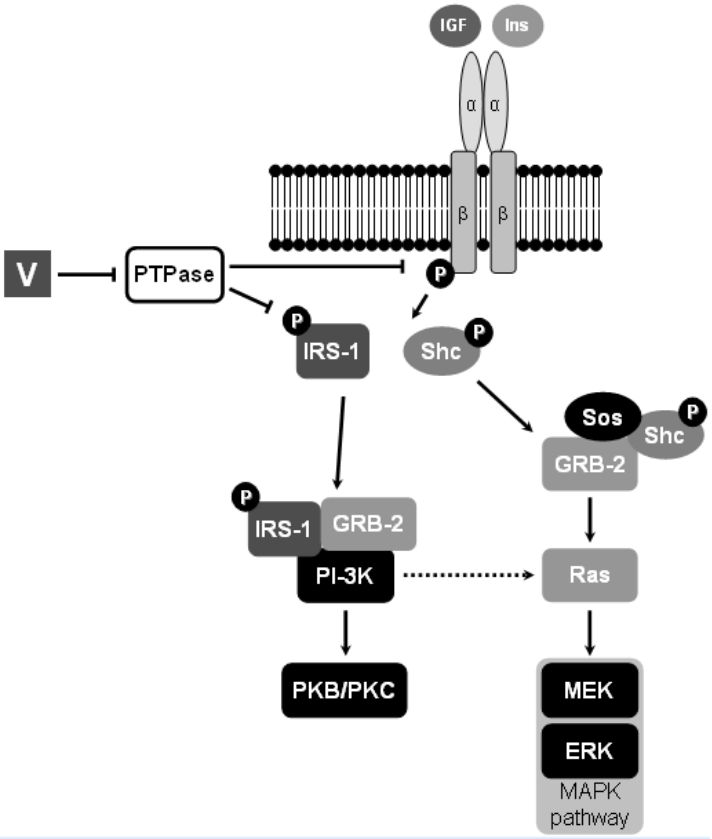

Figure 1.6 – Insulin (Ins) and insulin-like growth factor 1 and 2 (IGF) intracellular signalling pathways, and putative regulation by vanadium. **α** and **β** represent the subunits of insulin and IGF-1 receptors; **Circled P** represents phosphorylation of β subunit and signalling peptides; **V** indicates vanadium. **Filled arrows** indicate activation by previous protein/complex; **dashed arrow** indicates PI-3K\Ras\ERK pathway; **intersected line (┬)** indicates inhibition or inactivated. IRS-1, GRB-2, PKB and PKC indicate activated intermediates in PI-3K pathway. Shc, Sos, GRB-2 (also intermediate in PI-3K), Ras, MEK and ERK indicate intermediate proteins in MAPK pathway. *Adapted from Tiago et al. 2008*.

1.2. Insulin-like activity in vertebrate bone

Vertebrate linear bone growth is a process tightly regulated by numerous and complex cellular signalling pathways, which are regulated by various growth factors and hormones [79-81], including insulin and IGFs [82,83]. *In vivo* and *in vitro* experiments have demonstrated an association of insulin and IGFs with osteogenesis [84-86], bone mineral density and bone formation rate [20,22,87-90]. These processes are highly dependent on the effects promoted during development by three major skeleton specific cell types: the chondrocyte, the osteoblast and the osteoclast.

1.2.1. Skeleton formation

Vertebrate skeleton is composed of cartilage and bone tissues, which are mainly formed by 3 major cell types: chondrocytes (cartilage specific), osteoblasts and osteoclasts (both bone specific) [91]. However, bone and cartilage cell types have different progenitor cells. Chondrocytes and osteoblasts derived from mesenchymal cell lineage and osteoclasts derived from monocyte cell lineage (Figure 1.7).

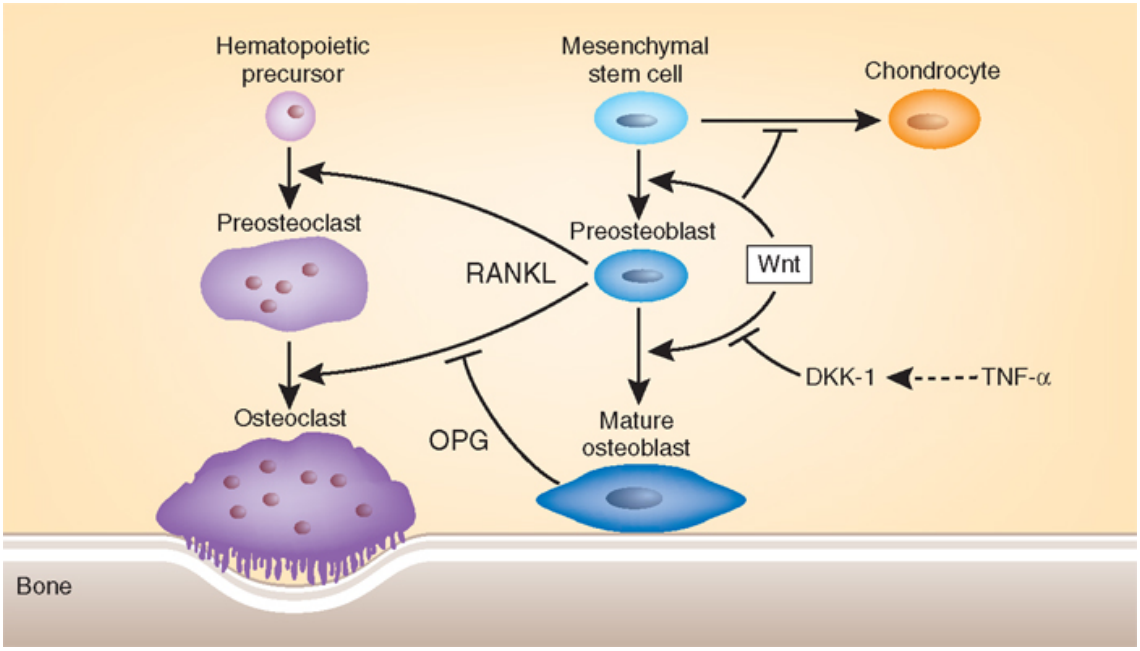

Figure 1.7 – Chondrocyte, osteoblast and osteoclast differentiation, its precursors and regulation. **OPG** indicates osteoprotegerin, **RANKL** indicates receptor activator of NF-kB ligand, **TNF-α** indicates tumor necrosis factor alpha, **Wnt** indicates wingless-int-1 oncogene, **DKK-1** indicates Dickkopf-1 (inhibitor of Wnt); **arrows** indicate activation and **intersected line (⊤)** indicates inhibition. *From Goldring and Goldring, 2007.*

After being completely formed, the skeleton is mostly made of bone tissue. Nevertheless, specific processes during development involve formation of cartilage templates in intermediary steps. Such events occur during endochondral ossification in long bones, which involve: (i) mesenchymal stem cells condensation; (ii) differentiation of condensed stem cells into chondrocytes to form a cartilaginous template; (iii) chondrocyte proliferation; (iv) chondrocyte differentiation through a process named

hypertrophy; (v) ECM calcification by hypertrophic chondrocytes; (vi) chondrocyte apoptosis; (vii) vascularisation and degradation of calcified ECM by chondroclasts; (viii) condensation of osteoblast progenitor cells; (ix) osteoblast differentiation (Figure 1.8) [91]. During hypertrophy, chondrocyte cells produce type II collagen, which are randomly oriented fibers that confer tensile strength, and aggrecan, which is a proteoglycan that provides a solid base for the ECM [93]. Hypertrophic chondrocytes no longer produce type II collagen but instead they synthesize type X collagen.

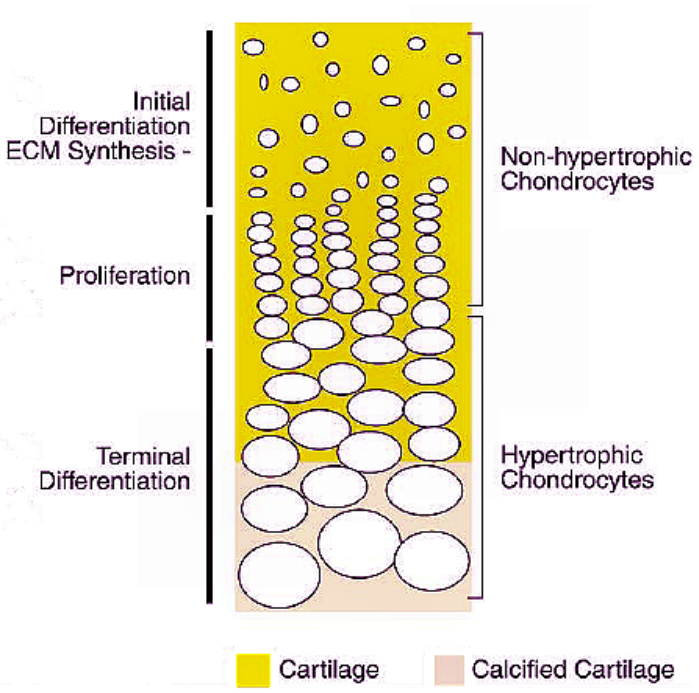

Figure 1.8 – Representation of growth plate column in long bones. From top to the bottom are represented are represented non-differentiated cells, then proliferating non-hypertrophic chondrocytes and finally hypertrophic chondrocytes with calcified ECM. Adapted from *Karsenty et al., 2002*

Endochondral ossification is controlled by several growth factors and transcription factors that regulate differentiation and proliferation of cells: Sox5, 6 and 9 (initial differentiation), Ihh (Indian hedgehog; proliferation and terminal differentiation), C-type natriuretic peptide (proliferation), fibroblast growth factor (FGF) receptor 3 (growth arrest), Wnt (wingless-int-1 oncogene; non-hypertrophic to hypertrophic

transition), Runx2 and parathyroid hormone related protein (terminal differentiation), and IGF-1 (proliferation and terminal differentiation) [91].

During flat bones formation, intramembranous ossification process takes place, involving condensation of mesenchymal stem cells and differentiation into osteoblasts. Differentiation of osteoblasts, whether in endochondral or intramembranous ossification, is also controlled by various growth and transcriptions factors, and in that sense Ihh and FGF-18 growth factors, and Cbfa1/Runx2 transcription factor seem to play key roles. Other factors, such as bone morphogenic proteins (BMPs), transforming growth factor-β and IGF, are also strongly implicated in proliferation and differentiation of osteoblasts, although their mode of action, either through direct or indirect pathways, remains uncompletely understood [91].

Differentiated osteoblasts are organized in bone as part of multicellular units named osteons, which synthesize a dense cross-linked type I collagen based matrix into which hydroxyapatite minerals ($Ca_{10}(PO_4)_6(OH)_2$) are deposited [94]. This process is assisted by several proteins, including the tissue non-specific ALP (TNAP; which cleaves pyrophosphate, an inhibitor of ECM mineralization), osteopontin (also named bone sialoprotein; an extracellular structural protein) and osteocalcin (OC, also named bone Gla protein – BGP – a calcium-binding protein essential for correct mineral maturation) [93,94]. Nevertheless, recent results demonstrate that coexpression of TNAP and fibrillar collagen (e.g. type I collagen) is apparently sufficient for ECM mineralization to occur [94].

In general, bone growth, regeneration and homeostasis occurs through a process involving sequential osteoblast and osteoclast differentiation (and cell death) which, through their specific activities, will form or resorb the mineralized matrix, respectively [93]. In this process, osteoclast formation is induced by the release of receptor activator

nuclear factor κB (NF-κB) proteins by osteoblasts, which are in turn stimulated by parathyroid hormone, vitamin D and several cytokines [93].

1.2.2. Insulin and IGF in vitro effects in bone-derived systems

IGFs are the most abundant growth factors in bone, where they have an autocrine/paracrine mode of action [81]. In addition, insulin and IGFs also assume important roles in bone through an endocrine mode of action [3]. *In vitro*, insulin and IGF (particularly IGF-1) have been shown to induce proliferation [95,96], differentiation (measured through ALP activity) [97-100], collagen synthesis (in combination with the inhibition of collagen degradation) [21,23,101-105] and anti-apoptotic effects [106] in osteoblast and osteoblast-like cell cultures (*e.g.* mouse primary osteoblasts and pre-osteoblastic cells MC3T3-E1, and human osteosarcoma cells MG63). Both MAPK and PI-3K pathways were shown to mediate mitogenic and anti-apoptotic effects (see also section 1.1.4) but ERK activation seems to be central in these effects. Evidences suggest that activation of MAPK pathway is essential for osteoblast differentiation through IGF-1 effects. Although data concerning insulin-like activity in chondrocytes or osteoclasts is somewhat limited, evidences point towards IGF-1 stimulation of: (i) proliferation [107,108], differentiation [109] and matrix synthesis in chondrocytes [19]; and (ii) differentiation of osteoclasts [97,110]. Studies developed in mouse ATDC5 chondrocyte cells have suggested that ERK activation triggers chondrocyte proliferation while inhibiting its differentiation [108]. Osteoclast formation and activity is apparently induced by both IGF-1 and IGF-2 in isolated rat osteoclast cultures but only in the presence of osteoblast cells (co-culture with primary osteoblast cultures or MG63 pre-osteoblast cells) [110].

1.2.3. Insulin and IGF in vivo effects in bone

Insulin and IGFs exhibit distinct effects *in vivo* on chondrocytes, osteoblasts and osteoclasts, as already stated in a previous section describing their *in vitro* effects. These *in vivo* effects have been studied by reverse genetics through knockout and overexpression (constitutive or restricted to osteoblasts) experiments in mice. Resulting phenotypes, summarized in Table I.1, clearly associate IGF-1, but not IGF-2, to bone formation rate and mineral density [3].

Table 1.1 – Mouse with mutations in IGF system and respective bone phenotype. *Adapted from Dupont and Holzenberger, 2003*.

Model	Phenotype	Reference
IGF-1 overproduction in osteoblasts in early development	↑ Bone formation ↑ mineral density	[20]
IGF-1 constitutive knockout	↓ Mineral density, short bones	[9]
IGF-2 constitutive knockout	No delay in ossification	[111]
IGF-1R conditional knockout in osteoblasts	↓ mineralization rate, ↓ mineral density	[16]
IRS-1 constitutive knockout	↓ Bone formation	[112]

Mice with altered IGF-1 and IGF-1R gene expression exhibit mineralization defects, demonstrating an important role for IGF-1 signalling during *in vivo* mineralization of the osteoblast ECM [16,20]. Experiments involving specific disruption of IRS-1 gene (see previous section) confirm a role of IGF signalling in osteoblast differentiation and additionally demonstrate important functions in osteoclastogenesis and bone turnover regulation [112]. Furthermore, IGF-1 effects during endochondral ossification have been linked to both stimulation of proliferation [113] and hypertrophy [19] of chondrocytes. Surprisingly, no significant bone-related phenotypes have been observed in IGF-2 knockout mice, suggesting a secondary role for this peptide in that

tissue [111]. In humans, low levels of IGF-1 in serum (resulting from a polymorphism in IGF-1 gene promoter) have been tentatively associated with a higher susceptibility to osteoarthritis and osteoporosis [114,115]. In a similar way, studies regarding insulin have mainly attempted to link type I diabetic condition in mice and human with particular bone-related phenotypes [82,87]. In streptozocin-treated mice (induced diabetes) intramembranous ossification was apparently accompanied by decreased gene expression of important transcription factors (*e.g.* Runx2). As a result, differentiation of osteoblasts was seriously hampered and a significant decrease in synthesis of bone matrix proteins such as OC and type I collagen [82] has been observed. In humans, diabetes is generally associated with an increased risk of fracture and osteoporosis. Histological studies have revealed lower levels of osteocalcin and decreased bone matrix formation rate [87].

1.2.4. Vanadate and its effects in bone

While adipose tissue has been the focus of most studies related to insulin-like properties of vanadium, bone has more recently emerged as a system of interest as a result of various observations: (i) vanadium has been shown to promote bone-related insulin-like effects [18,47,116,117], (ii) it accumulates in mammalian bones [118] and (iii) it affects bone formation if absent from diet [50,119]. In fact, bone is the main tissue for vanadium storage in mammals, *e.g.* approximately 2.4 µg V/g dry matter in goat carpal bones against only 1.6 µg V/g dry matter in kidney (the second highest concentration of vanadium in tissues) [50]. This accumulation has been proposed to be due to vanadium substitution of phosphate anions in the hydroxyapatite lattice and also to be related to a detoxification process [120,121]. However, severe malformations occurring in bone of animals (*e.g.* in the forelegs of goats) lacking vanadium (Figure

1.9) suggested a mechanism involving specific interaction with growth factors signalling, in particular those known to control bone development: platelet-derived growth factor (PDGF), fibroblast growth factors (1 and 2), insulin, IGFs, transforming growth factors β (1, 2 and 3), and various BMPs [79,116]. In fact, vanadate action closely resembled insulin and IGF due to its specific effects on osteoblast differentiation, interference with TKR and specific regulation of insulin/IGF associated signalling [122].

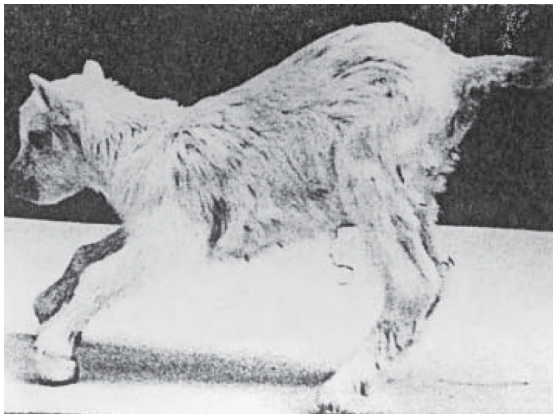

Figure 1.9 – Newborn vanadium-deficient goat with severely deformed forelegs. *In Anke et al., 2004*.

Vanadium effects in bone-derived systems in vitro

Primary culture from rat and chicken calvaria were the first *in vitro* systems used to investigate vanadium insulin-like effects in bone [117,123], in particular the inhibition of ALP activity and the stimulation of type I collagen synthesis [122]. Two mammalian cell lines, MC3T3-E1 (developed from newborn mouse calvaria, composed of pre-osteoblasts and able to mineralize its ECM [124]) and UMR106 (developed from rat osteosarcoma, composed of differentiated osteoblasts and unable to mineralize its ECM) were later shown to be particularly useful in understanding cellular mechanisms of vanadium, insulin- and IGF-like effects. In early studies, vanadium salts (*i.e.* vanadate, vanadyl, hydroperoxo- and peroxovanadium) have been shown to (i) affect osteoblast cell differentiation (monitored through the measurement of ALP activity) [125]

and stimulate cell proliferation at low doses (*i.e.* below 25 μM), and (ii) severely impair growth at higher doses [126]. Later on, other vanadium complexes (*i.e.* vanadium oxalate, citrate, tartrate and nitrilotriacetate) were tested on MC3T3-E1 and UMR106 cells proliferative and mineralogenic ability, revealing effects similar to those observed for vanadate [127] but still associated with a high cytotoxicity. Promising results arose recently from a new generation of vanadium complexes (*i.e.* bis(maltolato)oxovanadium(IV), bis(maltolato) dioxovanadium(V), vanadyl/aspirin, vanadyl/trehalose and vanadyl/ascorbate). These complexes have revealed a lower cytotoxicity while exhibiting effects similar to those promoted by vanadium salts (in particular vanadate). They have also allowed a better characterization of cellular mechanisms associated with bone-related vanadium effects, e.g. (i) strong inhibition of PTPase, (ii) stimulation of phosphorylation of tyrosine residues and insulin/IGF signalling cascade intermediates [128,129]; and (iii) activation of MAPK and PI-3K signalling pathways (analyzed using pathways inhibitors) [130-133]. In summary, while stimulation of cell proliferation and type-I collagen synthesis were shown to be mediated by insulin-dependent mechanisms, inhibition of ALP activity was apparently insulin-independent [122]. Since ALP and collagen are critical intermediates in ECM mineralization (*vide supra* **section 1.2.1**), it is likely that vanadium biological effects in bone depend greatly on its effect on these proteins. Nevertheless, the involvement of signalling mechanisms in these effects is still poorly understood and will need to be further investigated.

1.3. Fish as a model organism to study vertebrate bone formation

Fish systems have recently emerged as a promising alternative to more classical models (*i.e.* mammalian systems such as mouse, rat or mouse) to investigate vertebrate

development and various studies using *Danio rerio* (zebrafish) have demonstrated the suitability of fish models (see review by McGonnell and Fowkes [134]). Important features have recently demonstrated the suitability of fish to study vertebrate skeletogenesis, including: (i) the presence of fish orthologs for most mammalian genes, (ii) the strong resemblance of biochemical and physiological processes between fish and mammals and (iii) their important similarities in organ morphology and systems composition. In addition, fish systems present various technical advantages such as large progeny, external reproduction and fast growth.

Skeleton formation has been an important subject of study in fish. Interest in fish bone investigation has greatly increased after the detection of pathologies in zebrafish similar to those found in human systems: (i) *chihuahua* mutation in type 1 collagen gene can model human osteogenesis imperfecta and (ii) cranial neural crest formation in zebrafish can model human craniofacial birth defects [134,135]. Moreover, and from an economical point of view, the presence of a high rate of skeletal abnormalities in aquaculture fish species has also contributed to increase the interest in fish skeletogenesis. In that sense, skeletal development of aquaculture fish species has been extensively characterized in recent years [136]: important bone markers, such as matrix Gla protein (MGP), BMP-2, osteopontin, osteocalcin, etc, have been identified (gene and/or protein) and their role in fish tissue mineralization and bone formation has been investigated [137-141]. Conversely, important efforts have been made towards the development of biochemical, molecular and cellular biology tools from fish systems: the genomes of zebrafish, Japanese and green spotted pufferfish, Japanese medaka and stickleback have been sequenced and are available (*e.g.* at Ensembl sequence database – www.ensembl.org), microarrays containing thousands of genes have been constructed and cell lines have been developed. Remarkably, despite numerous fish cell lines being

available, none was derived from bone, and therefore suitable to study mechanism of tissue mineralization, until the recent development in our laboratory of two cell lines derived from the vertebra of the marine teleost fish *Sparus aurata* (gilthead seabream) [142].

1.3.1. Fish bone-derived cell lines: VSa13 and VSa16 cells

VSa13 and VSa16 (Figure 1.10) are bone-derived cell lines with chondrocytic and osteoblastic properties, respectively, and capable of mineralizing their ECM under appropriate conditions, although to different extents and rates [142].

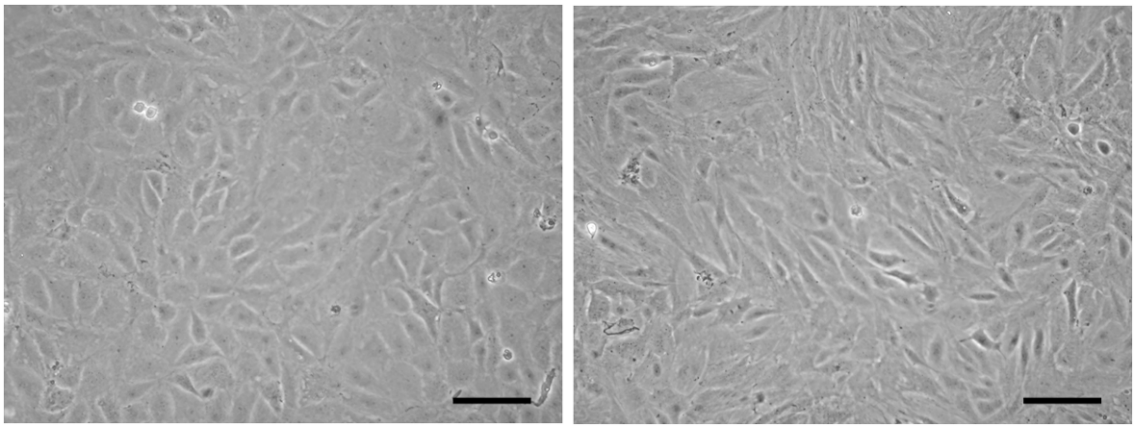

Figure 1.10 – Phase contrast micrographs of VSa13 (left) and VSa16 cells (right). Cells were cultured in Dulbecco's modified Eagle medium supplemented with 10% fetal bovine serum, 2 mM glutamine and 1% antibiotics and antimycotics. Pictures were obtained using a Zeiss Axiovert 25 microscope and an Olympus C-3030 Zoom digital camera. *Bar* = 100 μm.

During ECM mineralization, both cell types deposit calcium/phosphate nodules with chemical composition similar to that of hydroxyapatite (demonstrated by X-Ray diffraction), and this process has been quantified / analyzed using staining techniques specific for phosphate (von Kossa) or for calcium (Alizarin red) [136,142]. Both cell lines express MGP and osteocalcin genes in a mutually exclusive manner (*i.e.* MGP is only expressed in VSa13 cells where it is down-regulated during mineralization and

osteocalcin is only expressed in VSa16 where it is upregulated during mineralization), further demonstrating their relation with distinct bone cell types (*i.e.* chondrocyte-like and osteoblast-like respectively) [143]. [143]. Finally, both cell lines produce alkaline phosphatase and fibrilar collagen in quantity suitable for in vitro studies of ECM mineralization.

1.4. Objective

The effects of insulin, IGF-1 and vanadate on bone metabolism/formation are still poorly understood and have been exclusively characterized using classical mammalian systems. There are only few data available concerning other vertebrates, and none for fish. We proposed to characterize insulin, IGF-1 and vanadate effects on VSa13 (chondrocyte-like) and VSa16 (osteoblast-like) cell proliferation and ECM mineralization, and investigate intracellular signalling mechanisms, as well as important bone-related targets (*i.e.* ALP activity and collagen synthesis), involved in proliferative and mineralogenic effects. Ultimately, a comprehensive knowledge of IGF system in seabream (and fish in general) is proposed through the cloning of IGF-1 transcript(s) and the characterization of gene expression pattern during development and in adult tissues.

Chapter II

2. Methods

2.1. Preparation of peptide, vanadate, PD98059 and wortmannin solutions

Mature peptides of bovine insulin (Sigma Aldrich) and Australian snapper (Sparidae: *Pagrus auratus*) IGF-1 (Novozymes GroPep) were solubilised in pH 2.0 water (*i.e.* 1% v/v glacial acetic acid solution) at 10 μM and in pH 6.0 water at 0.1 mg/ml, respectively.

Metavanadate stock solution (50 mM, pH 6.7) was prepared from ammonium metavanadate (NH_4VO_3; Riedel-de-Haen). Decavanadate stock solution was obtained by adjusting the pH of the former solution to 4.0, as described elsewhere [55]. Acquired characteristic orange color in decavanadate solution upon acidification revealed the presence of decameric vanadate species (V10). Decavanadate stock solution was always adjusted to pH 7.0 immediately before using it. Both vanadate solutions were stored at 4°C. Although total vanadate concentration does not change, it should be noted that in case of decavanadate solutions the concentration in decameric vanadate species is effectively reduced 10-fold, meaning that stock decavanadate solutions contain 5 mM decameric vanadate species. However, vanadate concentrations are always given for monomeric vanadate (*i.e.* total vanadate).

PD98059 and wortmannin (Sigma Aldrich) stock solutions were prepared in DMSO at 6 and 10 mg/ml, respectively.

Milli-Q water (Millipore) was used to prepare solutions used in this work.

2.1.1. Characterization of vanadate solutions in cell culture medium

Composition of both vanadate solutions was analyzed by ^{51}V Nuclear Magnetic Resonance (NMR) spectroscopy as described elsewhere [55]. Briefly, the composition

of vanadate solutions upon dilution into Dulbecco's modified Eagle medium (DMEM #21969-035, Invitrogen; see Table AI.1in Appendix I) was analyzed in a Bruker AM-400 spectrometer at 105.2 MHz equipped with a 5-mm multinuclear inverse probe, using a 90º pulse Fourier transform technique. Spectra were acquired at room temperature using 0.5 ml of vanadate samples in the medium, containing at least 10 % D_2O, under the following conditions: spectral width 45455 Hz, accumulation time 0.05 s and relaxation delay 0.01 s. ^{51}V NMR chemical shifts are reported relative to an external reference of $VOCl_3$ (0 ppm). The relative areas of the several free or/and bound vanadate resonances were integrated and the line widths were obtained after subtracting the value (20 Hz) used in line broadening. The concentration of each vanadate oligomers V_x was calculated from the fractions of the total integrated areas observed in the recorded spectra as described (Equation 1). Symbol A corresponds to the area measured for the x vanadate species with the n aggregation number (number of vanadium atoms), A_t the sum of measured areas and $[V_t]$ corresponds to total vanadate concentration [52].

$$[V_x] = \frac{A_x}{A_t} \times \frac{[V_t]}{n} \qquad (1)$$

The calculated concentrations of vanadate oligomers were reproducible within 2-4%. For quantitative measurements all spectra parameters were kept constant. Vanadate concentrations are always given for monomeric vanadate, *i.e.* total vanadium. Unlike metavanadate, decavanadate solutions are instable. The partial de-oligomerization of decameric vanadate species present at the decavanadate solutions upon dilution in DMEM was analyzed by ultraviolet/visible spectroscopy (Shimadzu UV-2401PC spectrophotometer) at 400 nm, as described elsewhere [63].

2.2. Fish culture

Eggs collected from natural spawning of seabream (from January to March, 2006) were placed at 16ºC in a closed recirculating system with 35 ppt salinity water. Light was controlled with fluorescent lamps, maintaining a 12:12 hour light-dark photoperiod. Hatching took place 48 to 56 hours after fertilization (HAF; hatched larvae approx. size 3 mm). Developing larvae were fed with rotifers from 96 HAF to 20 days after hatching (DAH; approx. size 7-8 mm) and with newly hatched *Artemia nauplii* from 20 to 50 DAH (approx. size 15 mm), as described in table AIII.1 of appendix III. Rotifers and *A. nauplii* were fed with microalgae *Tetraselmis suecica* and *Isochrysis galbana*. Selco (INVE) was introduced into larval diet between 35 and 45 DAH through the use of Selco-enriched *A. nauplii*. Dry food was introduced into larval diet between 45 and 70 DAH (approx. size 20 mm) through the use of Selco/dry food mixture (initially 50% and then 100% food). After 70 DAH, larvae were maintained on a dry food diet. Definitive morphology reached at approximately 90 DAH (approx. size 30 mm). Juvenile and adult fish were bred at 16-20ºC in 100 l seawater tanks with a 12:12 hour light-dark photoperiod, aeration of 100 ml/minute, and renewal flow of 1 tank/day and fed with artificial food (Sorgal).

2.3. Cell culture maintenance

Cultured VSa13 and VSa16 cells were maintained as described elsewhere [142]. Briefly, cells were cultured in DMEM (see Table AI.1 in Appendix I) supplemented with 1 % penicillin-streptomycin, 1 % fungizone, 2 mM L-glutamine and 10 % fetal bovine serum (Invitrogen), and incubated at 33 ºC in a 10 % CO_2 humidified atmosphere. Confluent cultures were divided (1:2) every 3-4 days using trypsin-EDTA solution (solution T; see appendix I table AI.2).

2.4. RNA preparations

2.4.1. RNA extraction from larvae and tissues

At appropriate times, pools of at least 10 eggs/larvae/juveniles or tissues from 1 female and 3 male adult fish (males approx. weight was 0.5 kg and female approx. weight was 2 kg; equal amount of male and female tissues were mixed) were sampled. Fish and tissue samples were washed twice in phosphate-buffered saline solution (PBS 1×; see Table AI.2 in Appendix I) before storage at -80ºC in at least 5 ml of Trizol (see Table AI.3 in Appendix I). Total RNA was extracted as described by Chomczynski and Sacchi [144]. Briefly, samples were ground to powder in liquid N_2 (hard tissues) and homogenised in Trizol using a syringe with a 20 G needle. Total RNA was first extracted from tissue homogenate with 0.2 volume of chloroform/isoamyl alcohol mixture (49:1, freshly prepared) then precipitated from aqueous phase (obtained after 15 min of centrifugation at 12000×g and 4ºC) with 1 volume of 100% isopropanol. After 1 h at -30ºC, total RNA was finally pelleted by centrifugation at 12000×g (15 min, 4ºC). RNA pellets were washed twice with ice-cold 75% ethanol and re-suspended in RNase-free MilliQ water. Total RNA concentration was determined by spectrophotometry at 260 nm using GeneQuant spectrophotometer (Pharmacia). Quality of all RNA samples was assessed on agarose-formaldehyde gels.

2.4.2. RNA preparation from cultured cells

Total RNA was extracted from cultured cells using a method adapted from Chomczynski and Sacchi [144]. Cells were washed with PBS 1×, scraped from plates, homogenized in 5 ml of solution D (see Table AI.3 in Appendix I) using a syringe with

a 20 G needle (to shear genomic DNA). Total RNA was first extrated from cell homogenate with 0.1 volume of 2 M sodium acetate pH 4 (mixed by inversion), 1 volume of phenol pH 4 (mixed by inversion) and 0.2 volume of chloroform/isoamyl alcohol mixture (49:1, freshly prepared), then precipitated from aqueous phase (obtained after 15 min centrifugation at 10000×g and 4ºC) with 1 volume of 100% isopropanol. After 1 h at -30ºC, total RNA was finally pelleted by centrifugation (30 min at 10000×g, 4ºC). RNA pellets were solubilized in solution D and RNA was again precipitated, washed with ice-cold 75 % ethanol, air dried and finally sollubilized in RNase-free MilliQ water. Total RNA concentration was determined by spectrophotometry at 260 nm using GeneQuant spectrophotometer (Pharmacia). Quality of all RNA samples was assessed on agarose-formaldehyde gels.

2.5. Construction of genomic and complementary DNA libraries

2.5.1. Construction of genomic DNA library

Seabream genomic DNA was prepared from a pool of tissues using DNeasy Tissue kit (QIAGEN) according to manufacturer instructions, then digested with *Pvu*II or *Sca*I endonucleases. Libraries were constructed using GenomeWalker Universal kit (Clontech BD Biosciences) according to manufacturer instructions.

2.5.2. Construction of complementary DNA

Full-length cDNA library were prepared using Marathon cDNA Amplification kit (Clontech BD Biosciences) according to manufacturer instructions. Poly(A^+) RNA needed for library construction was purified using RNA QuickPrep Micro mRNA

Purification kit (Pharmacia) from total RNA extracted from seabream liver, kidney, brain and pituitary as described in section 2.4.

2.6. DNA amplification and cloning

Rapid amplification of cDNA ends (RACE) and amplification of full-length cDNAs were performed by polymerase chain reaction (PCR) using a 1:50 dilution of a Marathon cDNA library, Advantage *Klen Taq* Polymerase mix (Clontech BD Biosciences) and primers listed in Table AII.1 of Appendix II, according to manufacturer's instructions. Amplification of genomic fragments was performed by PCR using GenomeWalker libraries, Advantage *Klen Taq* Polymerase mix and primers listed in Table AII.1 of Appendix II, according to manufacturer's instructions. PCR products were size-separated by agarose gel electrophoresis, purified using the GFX PCR DNA and Gel Band Purification kit (Amersham Biosciences) and cloned into pCRII-TOPO vector (Invitrogen). Final fragment identification was achieved by DNA sequencing (Macrogen) and analyzed using BLAST facilities at NCBI (www.ncbi.nlm.nih.gov).

2.7. Sequence reconstruction

GenBank sequence database was searched in October 2006 using BLAST facilities at NCBI for sequences showing similarities to seabream IGF-1 transcripts. Species-specific sequences were first clustered, and elements of each cluster were assembled using ContigExpress module of Vector NTI Suite 10 (Invitrogen) to generate, after manual correction, accurate consensus sequences. Virtual transcripts and alternative splicing events were deduced from consensus sequences using stringent overlap criteria.

2.8. Genomic southern analysis

Aliquots (10 µg) of seabream genomic DNA, prepared using DNeasy Tissue kit were digested with 25 units of selected endonucleases (*Bgl*I, *Bgl*II, *Eco*RI, *Hin*dIII, *Pst*I, and *Sca*I) and DNA fragments were size-separated on a 0.8 % (w/v) agarose gel for 10 h at 50 V. DNA was transferred onto a Hybond-XL nylon membrane (Amersham Biosciences) by capillarity blotting with standard saline citrate buffer 10× (SSC 10×; see composition in Table AI.6 of Appendix I). IGF-1 cDNA probe (199 bp corresponding to cDNA positions 357 to 555 bp) was radiolabeled with [α-^{32}P]dCTP (3000 Ci/ml) using the Rediprime II kit (Amersham Biosciences) and purified from unincorporated nucleotides using MicroSpin G-50 columns (Amersham Biosciences). Hybridization of the blot was performed overnight at 42°C in ULTRAhyb solution (Ambion). Blots were washed 2×5 min in low stringency solution (SSC 2× and 0.1 % SDS) and 3×15 min in high stringency solution (SSC 0.1× and 0.1 % SDS) at 60°C, then autoradiographed.

2.9. Quantitative real-time PCR

Real-time PCR (qPCR) was performed using iCycler PCR system and software (Bio-Rad). Total RNA (1 µg) samples from seabream were treated with RQ1 RNase-free DNase (Promega) and reverse-transcribed using moloney murine leukemia virus reverse transcriptase (Invitrogen) and specific reverse primers listed in Table AII.2 of Appendix II. The following reverse transcription reaction conditions were used: 3 min at 60ºC, 5 min at 4ºC, 1 h at 37ºC and 5 min at 95ºC. PCR amplification of cDNA fragments was performed using the iQ SYBR Green I mix (Bio-

Rad), 10 ng of reverse-transcribed RNA and specific primers listed in Table AII.2 of Appendix II. The following PCR conditions were used: 4 min at 95ºC, 40-50 cycles (each cycle is 30 s at 95ºC, 15 s at 68ºC). Changes in gene expression were determined through normalization of each transcript threshold cycle with that of corresponding housekeeping gene (β-actin or ribosomal protein L27a (RPL27a), assumed to be invariant) [145]. This operation was performed using Bio-Rad RelQuant excel sheet.

2.10. Cell viability assay

Cytotoxic and proliferative effects on cells were assessed through cell viability analysis using the CellTiter 96 non-radioactive proliferation assay kit (Promega) according to manufacturer's instructions (adapted from the protocol developed by Mosmann [146]. Briefly, tetrazolium reagent (3-(4,5-dimethylthiazol-2-yl)-5-(3-carboxy-methoxyphenyl)-2-(4-sulfophenyl)-2H-tetrazolium; inner salt, MTS) and the electron-coupling reagent, phenazine methosulfate, were mixed in solution in a 20:1 proportion. Once added to cell culture, MTS is reduced into formazan by a mitochondrial dehydrogenase found in metabolically active cells. Formazan formation, which is proportional to the number of living cells [147], was followed at 490 nm in 96-well tissue culture dishes using a Bio-Rad Benchmark microplate reader. Incubation with 20 µl of reagent mixture during 1 h was determined to be the optimal after being observed linearity between number of cells and formazan absorbance at 490 nm wavelength (see Figure AIV.1 in Appendix IV,). Effects were either analyzed in confluent cell cultures or low-density cell cultures (starting from 1.5×10^3 cells/well).

2.11. ECM mineralization and nodule detection

Cells were seeded in 24-well plates at 2×10^4 cells/well using culture conditions described in section 2.3. To induce ECM mineralization, cells were treated with 50 µg/ml L-ascorbic acid (vitamin C), 10 mM β-glycerophosphate and 4 mM $CaCl_2$ during 4 weeks. At appropriate times, cells were washed 3 times with ice-cold PBS, fixed with 10% formaldehyde (in PBS 1×) for 1 h at 4ºC, washed 3 times with MilliQ water, then incubated with 5% silver nitrate for 30 min under ultraviolet light. Relative levels of ECM mineralization were determined by densitometric analysis using Quantity One software (Bio-Rad).

2.12. Protein quantification

Protein concentration in cell extracts was determined using Bradford reagent (Sigma Aldrich) according to manufacturer's protocol (adapted from Bradford [148]). Standards and samples were prepared according to Table AIII.2 of Appendix III using 2 mg/ml bovine serum albumin (BSA; Pierce) or 10 µl of each sample, then incubated approximately 10 min with reagent. Absorbance was measured at 595 nm in a Thermo Helios-γ spectrophotometer.

2.13. ALP activity

Cells were washed 3 times with PBS 1× and scrapped using 500 µl of 0.1% Triton X-100. Samples were centrifuged at 16000×g and supernatants collected and stored at -20 ºC until further analysis. Protein content was determined as described in section 12 of Methods. ALP activity was measured at 37ºC through spectrophotometric analysis of initial rates of hydrolysis of p-nitrophenyl phosphate (Sigma Aldrich) into p-nitrophenol

at 405 nm, using a Shimadzu UV-2401PC spectrophotometer. The following reaction mixture has been used: 800 µl of ALP reaction buffer (see Table AI.4 of Appendix I), 100 µl of p-nitrophenyl phosphate (5 mM in reaction buffer) and 100 µl of supernatant (used to set the reaction). ALP activity was normalized with protein content and presented as nmol of p-nitrophenol (considering $\varepsilon = 18200\ M^{-1}\ cm^{-1}$) formed per min and per mg of total protein.

2.14. Total collagen content

Collagen fibbers of ECM were stained using Sirius red dye as described by Tullberg-Reinert and Jundt (1999) [149]. Briefly, cell cultures were washed 3 times with PBS 1× then fixed for 1 h using Bouin's fluid (see Table AI.5of Appendix I). After fixation, cells were washed with running tap water during 15 min, air dried and incubated 1 h (gentle agitation) with Sirius red staining solution (see Table AI.5 of Appendix I). Unbound dye was removed by extensive wash using 0.01 N HCl. Coloration was observed under an Axiovert 25 inverted light microscope (Zeiss) and quantified in a Bio-Rad Benchmark microplate reader at 550 nm after dye re-suspension in 200 µl of 0.1 N NaOH solution.

2.15. Vanadium accumulation in cell extracts

Cells were incubated with vanadate solutions during 24 h. At appropriate times, cultures were washed 3 times with PBS 1×, supplemented with 1 ml of MilliQ water and placed at -80ºC for at least 12 h. Frozen cells, thawed at room temperature, were scrapped from plates and transferred into 2-ml microcentrifuge tubes. Plates were washed with 1 ml of MilliQ water then pooled with first extract (total volume sample

was 2 ml). Total protein content in samples was quantified as described in section 12 of Methods. Remaining sample was digested at 100ºC with 30 µl of 65 % HNO_3 and final solid residues dissolved in 5% HCl solution. Vanadium concentration was determined by atomic absorption spectrometry analysis using a GBC Avanta atomic absorption spectrometer equipped with a GBC GF 3000 graphite furnace system and a GBC PAL 3000 auto sampler working at a furnace program of 63 s with an argon gas flow of 3.0 l/min. The vanadium lamp was operated at 318.2 nm, with slit width of 0.2 nm, and the instrument was calibrated against a series of solutions containing 12.5, 25, 37.5 and 50 ppb of vanadium. Calibrating standards were obtained by successive dilutions of a standard solution of vanadium 1002 ± 2 mg/l (Merck). The detection and quantification limits of the instrument for these analysis conditions, determined according to ISO 8466-1, were 5 and 11 ppb, respectively.

Chapter III

3. Results

3.1. Short exposures of vanadate oligomers differently affect VSa13 cells

3.1.1. Spectral analysis of metavanadate and decavanadate oligomers in DMEM

^{51}V NMR spectroscopy of decavanadate-DMEM solutions (1 and 5 mM at pH 7.0), revealed three signals attributed to three specific vanadium atoms in V10 structure: V10A at -515 ppm, V10B at -498 ppm and V10C at -425 ppm (Figure 3.1 A). Similarly, signals detected in metavanadate-DMEM solutions (1 and 5 mM at pH 7.0) were attributed to mono- (V1), di- (V2), tetra- (V4) and pentameric (V5) vanadate species at -556 , -571 , -579 and -587 ppm, respectively (Figure 3.1 A). Monomeric NMR signal is clearly broadened, with a half line-width value (270 Hz) approx. 3.4-fold of normal value (80 Hz) [65], probably due to vanadate interactions with compounds present in DMEM such as glucose (25 mM) and pyruvate (1 mM), or even interactions with proteins from FBS, also present in culture medium [53,65]. Concerning each vanadate oligomers concentrations in metavanadate solutions in DMEM (1 and 5 mM), different profile has been observed (Figure 3.1 B). Interestingly, different profiles have been observed for each concentration of metavanadate in DMEM: while tetrameric species were predominant at 5 mM, monomeric vanadate was the most abundant at 1 mM (Figure 3.1 B). On the contrary, the profile of decavanadate solutions was similar since decameric species present in the solutions increased linearly with total vanadate concentration (Figure 3.1 C).

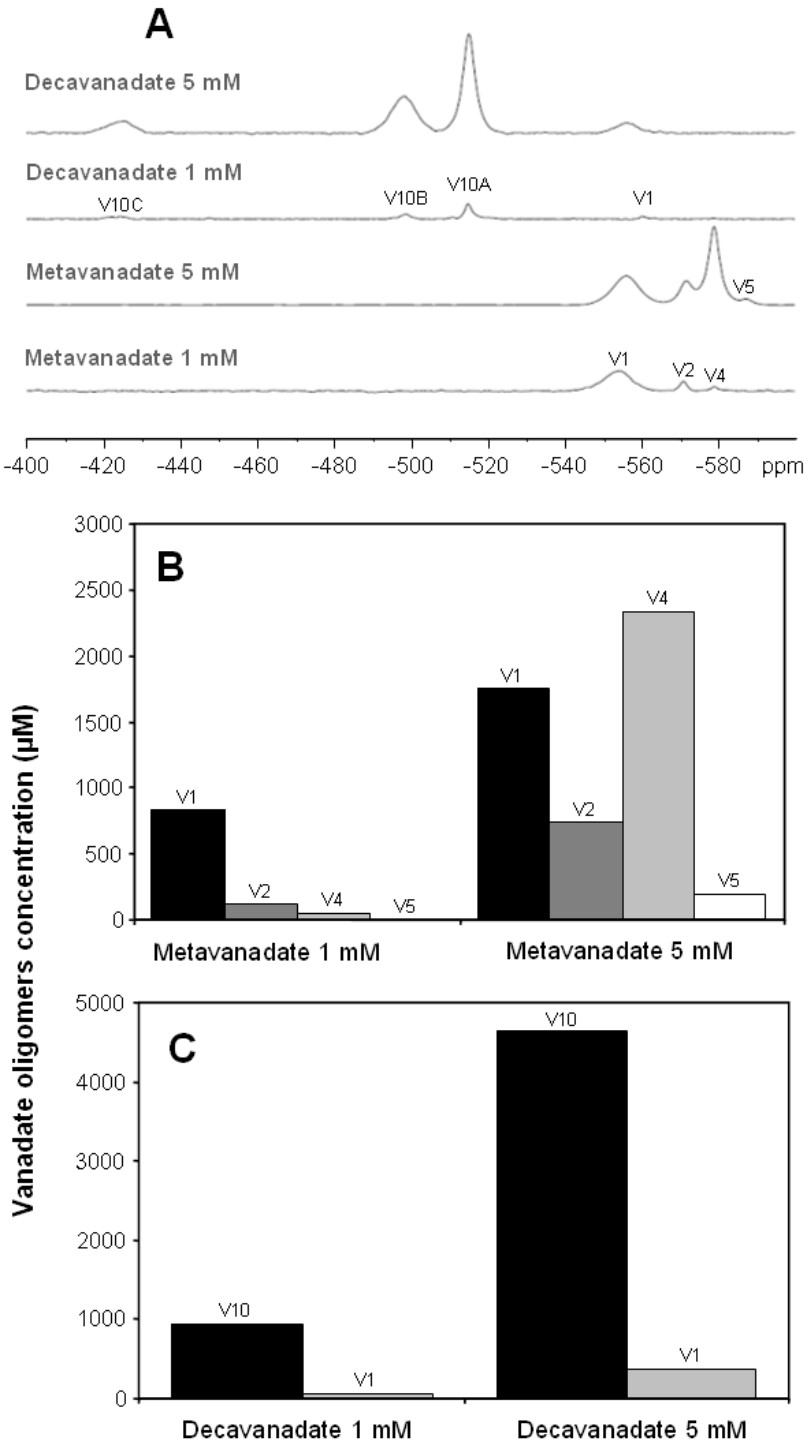

Figure 3.1 - ^{51}V NMR spectra of metavanadate and decavanadate solutions in DMEM. Spectra were performed at 22°C and pH 7.1. (**A**) V1 and V2 correspond to monomeric ($H_2VO_4^-$) and dimeric ($HV_2O_7^{3-}$ and $H_2V_2O_7^{2-}$) vanadate species, respectively, and independently of protonation state; V4 and V5 correspond to cyclic tetrameric ($V_4O_{12}^{4-}$) and pentameric ($V_5O_{15}^{5-}$) vanadate specie; V10A, V10B and V10C signals correspond different to vanadium atoms in the decameric vanadate specie ($V_{10}O_{28}^{6-}$) structure. (**B** and **C**) Each vanadate (V) specie concentration was calculated from the fractions of the total integrated areas observed in the spectra (as described in section 1.1 of Methods. For quantitative measurements, spectral parameters were kept constant and normalized using that of 5 mM decavanadate.

3.1.2. Decavanadate stability in DMEM

^{51}V NMR spectroscopy is an essential tool to analyze vanadate oligomers composition and interactions in a solution; however, it is not suitable when analyzing the presence of vanadate species at low concentrations (in the μM range). Consequently, the stability of vanadate species in culture medium were followed through ultraviolet/visible spectroscopy and decomposition rate was determined at 33ºC through the time-course analysis of the absorbance (400 nm) of a decavanadate solution prepared in DMEM (250 μM, meaning 25 μM decameric species). In these conditions, decameric species were shown to decompose through a first order kinetic (Figure III.2), which can be mathematically described by equation 1. In this equation, $\mathbf{t_{1/2}}$ is the half-life time of the reaction, $\mathbf{[V_{10}]}$ is the concentration of decameric species at a given time, $\mathbf{[V_{10}]_0}$ is the initial concentration of decameric species and **k** is the kinetic constant (which corresponds to the slope of the straight line in a first order kinetic).

$$\ln ([V_{10}]/[V_{10}]_0) = -kt \quad (1)$$

At $t_{1/2}$, $[A] = ½ [A]_0$, and substituting this values in equation 1 we obtain equation 2.

$$t_{1/2} = \ln(2)/k \quad (2)$$

From the graphic in Figure III.2, k is 0.00462 min^{-1} and substituting values in equation 2 it has been determined that $t_{1/2}$ of decavanadate decomposition is approx. 150 min.

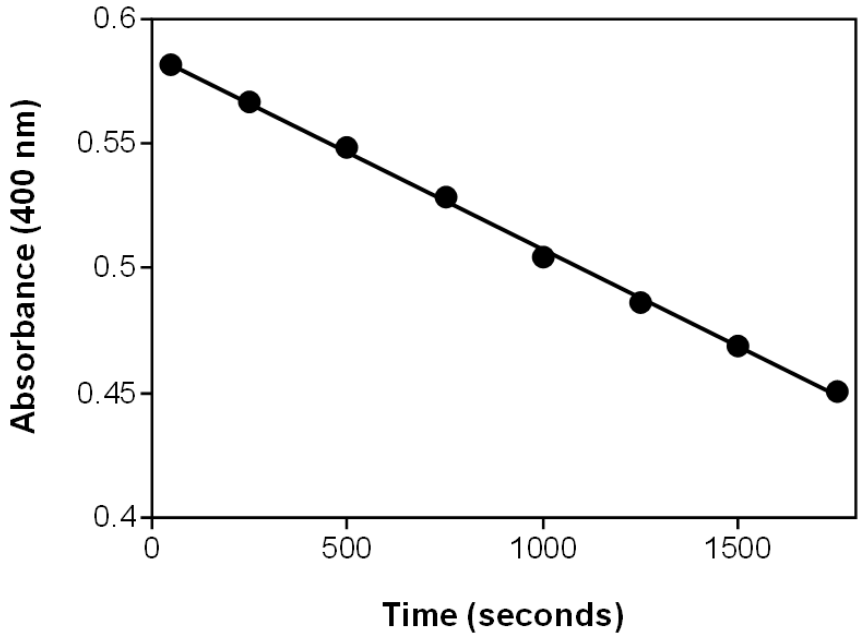

Figure 3.2 – Decameric species de-oligomerization kinetic in DMEM at 33ºC and pH 7.4, from 250 µM decavanadate solution. Before dilution in DMEM of the decavanadate stock solution (50 mM), pH was adjusted to 7.4; DMEM was used as absorbance blank at 400 nm; decavanadate in DMEM absorbance was measured during approximately 30 min using Shimadzu UV-2401PC spectrophotometer.

3.1.3. Short- and long-term cytotoxic effects of vanadate oligomers in VSa13 cells

Cytotoxicity of vanadate oligomers was tested in confluent cultures of VSa13 cells for 15 days using concentrations up to 250 µM (chronic toxicity) or for 4 h using a concentration of 1 mM (acute toxicity). Prolonged exposure to metavanadate or decavanadate similarly affected VSa13 cell viability (Figure 3.3): treatments using concentrations up to 7.5 µM did not decrease cell viability (a slight increase was even observed after 15 days) while treatments using 10 to 250 µM concentrations seriously affected cell viability, most of the cells being killed at the highest concentrations.

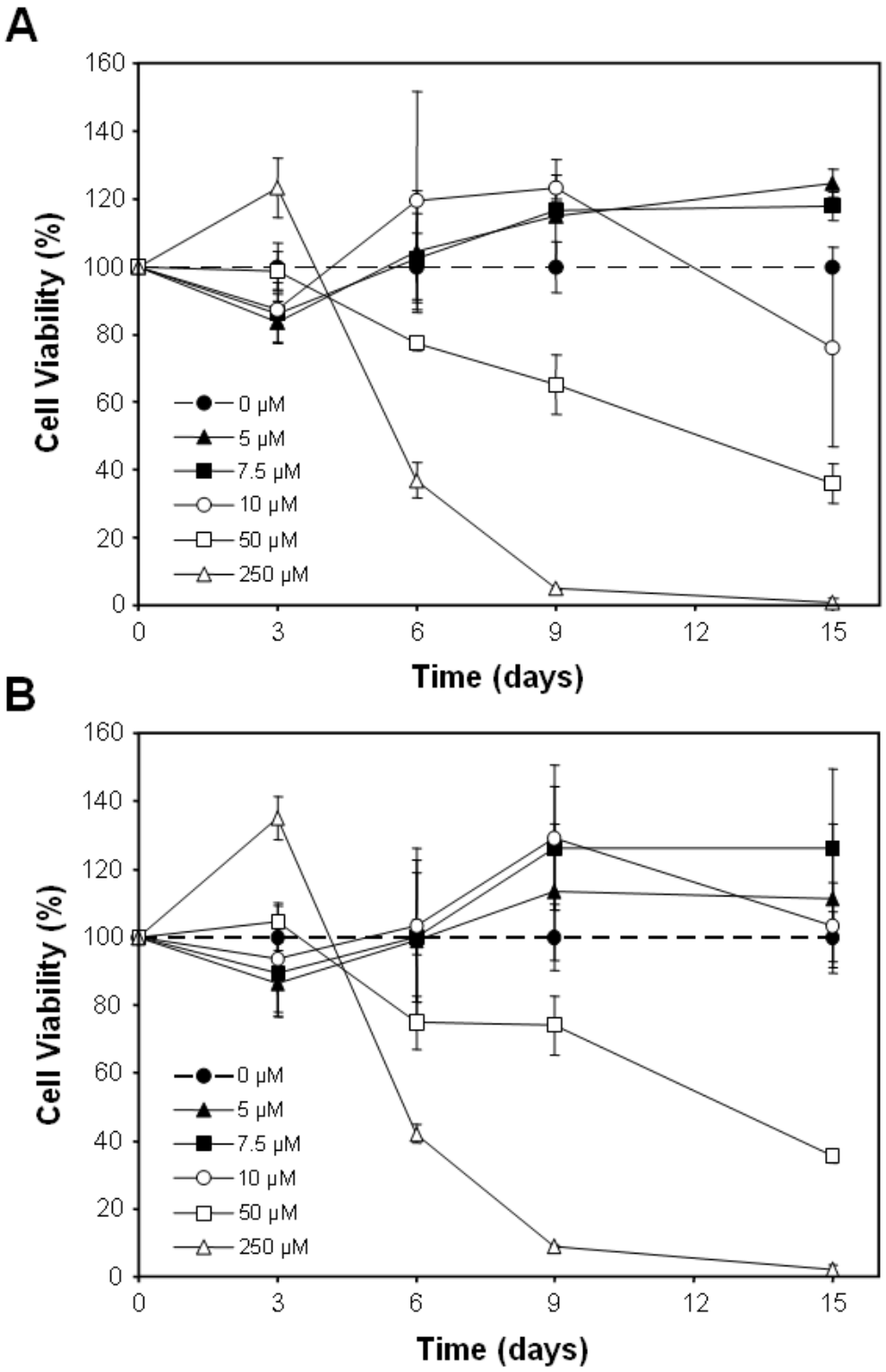

Figure 3.3 - Long-term effect of metavanadate and decavanadate on VSa13 cell viability. VSa13 cells were seeded in 96-well plates, grown in DMEM until confluence then treated with metavanadate (**A**) and decavanadate (**B**) using concentrations ranging from 5 to 250 µM. Cell viability was evaluated at appropriate times using MTS assay and is presented as the percentage of control value (set to 100%). Values are the mean of at least three independent experiments.

On the contrary, short-term exposure to metavanadate and decavanadate differentially affected VSa13 cell viability (Figure 3.4): while 1 mM decavanadate significantly reduced cell viability after 2 h, 1 mM metavanadate showed no effects. After 4 h, both solutions significantly reduced the cell viability to levels near 50% (ANOVA – analysis of variances).

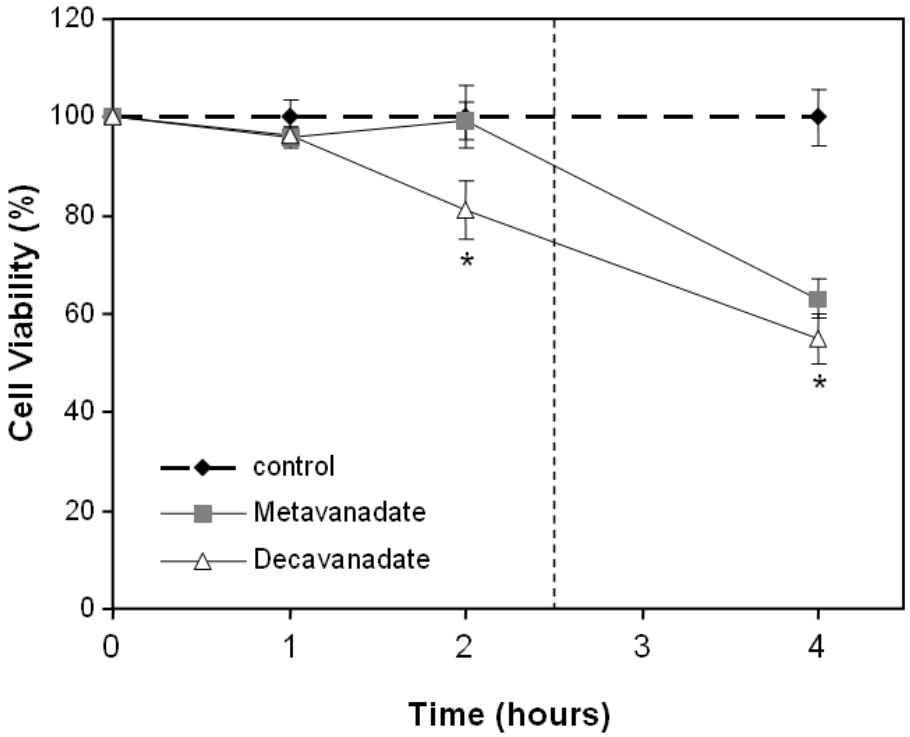

Figure 3.4 - Short-term effect of metavanadate and decavanadate on VSa13 cell viability. VSa13 cells were seeded in 96-microwell plates, grown in DMEM until confluence then treated with 1 mM metavanadate and decavanadate. Cell viability was evaluated at appropriate times using MTS assay and is presented as the percentage of control value (set to 100%). Values are the mean of at least three independent experiments. Asterisk indicates that values are statistically different in comparison to the respective control ($P < 0.05$; one-way ANOVA). Dashed line indicates the half-life of decavanadate in DMEM estimated at 2.5 h.

This observation suggests that decameric vanadate species, still present in culture medium after 2 h, are likely to induce more toxicity effects than monomeric vanadate species, certainly the most abundant vanadate form found in culture medium after 4 h (half-life time of decavanadate in DMEM was estimated at 2.5 h) upon decameric vanadate desintegration.

3.1.4. Vanadium accumulates differently in VSa13 cells upon vanadate exposure

A time-course of vanadium accumulation in VSa13 cells was determined in confluent cultures treated with 10 µM metavanadate or decavanadate (shown not to be toxic at 24 h; see Figure 3.3). After subtraction of vanadium content measured in non-treated cells (2.54 ± 0.43 µg V/g of protein; Figure 3.5), vanadium accumulation after 1 h of treatment was significantly higher (according to Student's test) in cells treated with metavanadate (4.61 ± 0.29 µg V/g of protein) than in cells treated with decavanadate (3.24 ± 0.24 µg V/g of protein). A similar but more pronounced difference in vanadium accumulations was observed after 2 h of treatment (6.85 ± 0.4 µg and 3.95 ±0.1 µg V/g of protein, respectively). Although longer incubation resulted in higher vanadium accumulation (approximately 18-fold increase above control value at 24 h), no significant differences have been observed between metavanadate and decavanadate treatments. These results suggest that monomeric species enter and accumulate more easily in VSa13 cells than decameric species. Furthermore, accumulation rates only become similar at longer exposures which is consistent with decameric molecules decomposition ($t_{1/2}$ = 150 minutes).

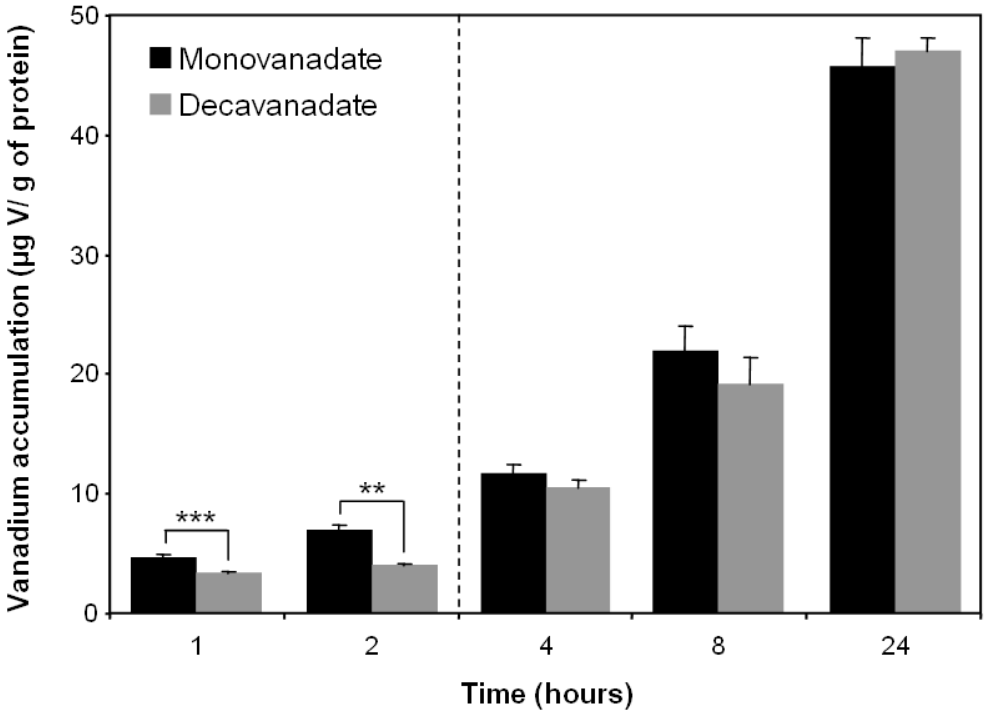

Figure 3.5 - Vanadium accumulation in VSa13 cells upon vanadate exposure. VSa13 cells were seeded in 100-mm plates, grown in DMEM until confluence then treated with 10 µM metavanadate or decavanadate. At appropriate times, vanadium content was determined by atomic absorption from cellular extract and normalized with protein content. Vanadium content measured in non-treated samples (2.54 ± 0.43 µg V/g of protein) was subtracted to each value. Asterisks indicate statistically significant differences between metavanadate and decavanadate according to Student's test (** $p < 0.005$ and *** $p < 0.001$). Values are the mean of at least three independent experiments. Dashed line indicates the half-life of decavanadate in DMEM estimated at 2.5 h.

3.2. Vanadate insulin-like effects on VSa13 cells

3.2.1. Vanadate and IGF-1 stimulate VSa13 cells proliferation

Vanadate effect on VSa13 cell proliferation rate was investigated in dividing cultures. Both metavanadate and decavanadate (maximum at 7.5 µM) stimulated VSa13 cell proliferation to a similar extent (consequently only data from metavanadate exposure are shown; Figures 3.6, 3.7 and 3.8). In separate experiments, IGF-1, but not insulin (up to 100 nM each; concentrations used in mammalian bone-derived cell

systems [150,151]) stimulated VSa13 cells proliferation to an extent similar to that of vanadate (maximum stimulation at 10 nM) (Figures 3.6, 3.7 and 3.8).

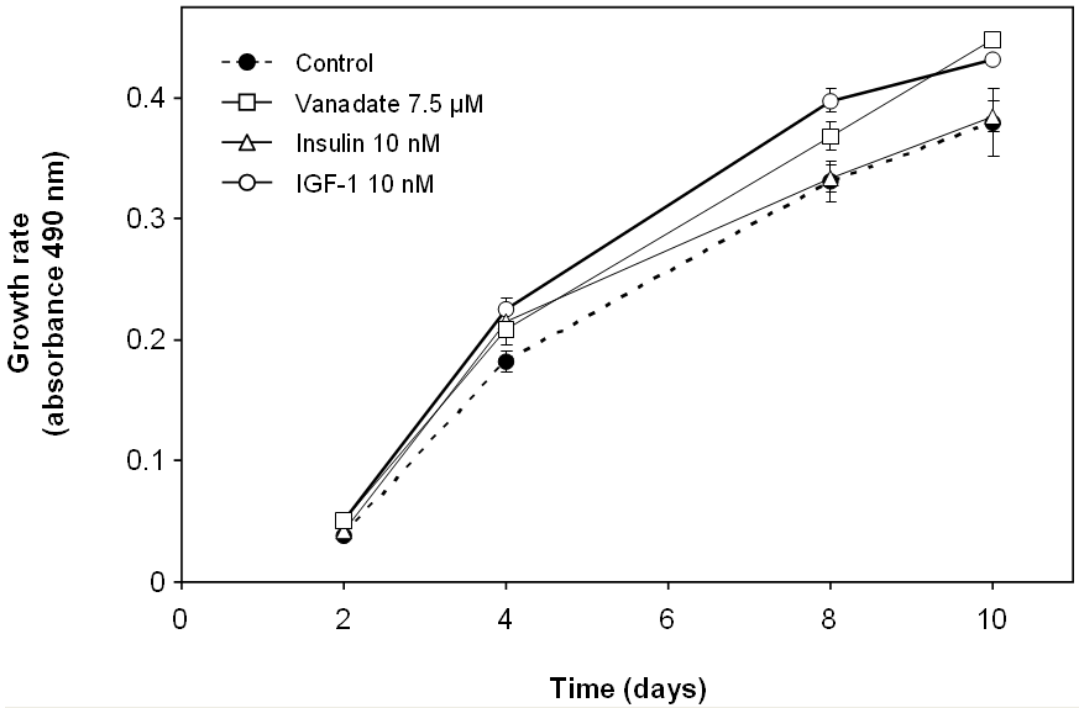

Figure 3.6 - Effect of vanadate, insulin and IGF-1 on VSa13 cells proliferation. VSa13 cells were seeded in 96-well plates at 1.5×10^3 cell/well then treated either with 7.5 µM vanadate (metavanadate or decavanadate), 10 nM insulin or 10 nM IGF-1. Cell proliferation was evaluated at appropriate times using MTS assay. Values are the mean of at least three independent experiments.

These results suggest that proliferative effect of vanadate may involve IGF-1 signalling pathway, but not that of insulin. It is worth noting that no proliferative effects were observed for insulin using concentrations up to 100 nM (Figure 3.7).

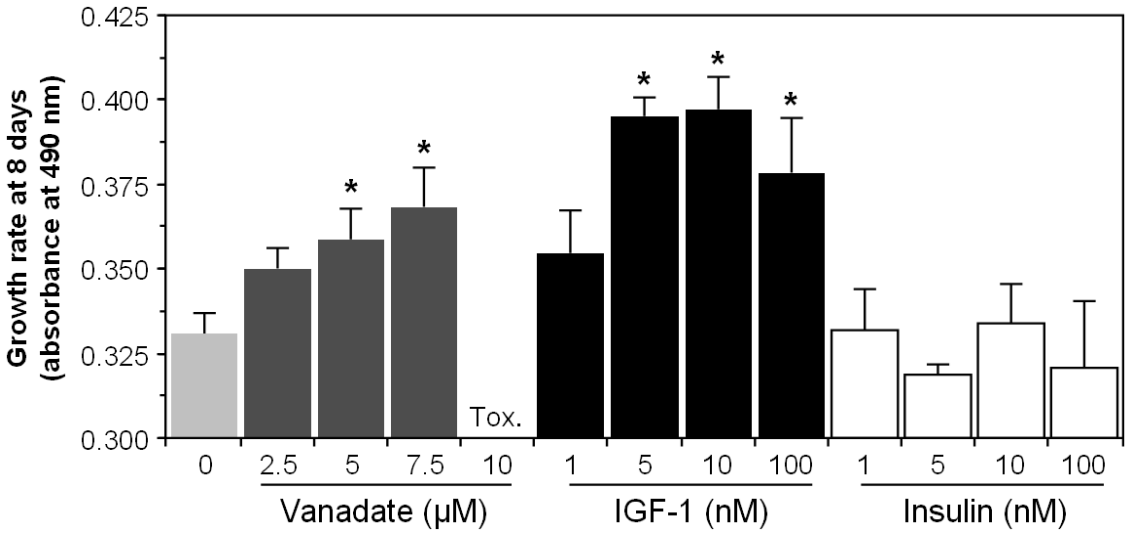

Figure 3.7 - Effect of vanadate, insulin and IGF-1 doses on VSa13 cells proliferation. VSa13 cells were seeded in 96-well plates at 1.5×103 cells/well then either left untreated (0) or treated with vanadate (2.5-10 µM), insulin (1-100 nM) or IGF-1 (1-100 nM). Cell proliferation was evaluated after 8 days using MTS assay. Asterisk indicates values statistically different from corresponding controls (n≥3; $P<0.05$; one-way ANOVA).

3.2.2. PD98059 similarly blocks vanadate and IGF-1 stimulation of VSa13 cell proliferation

Wortmannin and PD98059, known inhibitors of PI-3K and MAPK, respectively, were tested for their effect on VSa13 cell proliferation and for their capacity of reverting IGF-1 and vanadate stimulatory effects. Dividing cultures of VSa13 cells were treated for 8 days with 0.1 µM wortmannin, 100 µM PD98059 (non-toxic concentrations, see Figure AIV.2 of Appendix IV; added volumes of DMSO were non-toxic, data not shown), 10 nM insulin, 7.5 µM vanadate and/or 10 nM IGF-1. PD98059 but not wortmannin totally abolished vanadate and IGF-1 stimulation of cell proliferation, while inhibitors alone had no effect (Figure 3.8). These results provide strong evidence that proliferation of VSa13 cells is stimulated by micromolar concentrations of vanadate through the same mechanisms as IGF-1, *i.e.* through activation of the MAPK pathway.

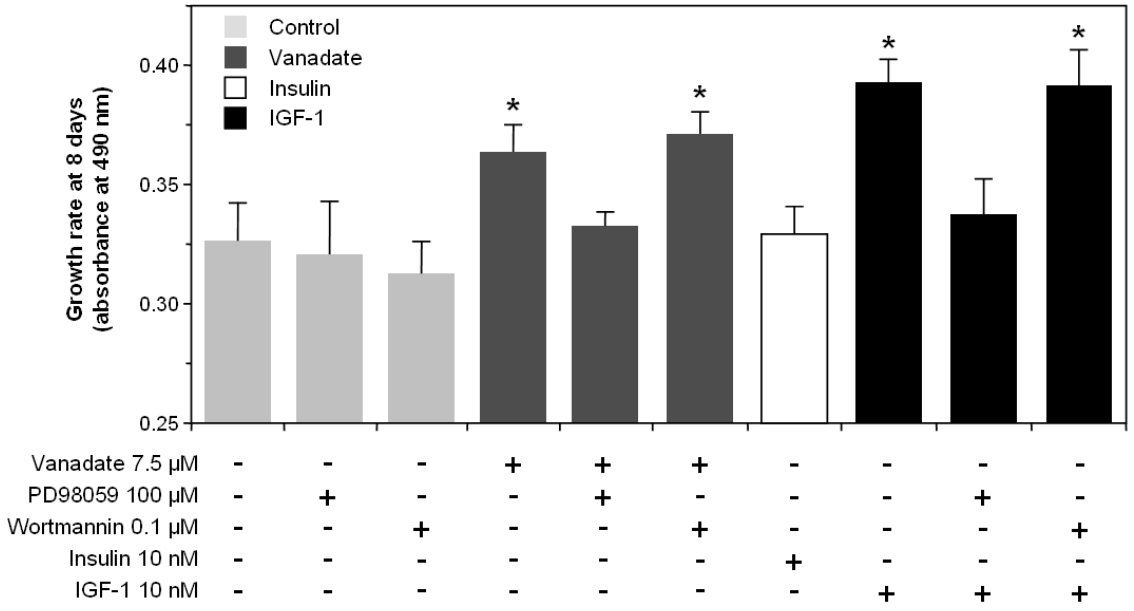

Figure 3.8 – Effect of vanadate, insulin, IGF-1, wortmannin and PD98059 on VSa13 cell proliferation. VSa13 cells were seeded in 96-well plates at 1.5×10^3 cells/well then either left untreated or treated with PD98059, wortmannin, vanadate, insulin or IGF-1, alone or in combinations. Cell proliferation was evaluated after 8 days using MTS assay. Values are the mean of at least three independent experiments. Asterisk indicates values statistically different from their respective control ($P<0.05$; one-way ANOVA).

3.2.3. Vanadate and insulin impair VSa13 ECM mineralization

Vanadate was then tested for its ability to affect cell differentiation using VSa13 cells cultured under mineralizing conditions for 4 weeks. ECM mineralization was evaluated by densitometric analysis of von Kossa staining. VSa13 cells were either treated with 5 µM metavanadate, 5 µM decavanadate, 10 nM insulin and 10 nM IGF-1 separately, or in combination (Figure 3.9). Both metavanadate and decavanadate induced similar effects on ECM mineralization and to a similar extent, therefore only metavanadate results have been reported. Vanadate 7.5 µM concentration was excluded from this experiment due to cytotoxic effects observed after 4 weeks of treatment (data not shown). Insulin and vanadate, but not IGF-1, decreased ECM mineralization (according to ANOVA), although to different extents: 30% and 87.5%, respectively. Our results also indicate that mineral deposition was almost abolished by a combination

of both insulin and vanadate, suggesting that both agents either activate different pathways resulting in anti-mineralogenic effect or, on the contrary, activate the same pathway but through a synergistic effect, e.g. vanadate would potentiate insulin effect.

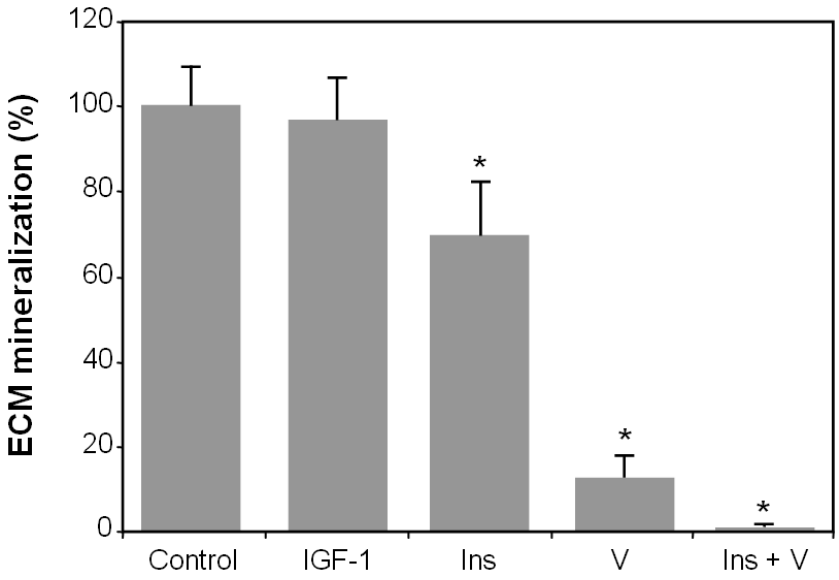

Figure 3.9 - Effect of vanadate, IGF-1 and insulin on ECM mineralization. VSa13 cells were seeded in 24-well plates, grown in DMEM until confluence then treated for mineralization. Mineralizing cultures were subsequently treated with 10 nM IGF-1 (IGF-1), 10 nM insulin (Ins), 5 μM vanadate (V), vanadate and insulin (Ins + V), or left untreated. Mineral deposition was revealed by von Kossa staining and evaluated by densitometric analysis. Values are the mean of at least three independent experiments. Asterisk indicates that values are statistically different in comparison to the respective control ($P<0.05$; one-way ANOVA).

3.2.4. PD98059 and wortmannin block both vanadate and insulin effects on VSa13 ECM mineralization

Wortmannin and PD98059 were then tested for their effect on ECM mineralization of VSa13 cells and for their capacity of reverting vanadate and insulin inhibitory effects. Mineralizing VSa13 cultures were treated for 4 weeks with 0.1 μM wortmannin, 100 μM PD98059, 10 nM IGF-1, 10 nM insulin, and/or 5 μM vanadate, then evaluated for mineralization. As already showed in Figure 3.9, and further demonstrated in Figure 3.10, mineral deposition was increasingly impaired by insulin (1.4 fold), vanadate (8 folds) and almost abolished by a combination of both agents, while not

altered by IGF-1. Interestingly, ECM of PD98059-treated cells, but not that of wortmannin-treated cells, exhibited a significant increase in mineral deposition (3.2 folds) suggesting an antagonist role of MAPK pathway in mineralization (Figure 3.10). This role was further confirmed by the reversion (100% and 72.5%, respectively) of insulin and vanadate anti-mineralogenic effect by PD98059. Surprisingly, wortmannin also reverted (100 % and 57.5%, respectively) insulin and vanadate anti-mineralogenic effect, suggesting also a role for PI-3K pathway in mineralization. As expected, impairment of mineralization by the combined effect of insulin and vanadate was reverted to an extent similar to that observed for vanadate alone. These results suggest that both MAPK and PI-3K pathways mediate vanadate and insulin anti-mineralogenic effect. However, vanadate anti-mineralogenic action apparently involved other mechanisms of action, given that neither PD98059 nor wortmannin completely revert its effects. ALP and collagen are important actors of ECM mineralization [94] and the action of vanadate on their activity and synthesis, respectively, will be evaluated in the next section.

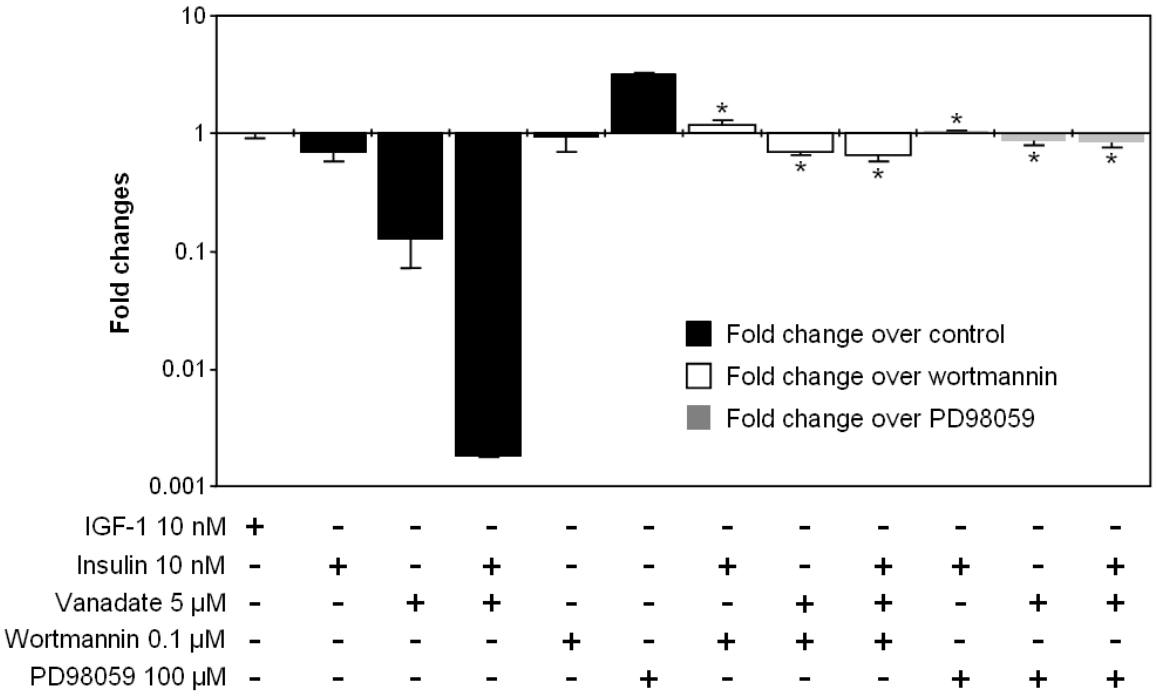

Figure 3.10 – Effect of IGF-1, vanadate, insulin, wortmannin and PD98059 on VSa13 ECM mineralization. VSa13 cells were seeded in 24-well plates at 2×10^4 cells/well, grown until confluence then treated for mineralization. Mineralizing cultures were then left untreated or treated with IGF-1, insulin, vanadate, PD98059, or wortmannin, alone or in combinations. Mineral deposition was revealed after 4 weeks by von Kossa staining and evaluated by densitometry analysis. Mineralization data are presented as the ratio of individual values with their respective control (non-treated, treated with wortmannin and treated with PD98059). Values are the mean of at least three independent experiments. Asterisk indicates values statistically different from their respective control ($P<0.05$; one-way ANOVA).

3.2.5. ALP activity is inhibited while collagen content is increased by micromolar concentrations of vanadate

ALP activity, a marker for osteoblast differentiation shown to be crucial in mineralization [94], was determined in mineralizing cell cultures treated with 5 µM vanadate and/or 10 nM insulin, and shown to increase by 40% following ECM mineralization, while activity remained similar to non-mineralizing control cells upon vanadate treatment (Figure 3.11, left panel). In similar experiments, collagen, another crucial protein in mineralization [94], was shown to increase by 57% in ECM

mineralized cultures and by an additional 17% when those cultures were also treated with vanadate (Figure 3.12). The stimulation of both ALP activity and collagen production in mineralized cultures is consistent with their role in mineralization mechanisms. The inability of insulin to affect ALP activity and collagen production suggests that vanadate action occurs through an insulin receptor-independent manner. ALP activity was then measured in cellular extracts of mineralized cultures (4 weeks) in the presence of increasing concentrations of vanadate: activity was stimulated at low concentration (5 µM) while strongly inhibited at higher concentrations (from 25 to 500 µM) of vanadate (Figure 3.11, right panel). Based on the capacity of VSa13 cells to accumulate vanadate (Figure 3.5) and on ALP direct inhibition only at higher vanadate concentrations (above 5 µM; Figure 3.11, right panel), it is likely that the mechanism for ALP activity down-regulation during mineralization (Figure 3.11, left panel) also involves higher vanadate concentrations (*i.e.* above 5 µM).

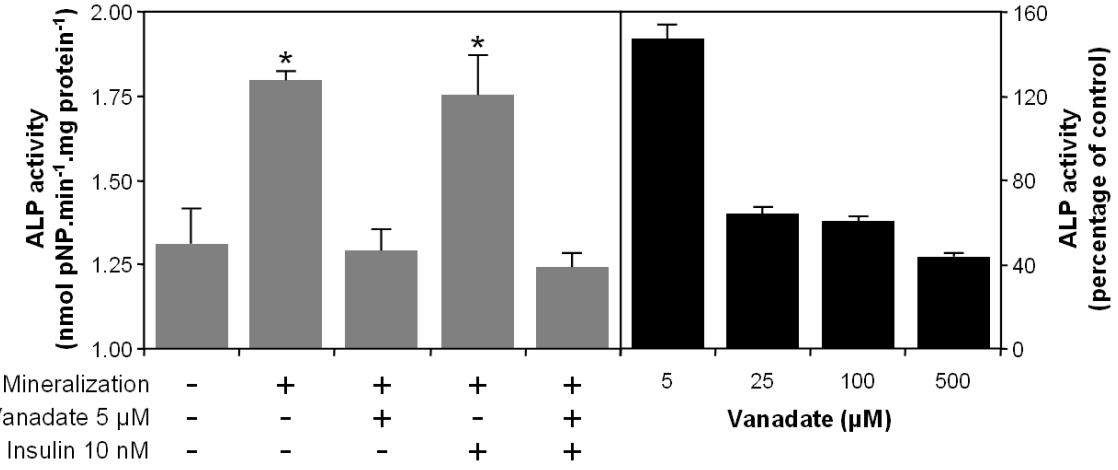

Figure 3.11 – ALP activity in mineralized cell cultures treated with insulin and vanadate. VSa13 cells were seeded in 24-well plates at 2×10^4 cells/well, grown until confluence then treated for mineralization. Mineralizing cultures were left untreated or treated with insulin and/or vanadate. ALP activity was measured in cell extracts after 4 weeks of treatment (left panel) or assayed in the presence of increasing concentration of vanadate (right panel). ALP activity was always measure in times lower than 5 minutes. Values are the mean of at least three independent experiments. Asterisk indicates values statistically different from their respective control ($P<0.05$; one-way ANOVA).

On the contrary, the increase of total collagen content in vanadate-treated mineralized cultures (most probably the result of increased type X collagen synthesis as observed in differentiated ATDC5 chondrocytes cells [91,93]) can hardly explain the decrease of ECM mineralization since increased collagen production is rather likely to benefit ECM mineralization.

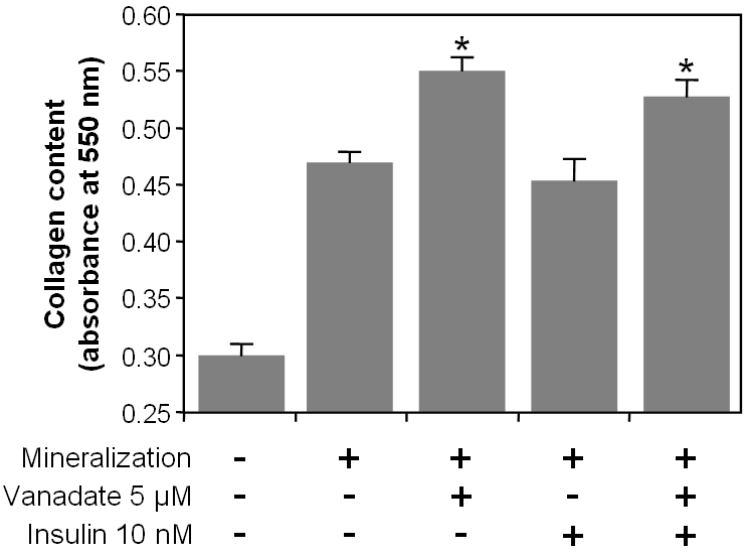

Figure 3.12 – Collagen content in mineralized cell cultures treated with insulin and/or vanadate. VSa13 cells were seeded in 24-well plates at 2×10^4 cells/well, grown until confluence then treated for mineralization. Mineralizing cultures were left untreated or treated with insulin and/or vanadate. Total collagen content was determined after 4 weeks of treatment through Sirius red staining. Values are the mean of at least three independent experiments. Asterisk indicates values statistically different from their respective control ($P<0.05$; one-way ANOVA).

3.3. Insulin-like effects on VSa16 cells

3.3.1. Proliferation of VSa16 cells is stimulated by IGF-1 but not by vanadate

Dividing cultures of VSa16 cells were treated for 8 days with 10 nM insulin, 10 nM IGF-1, 7.5 µM vanadate or left untreated, then cell proliferation was evaluated using the MTS assay and compared to that of VSa13 in similar experiments. Results illustrated in Figure 3.13 showed that cell proliferation of both cell lines was stimulated

by IGF-1, although to a different extent (20% over control in VSa13 cells and 11% over control in VSa16 cells), while unaltered by insulin. This observation suggests that, unlike insulin, IGF-1 exhibits strong mitogenic activity in fish bone-derived cells. Vanadate, in contrast to what has been observed for VSa13 cells, did not stimulate VSa16 cell proliferation (Figure 3.13), suggesting that vanadate mitogenic activity in fish bone-derived cells is cell type specific.

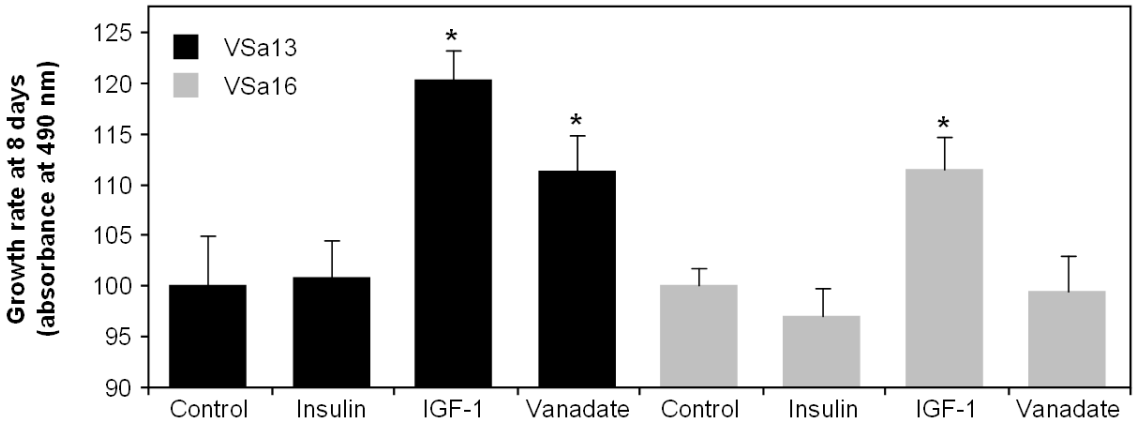

Figure 3.13 - Effect of vanadate, insulin and IGF-1 on VSa13 and VSa16 cells proliferation. Cells were seeded in 96-well plates at 1.5×10^3 cell/well then treated either with 10 nM insulin, 10 nM IGF-1 or 7.5 µM vanadate. Cell proliferation was evaluated after 8 days using MTS assay. Values are the mean of at least three independent experiments. Asterisk indicates values statistically different from their respective control ($P<0.05$; one-way ANOVA).

3.3.2. Vanadate and IGF-1 impair ECM mineralization in VSa16 cells

VSa16 cells were cultured under mineralizing conditions for 4 weeks and treated with 5 µM metavanadate, 10 nM insulin or 10 nM IGF-1. While insulin, but not IGF-1, significantly (ANOVA analysis) inhibited ECM mineralization in VSa13 cells, IGF-1, but not insulin, inhibited ECM mineralization in VSa16 cultures to a similar extent (*i.e.* 27% inhibition; figure 3.14). Altogether, these results suggest similar roles for insulin and IGF-1 in distinct bone-derived cells (osteoblast *versus* chondrocyte). Finally, vanadate was also shown to promote similar effects in both VSa13 and VSa16

cells, *i.e.* strong inhibition (88% and 66% of control mineralizing cells, respectively) without affecting cell viability (data not shown), respectively. Our results suggest that vanadate effects in involve similar mechanisms as in VSa13 cells, *i.e.* signalling pathway(s) activated by either insulin or IGF-1, or ALP activity inhibition.

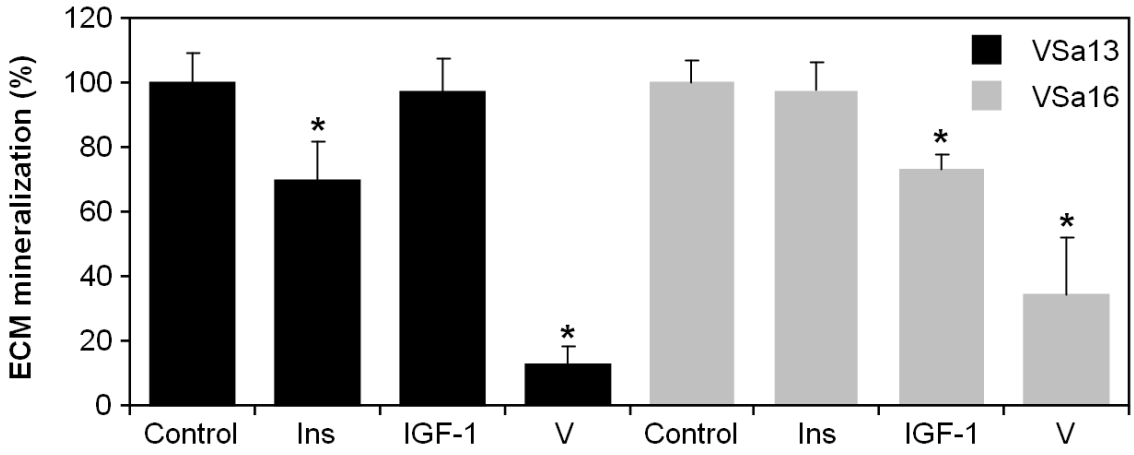

Figure 3.14 - Effect of vanadate, IGF-1 and insulin on ECM mineralization of VSa13 and VSa16 cells. Cells were seeded in 24-well plates, grown in DMEM until confluence then treated for mineralization. Mineralizing cultures were subsequently treated with 10 nM insulin (Ins), 10 nM IGF-1 (IGF-1), 5 μM vanadate (V), or left untreated. N.D. means non-detected. Mineral deposition was revealed by von Kossa staining and evaluated by densitometric analysis. Values are the mean of at least three independent experiments. Asterisk indicates that values are statistically different in comparison to the respective control ($P<0.05$; one-way ANOVA).

3.4. Alternative splicing of seabream IGF-1 transcript: Distribution and role of the splicing variants

3.4.1. Cloning of seabream IGF-1 transcripts

A 155 bp fragment was first amplified by 2 rounds of RACE-PCR using Marathon primers MarAP1 and MarAP2 combined with reverse primer IGF-1RV1 (see Table AII.1 of Appendix II), designed according to the partial sequence published by Duguay and colleagues [152]. This fragment was sequenced, identified as the 5' end of IGF-1 cDNA, and then used to design the forward specific primer IGF-1FW1 (see

Table AII.1 of Appendix II). Using this primer and Marathon primer MarAP1, two fragments of 2204 and 2285 bp were amplified by PCR. Both fragments were sequenced and identified as full-length IGF-1 cDNAs, then termed IGF-1a (longer transcript; GenBank accession number AY996779) and IGF-1b (shorter transcript; GenBank accession number EF688015). The comparison of both sequences identified a region of 81 bp present in IGF-1a but absent in IGF-1b (Figure 3.15) and localized between positions 492 bp and 572 bp in the sequence coding for IGF-1 E domain. Specific primers were designed in order to detect additional IGF-1 transcripts. Using primer sets IGF-1FW1 / MarAP1 and IGF-1FW2 / IGF-1RV2 (see Table AII.1 in appendix II), a third fragment was amplified, IGF-1c (GenBank accession number EF688016). The comparison of IGF-1c sequence with that of IGF-1a identified a region of 117 bp present only in IGF-1a (Figure 3.15) and localized between positions 492 bp and 608 bp in the sequence encoding IGF-1 E domain. No polyadenylation signal has been clearly identified but a putative one has been underlined in Figure 3.13. All transcripts identified in this study as seabream IGF-1 encode peptides containing the six canonical domains [153] but exhibiting different sizes for the E domain: 74, 47 and 35 aa for IGF-1a, 1b and 1c, respectively.

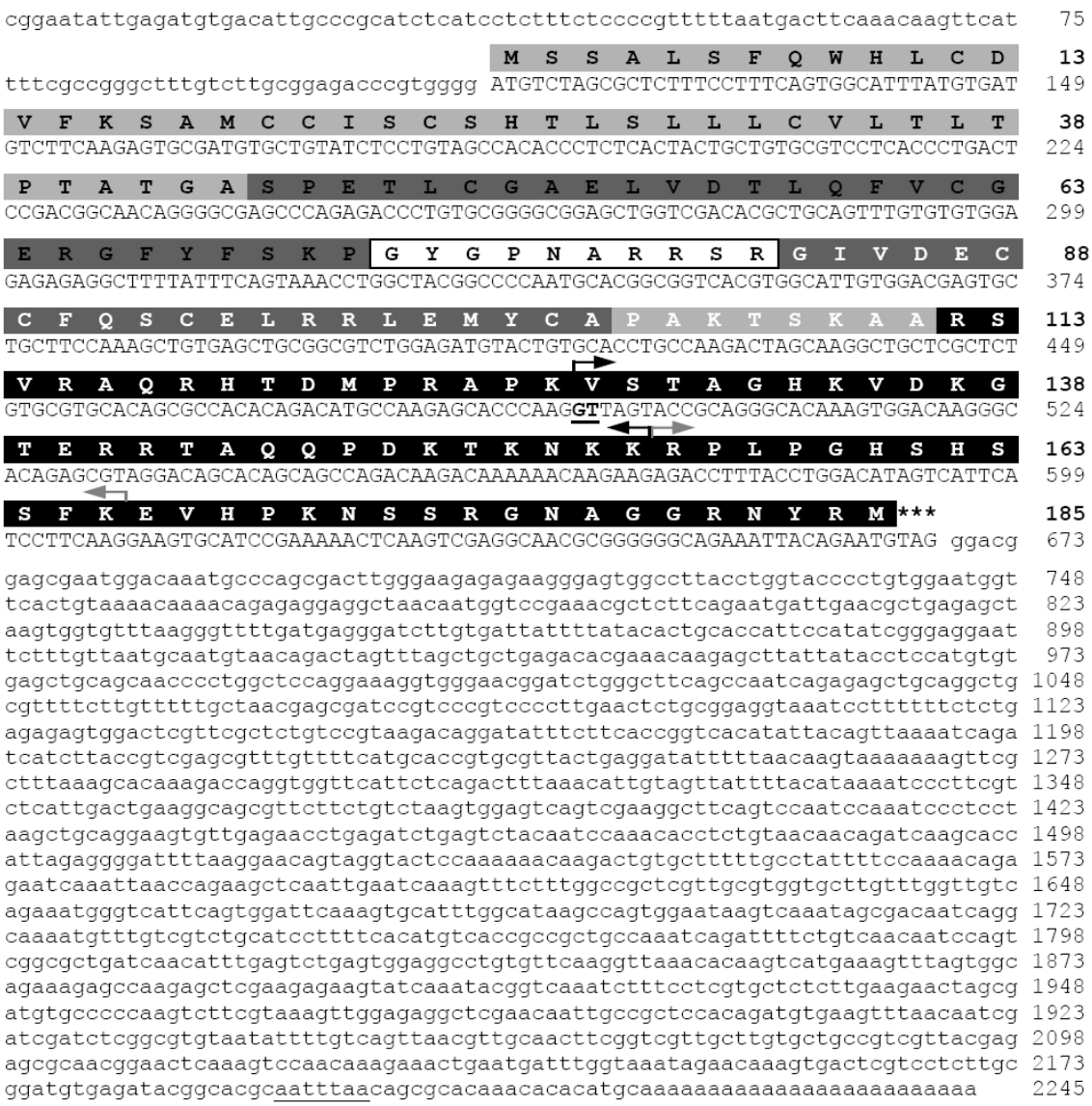

Figure 3.15 - Seabream IGF-1 full-length cDNA and deduced amino acid sequences. Light grey box and black letters indicate the signal peptide; dark grey box and black letters indicate the B domain; dark grey box and white letters indicate the C domain; white box indicates the A domain; light grey box and white letters indicate the D domain; black box and white letters indicate the E domain; asterisks indicate the stop codon; black arrows set the boundaries of the 81-bp alternatively spliced region present in IGF-1a transcript but absent in transcripts IGF-1b and IGF-1c (alternative GT donor splice site is bold-underlined); grey arrows set the boundaries of the 36-bp alternatively spliced region present in transcripts IGF-1a and IGF-1b but absent in transcript IGF-1c; putative polyadenylation signal sequence is underlined.

3.4.2. IGF-1 gene occurrence and structure

In order to determine whether previously identified transcripts originated from alternative splicing of a single IGF-1 gene or from several genes, seabream genome was analyzed by Southern blot. Probe was designed within putative exon 3 (determined by comparison of seabream cDNA with available IGF-1 genes from zebrafish, salmon and flounder), which is present in all 3 transcripts and does not contain restriction sites for the endonucleases used to digest DNA. A single signal was detected in each lane of the hybridized blot (Figure 3.16), suggesting the presence of a single copy of IGF-1 gene in seabream genome and consequently that the various IGF-1 transcripts obtained correspond to alternatively spliced variants.

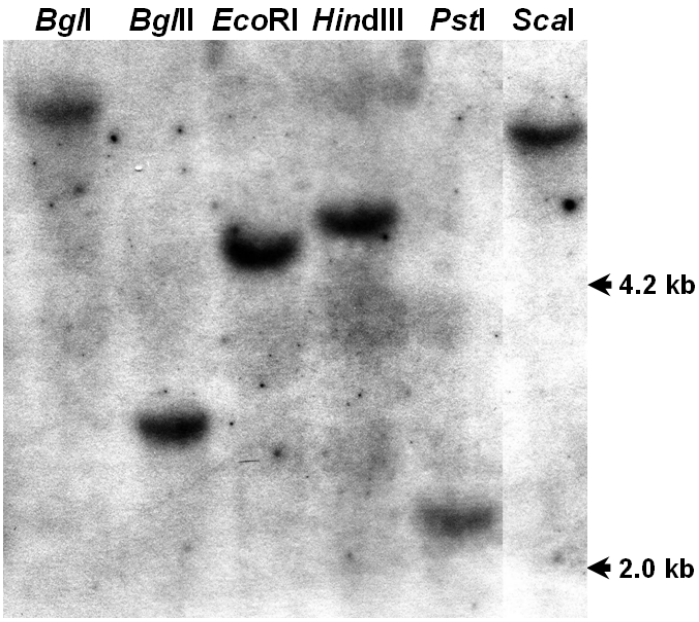

Figure 3.16 - Southern blot analysis of seabream genomic DNA. A 199-bp radiolabeled probe specific for exon 3 was used for hybridization; restriction enzymes used to digest genomic DNA (*Bgl*I, *Bgl*II, *Eco*RI, *Hin*dIII, *Pst*I and *Sca*I) are indicated above each lane; DNA marker sizes are indicated in the right.

Using primers IGF-1FW3 and IGF-1FW4, designed immediately upstream of alternatively spliced regions, in combination with GWAP1 and GWAP2 primers,

respectively (see Table AII.1 of Appendix II), a genomic fragment of approximately 4600-bp was amplified, sequenced and identified as partial seabream IGF-1 gene (GenBank accession number DQ118098). This genomic fragment was compared with each of the transcripts using the Spidey mRNA-to-genomic alignment tool at NCBI, allowing the reconstruction of partial IGF-1 gene structure (Figure 3.17). Exon 3 (partial), exon 4 and exon 5 (containing 3'UTR) were identified, coding for domains A (partial), D and E, respectively (Figure 3.17 A).

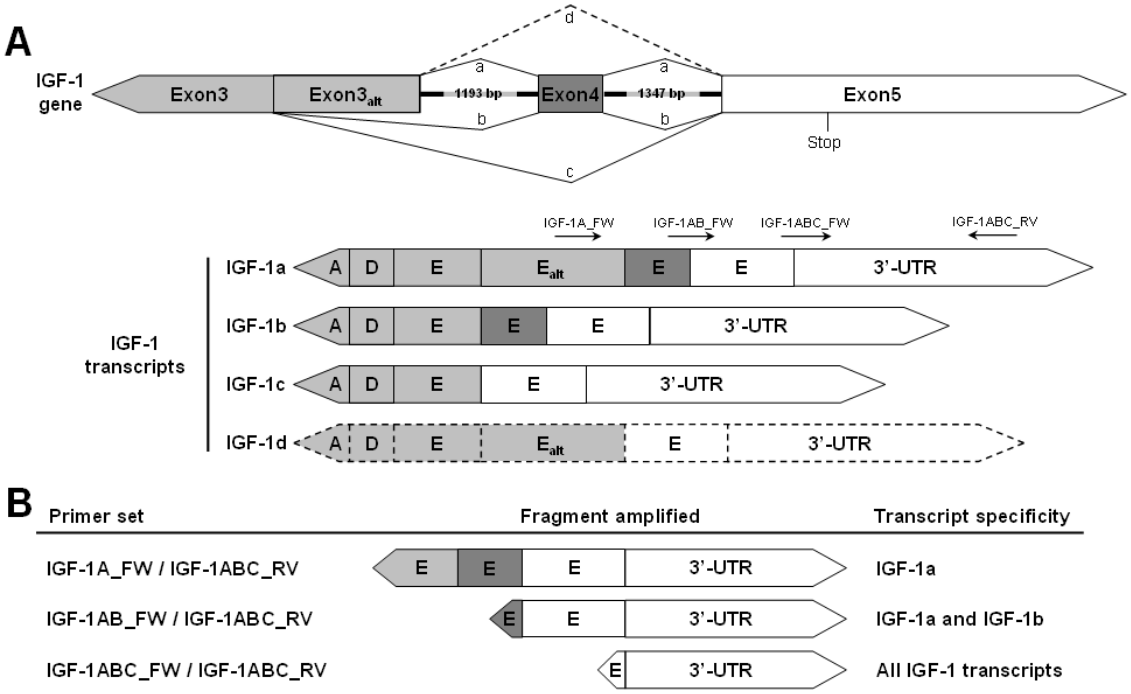

Figure 3.17 - Schematic representation of seabream partial IGF-1 gene and related cDNAs. (**A**) Exons and domains are represented by boxes; introns are represented by solid thick lines; light grey boxes indicate exon 3 and related domains, dark grey boxes indicate exon 4 and related domains and white boxes indicate exon 5 and related domains; boxes with dashed lines indicate putative alternative transcripts; alternative splicing events in exon 3 and exon 4 are represented by solid and dashed lines; primers used for *qPCR* amplification of alternative transcripts are indicated above IGF-1a cDNA; (**B**) *qPCR* fragments and primers used to amplify them; first primer set is specific for IGF-1a transcript and amplifies a 258-bp fragment; second primer set is specific for IGF-1a and IGF-1b transcripts and amplifies a 201-bp fragment; third primer set amplifies a 134-bp fragment common to all three transcripts.

Alternatively spliced regions were localized within exon 3 and exon 4 and shown to be removed through 2 different splicing mechanisms: (i) alternative donor site (two functional GT donor sites were localized 81 bp from each other) at the 3' extremity of exon 3 and (ii) alternative skipping of the entire exon 4. In all cases, the phase of intron insertion was conserved (phase 0; [154]) thus maintaining the same reading frame.

3.4.3. Expression of IGF-1 transcripts during development and in adult seabream

Relative expression of alternatively spliced transcripts was measured by *qPCR* in developing and adult seabream using three sets of variant-specific primers (see Table AII.2 of Appendix II and Figure 3.17): set 1 (IGF-1ABC) to amplify all isoforms, set 2 (IGF-1A) to amplify IGF-1a, and set 3 (IGF-1AB) to amplify simultaneously IGF-1a and IGF-1b (Figure 3.17 B). IGF-1b relative gene expression was determined by subtracting values from set 2 to those from set 3 while relative levels of IGF-1c gene expression were determined by subtracting values from set 3 to those of set 1 (Figures 3.18 and 3.18). IGF-1c was shown to be expressed at basal levels in unfertilized eggs and during early development (embryo) while strongly up-regulated (around 30-fold) in hatched larvae. Levels of IGF-1c expression remained high in juvenile fish. IGF-1a transcript was first detected in larvae at 20 DAH, exhibiting intermediate levels of expression that remained stable throughout larval and juvenile development. IGF-1b transcript was detected soon after hatching but levels remained low throughout larval and juvenile development. All 3 transcripts clearly exhibited different patterns of gene expression during development (different onset and extent), suggesting different roles during this particular physiological stage in fish.

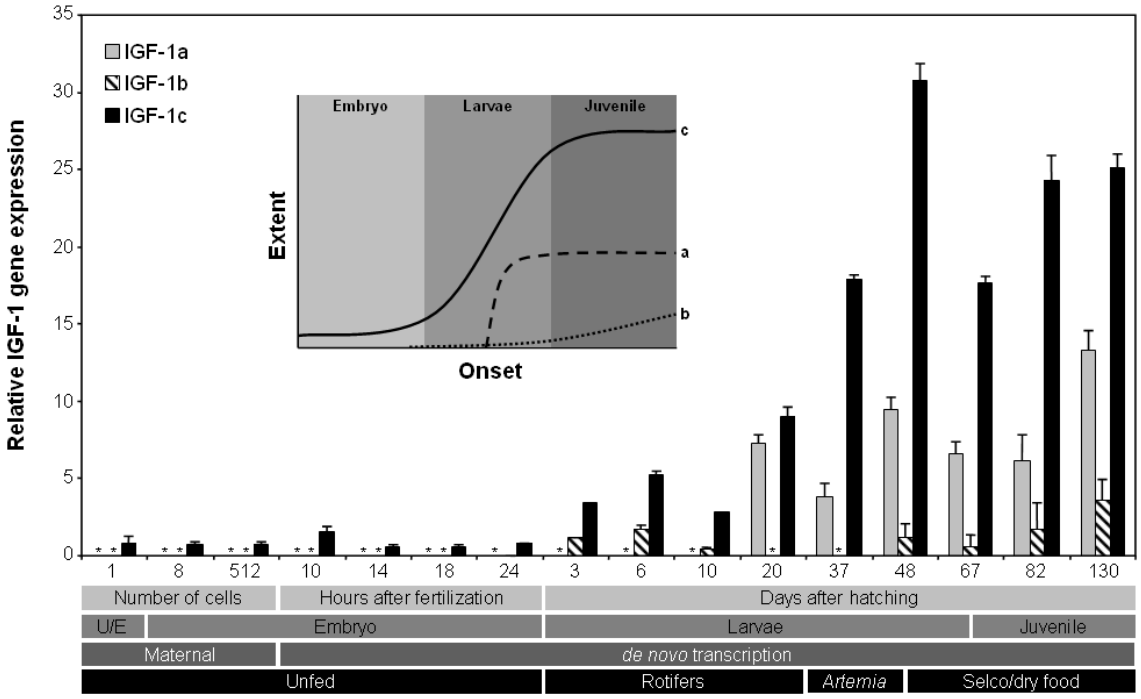

Figure 3.18 - Relative IGF-1 gene expression during seabream development measured by *qPCR*. IGF-1 gene expression was normalized using housekeeping gene β-actin; asterisks indicate that transcripts were not detected; U/E means unfertilized eggs; values are the mean of at least three independent *qPCR* experiments; insert illustrates the onset and extent of gene expression for each IGF-1 transcripts throughout seabream development.

Differences in transcript levels were also observed in adult tissues. IGF-1c was by far the most expressed transcript in all adult tissues, exhibiting highest levels of expression in liver, adipose tissue and pancreas, and moderate levels in brain, gall bladder, spleen and most of the calcified tissues, including poorly calcified branchial arches and gills. Both IGF-1a and IGF-1b were poorly expressed in most tissues analyzed, with the exception of liver. While high expression of IGF-1c transcripts in liver, adipose and pancreas is probably related to a systemic mode of action, lower levels of all transcripts in the remaining tissues could be associated to autocrine/paracrine regulation.

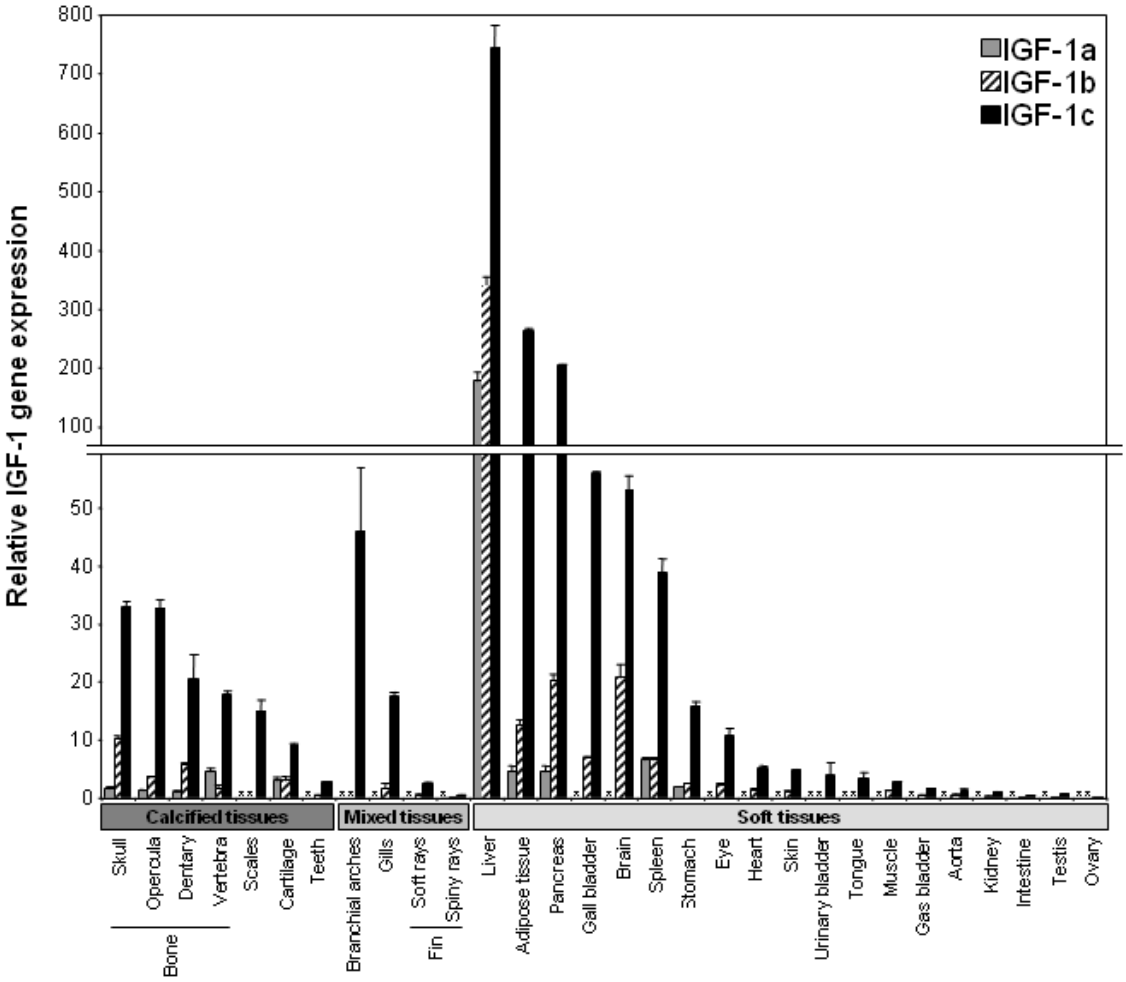

Figure 3.19 - Relative IGF-1 gene expression in seabream tissues measured by *qPCR*. IGF-1 gene expression was normalized using housekeeping gene RPL27a; asterisks indicate that transcripts were not detected; values are the mean of at least three independent *qPCR* experiments.

3.4.4. IGF-1 alternative splicing in vertebrates

In order to understand the occurrence of IGF-1 variants in seabream, orthologous sequences have been searched within GenBank sequence data base using Blast facilities at NCBI. Positive search results were considered to be members of the IGF-1 family if they showed significant sequence similarity to any of the previously identified members and if this similarity extended throughout the protein. Our search identified various sequences previously identified as IGF-1 and ESTs with similarities to previously characterized sequences, from which we could identify or reconstruct 52 IGF-1-related

cDNAs (Figure AIV.3 of Appendix IV). A total of 154 complete or nearly complete sequences (all with a complete E domain) have been identified from 41 species representing most classes of vertebrates (*i.e.* mammals, birds, amphibians and bony fish). One was identified in a cartilaginous fish (*Squalus acanthias*) but the homology within the E domain was weak making the identification dubious. Consequently, these sequences were not included in our analysis of alternative splicing in vertebrate IGF-1 gene. While sequences of all available bony fish, birds and amphibians were analyzed, only sequences from human and mouse were processed for mammals since almost nearly complete sets of sequences exist for both species. Our analysis identified 4 alternatively spliced IGF-1 transcripts in bony fish: three variants exhibited a splicing identical to those found in seabream and one was differently spliced (only exon 4 was alternatively spliced) and termed IGF-1d according to the nomenclature used in this study (Figure 3.17). A single transcript, spliced as seabream IGF-1c, was identified in birds and amphibians. Finally, three IGF-1 variants were identified in mammals, one spliced as seabream IGF-1c (IGF-1-Ea), and two variants specific to this taxonomic group: IGF-1-Eb, which includes exons 4 and 5 in the E domain, and IGF-1-Ec, which includes exons 4, partial 5 and 6 [155].

Analysis of the distribution of IGF-1 variants revealed that (i) IGF-1a transcript was specific of the Acanthopterygii and Protacanthopterygii, (ii) IGF-1b transcript was mainly found in Ostariophysi (also observed in few Acanthopterygii and Protacanthopterygii, (iii) IGF-1c was identified only in seabream and Salmonidae to date, and (iv) IGF-1d, the rarest variant, was exclusively found in Salmonidae (*Oncorhynchus kisutch* and *Oncorhynchus mykiss*). In general, only 6 Osteichthyes species expressed multiple IGF-1 variants, and the four fish-related transcripts were never simultaneously expressed, although some Salmonidae, if not all, are likely to have

the 4 of them. IGF-1c/Ea was shown to be the only variant common to all vertebrate taxa (Figure 3.20). On the contrary, other variants were shown to be specific for a taxon: IGF-1a, IGF-1b and IGF-1d were only observed in bony fish, and IGF-1-Eb and IGF-1-Ec were found exclusively in mammals. IGF-1c was not only the common variant in all analyzed classes, but also shown to be the only one present in amphibians and birds. IGF-1c/Ea pro-peptide is likely to play systemic role in fish as shown in mammals (or would have acquired this role throughout evolution), while other pro-peptides (*i.e.* 1a, 1b, 1d, Eb and Ec) would play specific and local roles that remain to be explored.

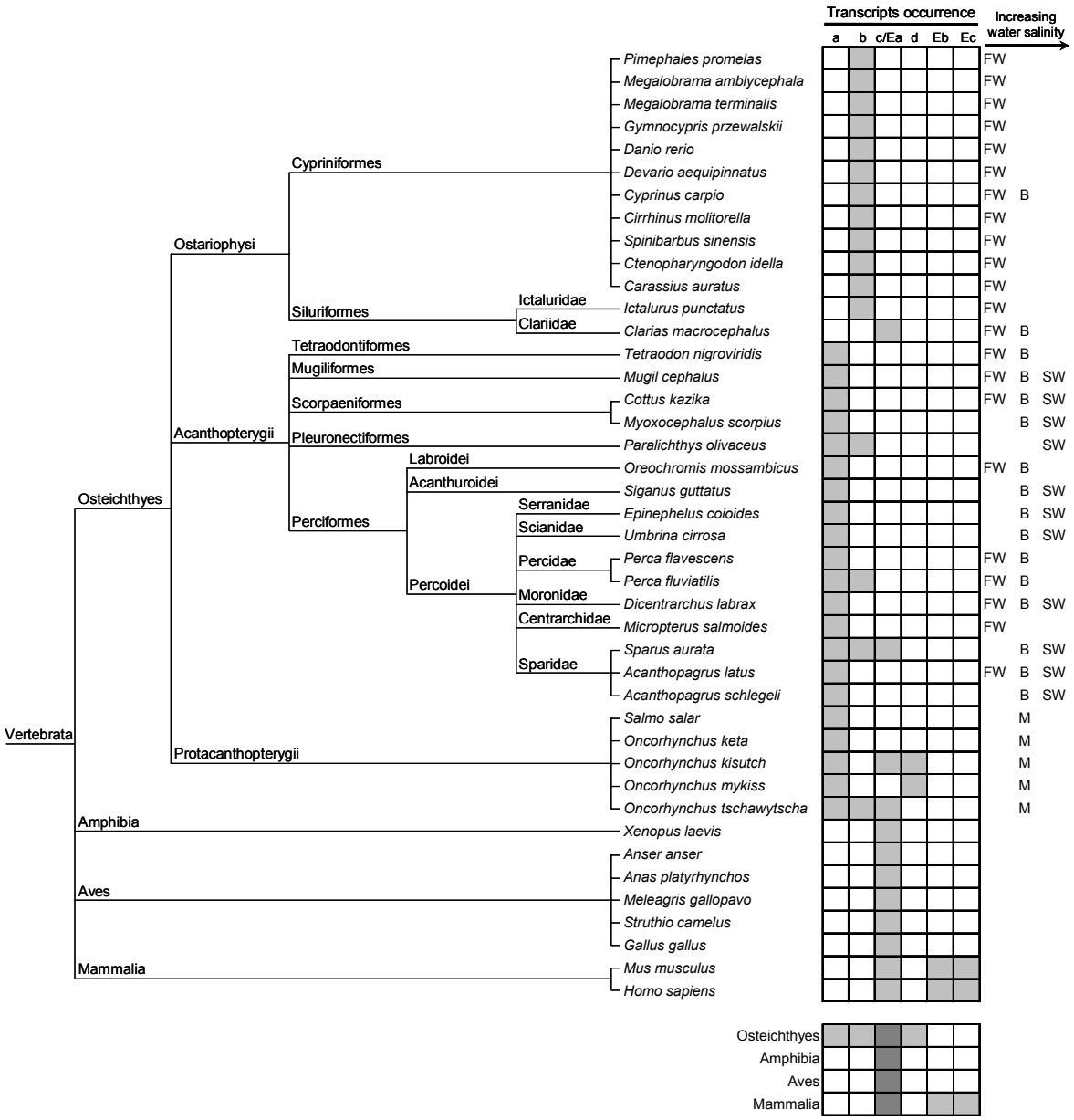

Figure 3.20 - Species and vertebrate distribution of IGF-1 alternatively spliced transcripts. Taxonomic tree of represented species; taxonomic data were retrieved (10-27-2006) from the Integrated Taxonomic Information System at www.itis.usda.gov and fish salinity environment data were retrieved from FishBase website at www.fishbase.org; *a*, b, c and d indicate IGF-1a, IGF-1b, IGF-1c and IGF-1d transcripts, respectively; Eb and Ec indicate the mammalian specific IGF-1 transcripts; grey boxes indicate the presence of a transcript in a species below, table indicates the distribution of IGF-1 transcripts in vertebrates taxons.

Chapter IV

4. Discussion

4.1. Metavanadate and decavanadate differently affect VSa13 cells

The effects of vanadium on bone biology have been extensively studied in mammalian *in vivo* and *in vitro* systems [50,117-119,122,156], but, to our knowledge, no studies have been performed using bone-derived systems of aquatic vertebrate origin. One of the goals of this study was to analyze, for the first time, the effects of different vanadate oligomers on the proliferation and differentiation/mineralization of fish bone-derived cell lines since the composition of vanadate solutions is very sensitive to vanadate concentration, pH, buffer, and other compounds used in biochemical studies [53,55,57,64,65,157]. Therefore, it was of primary importance to precisely characterize the species that can interact with a system before attempting to understand the effects promoted by vanadate solutions. Unlike metavanadate, containing several oxovanadates, decavanadate solutions contain mainly decameric vanadate species (V10). However, V10 is unstable in solution at pH 7, and decomposes into monomeric vanadate with half-life times of approximately 2 hours [53]. In this regard, species present in decavanadate-DMEM solutions have been characterized and its effects on VSa13 cells compared with those of metavanadate.

4.1.1. Differential effect of monomeric and decameric vanadate species on VSa13 cells upon short exposures

^{51}V NMR spectroscopy analysis of 1 and 5 mM vanadate solutions in DMEM, at pH 7.0, revealed the presence of: (i) V1, V2, V4 and V5 oligomers in metavanadate solution; and (ii) V1 and V10 oligomers in decavanadate solution. According to this analysis, lower metavanadate concentrations favour the formation of V1 species, while

the proportion of V1:V10 species are maintained upon decavanadate solution dilution. However, broadening of monomeric species NMR signal in DMEM (from 80 Hz in previous studies [65] to 270 Hz) indicated putative interactions with compounds present in medium, such as glucose (25 mM) and piruvate (1 mM), or even interactions with several proteins also present in medium, as it has been proposed in previous studies [53,65]. The half-life of decameric species decomposition in DMEM was approximately 150 minutes, a result which was in agreement with other decomposition kinetics determined in other systems [53], indicating that short exposure (less than 2.5 h) of VSa13 cells to decavanadate solutions would mainly result in effects caused by decameric species while long exposure (more than 2.5 h) would mainly result in effects caused by newly formed monomeric species. It was consequently not surprising to observe similar effects on cell proliferation and differentiation upon long exposure of decavanadate and metavanadate. On the contrary, short exposure of VSa13 cells to decavanadate was shown to be more toxic than for metavanadate. Considering that decavanadate solution contains 10 times less molecules (particularly in shorter exposure times, in which decameric species are predominant) than metavanadate (in which monomeric species are predominant), short-term toxicity of decavanadate is even more remarkable. This result is consistent with previous observations that decavanadate and metavanadate produce different oxidative stress levels in cardiac muscle in toadfish and gilthead seabream [54,56] and interact differently *in vitro* with specific proteins such as myosin and sarcoplasmic reticulum Ca^{2+}-ATPase [53,65,158].

Atomic absorption spectrometry analysis has revealed that vanadium differently accumulates in extracts from VSa13 cells treated with metavanadate or decavanadate solutions (less accumulation of vanadium after 1 and 2 h in decavanadate-treated cells), suggesting that the uptake mechanism for decameric species is probably inexistent or

less efficient. Although cellular accumulation of metavanadate has been previously demonstrated in mammalian systems, *e.g.* bovine kidney and Caco-2 cells [159,160], this process has never been related to the oligomerization of vanadium species until now. We propose that repeated exposures of the cells to vanadate may result in increasing intracellular accumulation of vanadium, possibly reaching concentrations toxic for cellular mechanisms.

4.2. Vanadate insulin-like effects on VSa13 cells

4.2.1. Insulin-like effects on VSa13 cells proliferation and ECM mineralization

Vanadate (*i.e.* metavanadate and decavanadate) stimulates VSa13 cell proliferation while inhibiting differentiation/mineralization. Similar proliferative effects have been reported in mammalian bone-derived cell lines and associated with the activation of IR [122]. The absence of proliferative effect in VSa13 cells upon insulin treatment suggests that vanadate effect is probably not mediated through IR in fish cells, but possibly through IGF-1 receptor/signalling in agreement with the observed stimulation of VSa13 cell proliferation by IGF-1. Alternatively, vanadate stimulation of VSa13 cells growth could also be mediated by other TKR, such as cytosolic TKR, previously proposed as a mediator of vanadate metabolic effects in rat adipocytes [75,161] or PDGF receptors [122]. Insulin-like effects on VSa13 cell differentiation/ECM mineralization were inhibitory: ECM mineralization was mildly reduced (~30%) by insulin, strongly impaired (~88%) by vanadate (regardless of its oligomerization - monomeric or decameric), and nearly abolished when both insulin and vanadate were present. Inability of IGF-1 to regulate mineralization is likely to be related to the

absence of its receptor during this process. Recently, we have analyzed the levels of gene expression in VSa13 cells undergoing mineralization using a microarray containing approx. 20,000 seabream genes, including IGF-1 receptor (but not insulin receptor). Preliminary data indicated the presence of IGF-1R in proliferating cells and its absence in mineralizing cells, which further supports our hypothesis. Nevertheless, regarding the effect of vanadate, results are not in agreement with those obtained in mammalian bone-derived cells, where it was shown to stimulate ECM mineralization [122,133]. The reasons for this discrepancy are not clear. However, differences in vanadate effects could be species-related (mammalian *versus* fish) and/or cell type-related (studies in mammalian were developed in osteoblast-like cell lines while fish VSa13 is a chondrocyte-like cell lines)

4.2.2. MAPK pathway transduces vanadate stimulation of cell proliferation

Prolonged exposure of VSa13 cells to low levels of metavanadate and decavanadate stimulated cell proliferation, in agreement with recent reports on the effect of ortovanadate and vanadium derivatives in mammalian bone-derived cell cultures MC3T3E1 and UMR106 [127-129,162], where vanadium effect was attributed to its ability to increase phosphotyrosine protein levels and to inhibit PTPase, thus regulating growth signalling pathways. Reversion of vanadate and IGF-1 proliferative effect by PD98059 demonstrated the involvement of the MAPK pathway in these mechanisms. Similar observations in mammalian osteoblast-like cell lines (*i.e.* MC3T3E1 and UMR106) [132,133], suggest a conservation of mechanisms of action throughout evolution and across bone cell types. Similar mechanisms (*i.e.* a key role of MAPK pathway in proliferative effect of IGF-1) have also been recently reported in the mouse chondrocyte ATDC5 cell line [108]. We propose on the basis of these results and those

reported in this study, a mechanism involving MAPK pathway that would regulate chondrocyte proliferation and also transduce vanadate effect (Figure 4.1).

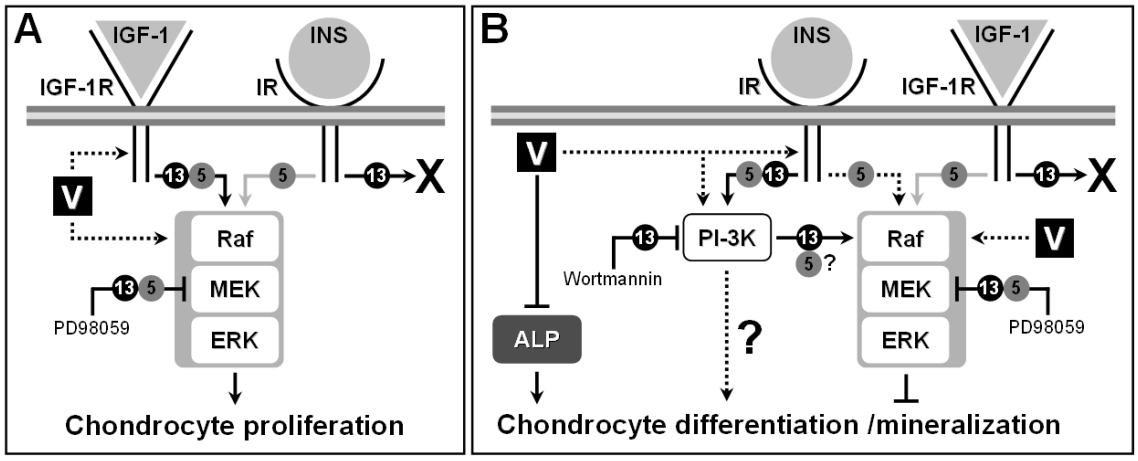

Figure 4.1 - Putative mechanisms of action for insulin, IGF-1 and vanadate in vertebrate chondrocyte cells. Circled 5 and 13 indicate pathways related to ATDC5 and VSa13 cell lines, respectively. Black, gray and dashed arrows indicate activated, moderately activated and putatively activated pathways, respectively. **X** indicates an absence of effect. **V**, vanadate. Raf, MEK and ERK are intermediates in the MAPK pathway.

4.2.3. PI-3K\Ras\ERK pathway mediates insulin and vanadate impairment of VSa13 ECM mineralization

The similarity in the anti-mineralogenic effects triggered by vanadate and insulin suggests that vanadate effect may occur through IR and/or signalling pathway, on the contrary to what has been proposed for its proliferative effect (*i.e.* involvement of IGF-1R and/or signalling pathway). The reversion of both insulin and vanadate effect by both PD98059 and wortmannin suggest a complex mechanism involving 2 signalling pathways, those of PI-3K and MAPK. We proposed, in agreement with recent results obtained in mouse MC3T3-E1 cells [163], that PI-3K\Ras\ERK pathway (a combination of MAPK and PI-3K pathways) may regulate VSa13 cell differentiation/ECM mineralization. We also propose, in agreement with recent results obtained in mouse ATDC5 chondrocyte cells [107,108], a mechanism involving PI-3K\Ras\ERK pathway

that would regulate chondrocyte differentiation/mineralization and transduce vanadate effect (Figure 4.1B)

4.2.3. Vanadate affects ECM mineralization through inhibition of ALP activity

Incomplete reversion of vanadate anti-mineralogenic effect by both PD98059 and wortmannin suggested that other differentiation/ECM mineralization-related mechanisms are affected by vanadate. ALP, by cleaving pyrophosphate, an inhibitor of ECM mineralization [93], and collagen, an essential structural component of ECM [94] are targets of choice for vanadate action. While vanadate treatments resulted in decreased ALP activity and increased collagen synthesis, insulin was unable to affect neither ALP nor collagen, suggesting that vanadate action on these two markers occurs through an IR-independent manner. We propose that vanadate not only inhibits ECM mineralization by interfering with intracellular Pi-3K/Ras/Erk signalling pathway, but also by interfering with ALP activity and pyrophosphate cleavage. Similar results, *i.e.* inhibition of ALP activity and stimulation of collagen synthesis by vanadate, have been reported in chicken [123] and mouse [117,125,133] bone-derived systems and we propose the conservation of these mechanisms throughout evolution and across bone cell types.

4.3. Insulin-like effects in chondrocyte-like versus osteoblast-like cells

4.3.1. IGF-1 stimulates both chondrocyte and osteoblast proliferation in fish

IGF-1, but not insulin, exhibited similar proliferative effects in both VSa16 and VSa13 cells, suggesting that IGF-1 growth-related mechanisms are probably conserved

across bone cell types. This hypothesis is consistent with data reported in mammalian osteoblast-like (*e.g.* MG-63) [95,96] and chondrocyte-like (ATDC5) cell lines [107,108], further demonstrating the conservation of mechanisms across species and throughout evolution. However, insulin incapacity to stimulate VSa13 and VSa16 cell proliferation contrasted with its stimulatory effects in mammalian chondrocyte- and osteoblast-like cell lines [104,107], suggesting a differential role for this peptide in fish and mammalian bone. In a similar manner, vanadate inefficacy to stimulate VSa16 cell proliferation also contrasted with its stimulatory effects in VSa13 cells and mammalian osteoblast-like cell lines (MC3T3-E1 and UMR106 cells) [127], which could indicate that either vanadate was unable to interact with intracellular targets (*i.e.* possible incapacity to enter cells), or its targets were absent during VSa16 cells proliferation. Further studies involving vanadium accumulation in VSa16 cell extracts and investigating signalling pathways mediating IGF-1 effects would need to be performed in order to explain these discrepancies.

4.3.2. IGF-1 and vanadate inhibit ECM mineralization of both fish chondrocyte-like and osteoblast-like cell lines

IGF-1 inhibition of ECM mineralization in VSa16 cells is consistent with similar effects observed in VSa13 cells. However, in opposition to what has been observed in the fish chondrocyte-like cells, these results suggest that IR is absent during ECM mineralization of the fish osteoblast-like cell line. Although, results are inconsistent with data showing mineralogenic effect of IGF-1 in mammals *in vitro* and *in vivo* [16,20,95,96], probably indicating that mechanisms have not been conserved across species, it was also recently demonstrated that mineral deposition in MC3T3-E1 cultures (also pre-osteoblasts) can be seriously hampered through ERK

activation (which is associated to insulin and IGF-1) [163]. We propose, in the light of all these data that IGF-1 stimulates proliferation of both chondrocytes and osteoblasts while it only affects osteoblast differentiation/ECM mineralization, a role played by insulin in chondrocytes. Finally, the severe anti-mineralogenic effect of vanadate on VSa13 cells through insulin/IGF-1 signalling pathways activation, as well as ALP activity inhibition, suggest the involvement of similar mechanisms of action in VSa16 cells. Further studies analyzing insulin and IGF-1 signalling, ALP activity and collagen synthesis as putative targets for vanadate action in VSa16 cells should be carried out.

4.4. Putative roles for alternatively spliced transcripts of IGF-1 in seabream

Recent reports on the existence of multiple forms of proIGF-1 in vertebrates have stimulated the interest of the scientific community in understanding its biological role, which remains largely controversial [155,164-173]. In this work, multiple proIGF-1 transcripts in the gilthead seabream have been identified. These transcripts are alternatively spliced within the region encoding the E domain and exhibit different patterns of expression during fish development and in adult tissues. *In silico* analysis revealed that alternative splicing is a common feature for IGF-1 expression in most vertebrates and identified taxon-specific transcripts.

4.4.1. Seabream IGF-1: one gene, several transcripts

Three alternatively spliced IGF-1 transcripts (IGF-1a, 1b and 1c) and corresponding gene have been identified in gilthead seabream through this work. A transcript, similar to seabream IGF-1a, was already available [152], but with what appears to have been an error in stop codon identification, and only a partial 3'UTR. In addition, two transcripts

(IGF-1b and 1c) were newly identified, as was the partial IGF-1 gene sequence. Alternative splicing was shown to occur within the sequence encoding the E domain, thus resulting in pro-peptides of different sizes. The IGF-1 alternative splicing identified in seabream resulted from the use of alternative donor sites in exon 3 and entire skipping of exon 4, consistent with previous observations in Salmonids and flounder [169,174]. In mammals, similar alternative splicing mechanisms have been shown to be at the origin of the different proIGF-1 variants (mammalian IGF-1Ea is similar to teleost IGF-1c) [155]. Based on alternative splicing mechanisms observed in Salmonids, a fourth transcript was predicted in seabream (IGF-1d; Figure 3.17 A). IGF-1d has however never been detected and is, therefore, either weakly or not expressed in seabream, or its expression is restricted to sites not explored in this work. IGF-1d variant could also be related to the existence of a second IGF-1 gene as in Salmonids, and consequently be absent in seabream where available evidence does not support the existence of 2 genes. However, existing data in Salmonids does not allow the association of any of the variants to a specific gene [174]. The presence of 2 genes in these species may be the consequence of (i) the fish-specific whole-genome duplication event that occurred in the teleost lineage after divergence from tetrapods, approximately 420 million years ago [175], the duplicated gene would then have been lost in seabream, or (ii) a recent whole-genome duplication event occurring 25-100 million years ago in the common ancestor of all salmonids [176]. High similarities between variants in Salmonids seem to indicate however that IGF-1 is more likely to have derived from a recent duplication event, in agreement with the second hypothesis. It has also been hypothesized that IGF-1 and IGF-2 genes may have diverged in the first whole-genome duplication event (420 million years ago) although this hypothesis has been ruled out in

a previous study performed in *S. acanthias*, in which two IGF-like peptides have been identified: one more similar to vertebrate IGF-1 and the other similar to IGF-2 [177].

4.4.2. The proIGF-1 variants are tightly regulated during seabream development

One of the goals of this study was to determine the expression profile of proIGF-1 variants during seabream development. Results have indicated: a) basal levels of IGF-1c expression in larval stages and strong up-regulation after hatching; b) onset of IGF-1b expression immediately after hatching and remaining at low levels; and c) onset of IGF-1a expression at 20 DAH and remaining at intermediate levels (when compared to IGF-1c). A similar analysis, although not quantitative, has been performed in coho salmon [170]: IGF-1b, IGF-1c and IGF-1d isoforms were detected in 6 week-old embryos and thereafter, and shown to be mainly expressed in liver, muscle and brain. The analysis of seabream proIGF-1 expression patterns during development suggests that IGF-1 pro-peptides may be involved in specific organ formation and/or development. Endocrine system, which has been shown to be active early in development, and GH initial expression at 3 DAH in seabream [178,179] are coincident with first detection of IGF-1b and strong up-regulation of IGF-1c. In the same period, it has been also observed in seabream an onset of mineralization (2 DAH) [140], primitive digestive tract differentiation (3-6 DAH) [179], red muscle development (from 1 DAH) [180]. Later in development, IGF-1a first appearance and second up-regulation of IGF-1c were coincident with previously observed intensification of tissue calcification (20 DAH) [139]. An intensification of IGF-1c expression, from 20 to 48 DAH, was observed during a period previously associated to increase in white muscle formation

(35 DAH until juvenile). The endocrine system has been previously shown to directly regulate IGF-1 expression (through GH) in vertebrates [171,181], which in part may explain IGF-1b and IGF-1c transcripts regulation after hatching. In mammals, its deficiency has been associated to smaller structures and osteoporosis but no specific variants have been related to these effects in fish. IGF-1 down-regulation in fish scales has been associated to decreased bone cell activity (osteoblast and osteoclast) [182]. In the present study, we hypothesize that different proIGF-1 isoforms may have different functions in fish bone development, with IGF-1c and IGF-1b assuming specific roles at the onset of mineralization, while IGF-1a could be more related to periods of intensive calcification. However, additional functional analysis is required to verify this hypothesis (*e.g.* different IGF-1 variants peptides effects in bone-derived cell lines, namely in VSa13 and VSa16 cells). In mammals, specific IGF-1 alternative transcripts have been shown to be involved in muscle formation [155,168,183], but in fish no specific functions have been attributed to any variant. In coho salmon, however, multiple IGF-1 transcripts have been detected in muscle [170], indicating a probable important role, as in mammals.

4.4.3. Variants of proIGF-1 in adult seabream tissues: systemic versus autocrine/paracrine modes of action

Various physiological mechanisms have been associated with IGF-1 action in mammals. It includes: i) stem cell differentiation into adipocyte and metabolic mechanisms of fasting and re-feeding in adipose tissue [25,26]; ii) pancreatic β-cell proliferation [27] and insulin release [29]; and iii) regulation of bone mineral density in developing structures [18]. Pattern of IGF-1 expression in adult seabream (*i.e.* main

expression is in liver, adipose tissue and pancreas; relatively high expression in calcified tissues) is in agreement with the reported role of mammalian IGF-1 in these processes. ProIGF-1 peptide resulting from IGF-1c (or E domain itself), the main transcript in liver (expression levels are 2-4 times higher than those for variants 1a and 1b), is likely to be involved in important physiological processes upon its release into circulation, an hypothesis consistent with previous observations in mammals, in which a systemic mode of action was demonstrated for IGF-1-Ea, the IGF-1c-like isoform in mammals [155]. It is hereby proposed that IGF-1c isoform assumes a similar role in seabream. Also of interest is our finding of relatively high IGF-1c expression in calcified tissues, which may indicate an autocrine/paracrine role of this variant in bone formation or metabolism. Following the same idea, variants 1a and 1b would assume local functions. Testing this hypothesis requires functional analysis, and again treatments with synthesized proIGF-1 or E domains variant peptides in isolated systems (*e.g.* in VSa13 and VSa16 cells) are suggested.

4.4.4. Mechanisms of IGF-1 alternative splicing in vertebrates are taxon-specific

Our *in silico* analysis of IGF-1 alternative splicing in vertebrates, indicates that a retention of IGF-1c/Ea has occurred in all taxa, suggesting that in fish, as in mammals, this variant may assume a systemic role, while other isoforms would play specific roles, a possibility that should be further explored. In order to identify these putative unexplored roles, taxonomic distribution of IGF-1 variants was tentatively related with various environmental adaptations or species characteristics. The distribution of IGF-1a and 1b in bony fish indicated a possible role in adaptations to different water salinities

(Figure 3.20). To test this hypothesis, analysis of IGF-1 variants expression during salinity adaptation is suggested. Since seabream which is a partially euryhaline species, it is proposed a study in which gene expression is analyzed upon specimen incubation in hypo-, iso- and hyperosmotic waters. In salmonids, IGF-1 potential role in osmoregulation has been previously studied and an up-regulation of IGF-1 expression in gills has been observed during seawater adaptation and smoltification process [184]. However, this process was never related to a specific IGF-1 variant and therefore this hypothesis could be tested by analyzing the expression of the different variants when specimens inhabit either rivers or seawater. Possible mechanisms, such as Na^+/K^+ ATPase regulation in gills, which has been previously related to IGF-1 [185], could also be correlated to expression of specific IGF-1 variants through the use of functional assays.

5. Conclusions and future perspectives

In this work, insulin-like activities of vanadate, insulin and IGF-1 were investigated in fish chondrocyte-like (VSa13) and osteoblast-like (VSa16) cell lines. Vanadate was shown to display different toxic effects and rates of intracellular accumulation according to its oligomerization state. Vanadate (independently of its oligomerization state) was shown to stimulate chondrocyte but not osteoblast cell proliferation, while strongly inhibiting differentiation/ECM mineralization in both cell types. IGF-1, but not insulin, stimulated cell proliferation of both cell type and inhibited cell differentiation/ECM mineralization of osteoblast cells. On the contrary, insulin, but not IGF-1, was shown to inhibit differentiation/ECM mineralization of chondrocyte cells. MAPK signalling pathway has been associated with the proliferative effect of vanadate and IGF-1 on chondrocyte cells, while PI-3K/Ras/ERK pathway has been associated with their anti-mineralogenic effect. Vanadate was shown to affect chondrocyte differentiation/ECM mineralization not only by interfering with intracellular signalling pathways but also by inhibiting alkaline phosphatase activity, which is crucial to prevent pyrophosphate inhibition of mineral deposition. Accordingly, we proposed that vanadate could affect chondrocyte proliferation through IGF-1 receptor/signalling pathway and chondrocyte differentiation through insulin receptor/signalling pathway.

In light of our results we proposed the conservation, throughout evolution, of those mechanisms regulating chondrocyte proliferation and differentiation and demonstrated the suitability of the fish VSa13 cell line to investigate mechanisms related to chondrogenesis in vertebrates. Although more data will be necessary to ascertain this hypothesis, we have hereby provided evidence towards the conservation of mechanisms involved in the IGF-1 dependent proliferative effect, across bone cell types and throughout evolution.

Finally, we report the existence of 3 transcripts for seabream IGF-1, alternatively spliced in the E domain, and their tight regulation during development and in adult tissues. We have tentatively associated the different isoforms (*i.e.* the pro-peptide or the E domain) to specific functions: IGF-1a and IGF-1b would be involved in the regulation of late developmental events (e.g. muscle and bone formation, and/or osmoregulation in teleosts), while IGF-1c would assume a systemic mode of action. Altogether, these results give new insights on bone-related insulin-like effects and further demonstrate the suitability of fish to study vertebrate development.

Although this work reports, for the first time, a detailed analysis of the insulin-like activities of IGF-1 and vanadate on the proliferation and ECM mineralization of fish chondrocyte-like and osteoblast-like cells, and provides new insights on the mechanisms (*i.e.* signalling and alternative targets) involved, there are still uncertainties that we would like to further investigate, such as the presence/activation of insulin and IGF-1 receptors during treatments, and/or the activation of downstream intermediates of PI-3K and MAPK pathways (*e.g.* phosphorylated forms of Akt and ERK). Although this could be performed through Western-blot analysis, there are no commercially available antibodies for these proteins in fish, therefore these experiments would require testing antibodies specific for the mammalian counterparts.

In VSa16 cells, the putative involvement of signalling pathways and other targets in insulin-like activities promoted by vanadate and IGF-1 are currently being investigated and preliminary results indicate involvement of MAPK in proliferative effects and PI-3K in anti-mineralogenic action.

Additionally, we are also performing microarray analysis using RNA samples from VSa13 and VSa16 cells during proliferation and ECM mineralization, and 4 x 44 k Agilent microarray slides specific for over 20.000 seabream genes. Preliminary results

in VSa13 cells indicate (i) 737 positive (up-regulated) and 587 negative (down-regulated) genes in control *versus* ECM mineralized cells, (ii) 207 positive and 379 negative genes in ECM mineralized *versus* ECM mineralized cells in the presence of vanadate, and (iii) 1710 positive and 2330 negative genes in control *versus* vanadate treated cells. We are currently identifying the most relevant genes (in terms of fold change and statistical significance) and its patterns of expression.

Concerning proIGF-1 alternative splicing, it would be interesting to investigate the activity of the distinct variants during VSa13 and VSa16 cell proliferation and ECM mineralization. Considering that adaptation to different water salinities was one of the putative roles identified for these variants in the course of this work, it would be important to analyze proIGF-1 alternative transcripts expression during incubation of seabream in different water salinities.

References

[1] Nakae, J., Kido, Y., and Accili, D. (2001). Distinct and overlapping functions of insulin and IGF-I receptors. *Endocr Rev* 22, 818-35.

[2] Cheatham, B., and Kahn, C.R. (1995). Insulin action and the insulin signaling network. *Endocr Rev* 16, 117-42.

[3] Dupont, J., and Holzenberger, M. (2003). Biology of insulin-like growth factors in development. *Birth Defects Res C Embryo Today* 69, 257-71.

[4] Munte, C.E., Vilela, L., Kalbitzer, H.R., and Garratt, R.C. (2005). Solution structure of human proinsulin C-peptide. *FEBS J* 272, 4284-93.

[5] Daughaday, W.H., and Rotwein, P. (1989). Insulin-like growth factors I and II. Peptide, messenger ribonucleic acid and gene structures, serum, and tissue concentrations. *Endocr Rev* 10, 68-91.

[6] Steiner, D.F., Smeekens, S.P., Ohagi, S., and Chan, S.J. (1992). The new enzymology of precursor processing endoproteases. *J Biol Chem* 267, 23435-8.

[7] Berg, J.M., Tymoczko, J.L., and Stryer, L. (2002) Protein structure and function. In *Biochemistry* (Stryer, L., ed)W.H. Freeman, New York and Basingstoke.

[8] Schmid, C. (1995). Insulin-like growth factors. *Cell Biol Int* 19, 445-57.

[9] Powell-Braxton, L., Hollingshead, P., Warburton, C., Dowd, M., Pitts-Meek, S., Dalton, D., Gillett, N., and Stewart, T.A. (1993). IGF-I is required for normal embryonic growth in mice. *Genes Dev* 7, 2609-17.

[10] Pessin, J.E., and Saltiel, A.R. (2000). Signaling pathways in insulin action: molecular targets of insulin resistance. *J Clin Invest* 106, 165-9.

[11] Cohick, W.S., and Clemmons, D.R. (1993). The insulin-like growth factors. *Annu Rev Physiol* 55, 131-53.

[12] Yakar, S., Liu, J.L., Stannard, B., Butler, A., Accili, D., Sauer, B., and LeRoith, D. (1999). Normal growth and development in the absence of hepatic insulin-like growth factor I. *Proc Natl Acad Sci U S A* 96, 7324-9.

[13] Baker, J., Liu, J.P., Robertson, E.J., and Efstratiadis, A. (1993). Role of insulin-like growth factors in embryonic and postnatal growth. *Cell* 75, 73-82.

[14] D'Ercole, A.J., Ye, P., and O'Kusky, J.R. (2002). Mutant mouse models of insulin-like growth factor actions in the central nervous system. *Neuropeptides* 36, 209-20.

[15] Ye, P., Li, L., Richards, R.G., DiAugustine, R.P., and D'Ercole, A.J. (2002). Myelination is altered in insulin-like growth factor-I null mutant mice. *J Neurosci* 22, 6041-51.

[16] Zhang, M. et al. (2002). Osteoblast-specific knockout of the insulin-like growth factor (IGF) receptor gene reveals an essential role of IGF signaling in bone matrix mineralization. *J Biol Chem* 277, 44005-12.

[17] Hayden, J.M., Mohan, S., and Baylink, D.J. (1995). The insulin-like growth factor system and the coupling of formation to resorption. *Bone* 17, 93-8.

[18] Canalis, E. (1993). Insulin like growth factors and the local regulation of bone formation. *Bone* 14, 273-6.

[19] Wang, J., Zhou, J., and Bondy, C.A. (1999). Igf1 promotes longitudinal bone growth by insulin-like actions augmenting chondrocyte hypertrophy. *FASEB J* 13, 1985-90.

[20] Zhao, G. et al. (2000). Targeted overexpression of insulin-like growth factor I to osteoblasts of transgenic mice: increased trabecular bone volume without increased osteoblast proliferation. *Endocrinology* 141, 2674-82.

[21] Canalis, E., Rydziel, S., Delany, A.M., Varghese, S., and Jeffrey, J.J. (1995). Insulin-like growth factors inhibit interstitial collagenase synthesis in bone cell cultures. *Endocrinology* 136, 1348-54.
[22] Bikle, D. et al. (2001). The skeletal structure of insulin-like growth factor I-deficient mice. *J Bone Miner Res* 16, 2320-9.
[23] Delany, A.M., Rydziel, S., and Canalis, E. (1996). Autocrine down-regulation of collagenase-3 in rat bone cell cultures by insulin-like growth factors. *Endocrinology* 137, 4665-70.
[24] Florini, J.R., Ewton, D.Z., and Coolican, S.A. (1996). Growth hormone and the insulin-like growth factor system in myogenesis. *Endocr Rev* 17, 481-517.
[25] Bertile, F., and Raclot, T. (2004). Differences in mRNA expression of adipocyte-derived factors in response to fasting, refeeding and leptin. *Biochim Biophys Acta* 1683, 101-9.
[26] Otto, T.C., and Lane, M.D. (2005). Adipose development: from stem cell to adipocyte. *Crit Rev Biochem Mol Biol* 40, 229-42.
[27] Kulkarni, R.N. (2005). New insights into the roles of insulin/IGF-I in the development and maintenance of β-cell mass. *Rev Endocr Metab Disord* 6, 199-210.
[28] Lingohr, M.K., Dickson, L.M., McCuaig, J.F., Hugl, S.R., Twardzik, D.R., and Rhodes, C.J. (2002). Activation of IRS-2-mediated signal transduction by IGF-1, but not TGF-α or EGF, augments pancreatic β-cell proliferation. *Diabetes* 51, 966-76.
[29] Hill, D.J., Sedran, R.J., Brenner, S.L., and McDonald, T.J. (1997). IGF-I has a dual effect on insulin release from isolated, perifused adult rat islets of Langerhans. *J Endocrinol* 153, 15-25.
[30] Laron, Z. (2002). Growth hormone insensitivity (Laron syndrome). *Rev Endocr Metab Disord* 3, 347-55.
[31] Holzenberger, M., Dupont, J., Ducos, B., Leneuve, P., Geloen, A., Even, P.C., Cervera, P., and Le Bouc, Y. (2003). IGF-1 receptor regulates lifespan and resistance to oxidative stress in mice. *Nature* 421, 182-7.
[32] Kiess, W., Blickenstaff, G.D., Sklar, M.M., Thomas, C.L., Nissley, S.P., and Sahagian, G.G. (1988). Biochemical evidence that the type II insulin-like growth factor receptor is identical to the cation-independent mannose 6-phosphate receptor. *J Biol Chem* 263, 9339-44.
[33] Rechler, M.M., and Nissley, S.P. (1985). The nature and regulation of the receptors for insulin-like growth factors. *Annu Rev Physiol* 47, 425-42.
[34] Rother, K.I., and Accili, D. (2000). Role of insulin receptors and IGF receptors in growth and development. *Pediatr Nephrol* 14, 558-61.
[35] LeRoith, D., Werner, H., Beitner-Johnson, D., and Roberts, C.T., Jr. (1995). Molecular and cellular aspects of the insulin-like growth factor I receptor. *Endocr Rev* 16, 143-63.
[36] Schlessinger, J. (2000). Cell signalling by receptor tyrosine kinases. *Cell* 103, 211-25.
[37] Kato, H., Faria, T.N., Stannard, B., Roberts, C.T., Jr., and LeRoith, D. (1994). Essential role of tyrosine residues 1131, 1135, and 1136 of the insulin-like growth factor-I (IGF-I) receptor in IGF-I action. *Mol Endocrinol* 8, 40-50.
[38] Wei, L., Hubbard, S.R., Hendrickson, W.A., and Ellis, L. (1995). Expression, characterization, and crystallization of the catalytic core of the human insulin receptor protein-tyrosine kinase domain. *J Biol Chem* 270, 8122-30.

[39] Hubbard, S.R. (1997). Crystal structure of the activated insulin receptor tyrosine kinase in complex with peptide substrate and ATP analog. *Embo J* 16, 5572-81.
[40] Jones, J.I., and Clemmons, D.R. (1995). Insulin-like growth factors and their binding proteins: biological actions. *Endocr Rev* 16, 3-34.
[41] LeRoith, D. (2000). Insulin-like growth factor I receptor signaling-overlapping or redundant pathways? *Endocrinology* 141, 1287-8.
[42] Cobb, M.H. (1999). MAP kinase pathways. *Prog Biophys Mol Biol* 71, 479-500.
[43] Parrizas, M., Saltiel, A.R., and LeRoith, D. (1997). Insulin-like growth factor 1 inhibits apoptosis using the phosphatidylinositol 3'-kinase and mitogen-activated protein kinase pathways. *J Biol Chem* 272, 154-61.
[44] Craparo, A., Freund, R., and Gustafson, T.A. (1997). 14-3-3 (ε) interacts with the insulin-like growth factor I receptor and insulin receptor substrate I in a phosphoserine-dependent manner. *J Biol Chem* 272, 11663-9.
[45] Furlanetto, R.W., Dey, B.R., Lopaczynski, W., and Nissley, S.P. (1997). 14-3-3 proteins interact with the insulin-like growth factor receptor but not the insulin receptor. *Biochem J* 327 (Pt 3), 765-71.
[46] Donnelly, R., and Qu, X. (1998). Mechanisms of insulin resistance and new pharmacological approaches to metabolism and diabetic complications. *Clin Exp Pharmacol Physiol* 25, 79-87.
[47] Nielsen, F.H., and Uthus, E.O. (1990) *Vanadium in biological systems*, Kluwer Academic Publishers. Boston.
[48] Crans, D.C., Smee, J.J., Gaidamauskas, E., and Yang, L. (2004). The chemistry and biochemistry of vanadium and the biological activities exerted by vanadium compounds. *Chem Rev* 104, 849-902.
[49] Rehder, D. (2003). Biological and medicinal aspects of vanadium. *Inorg Chem Commun* 6, 604-17.
[50] Anke, M. (2004). Vanadium - An element both essential and toxic to plants, animals and humans? *Anal Real Acad Nac Farm* 70, 961-99.
[51] Chasteen, N.D. (1983). The biochemistry of Vanadium. *Structure and bonding* 53, 105-38.
[52] Amado, A.M., Aureliano, M., Ribeiro-claro, P.J.A., and Teixeira-dias, J.J. (1993). Combined Raman and V-51 Nmr Spectroscopic Study of Vanadium (V) Oligomerization in Aqueous Alkaline-Solutions. *J Raman Spetrosc* 24, 699-703.
[53] Aureliano, M., and Gandara, R.M. (2005). Decavanadate effects in biological systems. *J Inorg Biochem* 99, 979-85.
[54] Aureliano, M., Joaquim, N., Sousa, A., Martins, H., and Coucelo, J.M. (2002). Oxidative stress in toadfish (Halobactrachus didactylus) cardiac muscle. Acute exposure to vanadate oligomers. *J Inorg Biochem* 90, 159-65.
[55] Aureliano, M., and Madeira, V.M. (1994). Interactions of vanadate oligomers with sarcoplasmic reticulum Ca(2+)-ATPase. *Biochim Biophys Acta* 1221, 259-71.
[56] Soares, S.S., Martins, H., Duarte, R.O., Moura, J.J.G., Coucelo, J., Gutiérrez-Merino, C., and Aureliano, M. (2007). Vanadium distribution, lipid peroxidation and oxidative stress markers upon decavanadate in vivo administration. *J Inorg Biochem* 101, 80-8.
[57] Tiago, T., Aureliano, M., Duarte, R.O., and Moura, J.J.G. (2002). Vanadate oligomers interaction with phosphorylated myosin. *Inorganica Chim Acta* 339, 317-21.

[58] Howarth, O.W., and Jarrold, M. (1978). Protonation of Decavanadate(6-) ion: a Vanadium-51 muclear magnetic resonance study. *J Chem Soc, Dalton Trans* 5, 503-6.

[59] Crans, D.C., Mahroof-Tahir, M., and Keramidas, A.D. (1995). Vanadium chemistry and biochemistry of relevance for use of vanadium compounds as antidiabetic agents. *Mol Cell Biochem* 153, 17-24.

[60] Aureliano, M., and Madeira, V.M.C. (1998) Energy transduction mechanisms as affected by vanadium (V) species: Ca2+-pumping in sarcoplasmic reticulum. In *Vanadium in the environment* (Nriagu, J.O., ed), 333-57. John Wiley & Sons, New York.

[61] Borges, G., Mendonca, P., Joaquim, N., Coucelo, J., and Aureliano, M. (2003). Acute effects of vanadate oligomers on heart, kidney, and liver histology in the Lusitanian toadfish (Halobatrachus didactylus). *Arch Environ Contam Toxicol* 45, 415-22.

[62] Soares, S.S., Aureliano, M., Joaquim, N., and Coucelo, J.M. (2003). Cadmium and vanadate oligomers effects on methaemoglobin reductase activity from Lusitanian toadfish: in vivo and in vitro studies. *J Inorg Biochem* 94, 285-90.

[63] Soares, S.S., Martins, H., and Aureliano, M. (2006). Vanadium distribution following decavanadate administration. *Arch Environ Contam Toxicol* 50, 60-4.

[64] Tiago, T., Aureliano, M., and Gutierrez-Merino, C. (2004). Decavanadate binding to a high affinity site near the myosin catalytic centre inhibits F-actin-stimulated myosin ATPase activity. *Biochemistry* 43, 5551-61.

[65] Tiago, T., Aureliano, M., and Moura, J.J. (2004). Decavanadate as a biochemical tool in the elucidation of muscle contraction regulation. *J Inorg Biochem* 98, 1902-10.

[66] Shechter, Y., and Karlish, S.J. (1980). Insulin-like stimulation of glucose oxidation in rat adipocytes by vanadyl (IV) ions. *Nature* 284, 556-8.

[67] Dubyak, G.R., and Kleinzeller, A. (1980). The insulin-mimetic effects of vanadate in isolated rat adipocytes. Dissociation from effects of vanadate as a (Na+-K+)ATPase inhibitor. *J Biol Chem* 255, 5306-12.

[68] Shechter, Y., and Ron, A. (1986). Effect of depletion of phosphate and bicarbonate ions on insulin action in rat adipocytes. *J Biol Chem* 261, 14945-50.

[69] Heyliger, C.E., Tahiliani, A.G., and McNeill, J.H. (1985). Effect of vanadate on elevated blood glucose and depressed cardiac performance of diabetic rats. *Science* 227, 1474-7.

[70] Meyerovitch, J., Farfel, Z., Sack, J., and Shechter, Y. (1987). Oral administration of vanadate normalizes blood glucose levels in streptozotocin-treated rats. Characterization and mode of action. *J Biol Chem* 262, 6658-62.

[71] Shechter, Y. (1998). Insulin-like effects of vanadium: Mechanisms of action, clinical and basic implications. *Lett Pept Sci* 5, 319-22.

[72] Goldwaser, I., Gefel, D., Gershonov, E., Fridkin, M., and Shechter, Y. (2000). Insulin-like effects of vanadium: basic and clinical implications. *J Inorg Biochem* 80, 21-5.

[73] Thompson, K.H., and Orvig, C. (2000). Design of vanadium compounds as insulin enhancing agents. *J Chem Soc, Dalton Trans* 17, 2885-92.

[74] Shechter, Y., Li, J., Meyerovitch, J., Gefel, D., Bruck, R., Elberg, G., Miller, D.S., and Shisheva, A. (1995). Insulin-like actions of vanadate are mediated in an insulin-receptor-independent manner via non-receptor protein tyrosine kinases and protein phosphotyrosine phosphatases. *Mol Cell Biochem* 153, 39-47.

[75] Shisheva, A., and Shechter, Y. (1993). Role of cytosolic tyrosine kinase in mediating insulin-like actions of vanadate in rat adipocytes. *J Biol Chem* 268, 6463-9.
[76] Drake, P.G., and Posner, B.I. (1998). Insulin receptor-associated protein tyrosine phosphatase(s): role in insulin action. *Mol Cell Biochem* 182, 79-89.
[77] Pandey, S.K., Anand-Srivastava, M.B., and Srivastava, A.K. (1998). Vanadyl sulfate-stimulated glycogen synthesis is associated with activation of phosphatidylinositol 3-kinase and is independent of insulin receptor tyrosine phosphorylation. *Biochemistry* 37, 7006-14.
[78] Tiago, D.M., Laizé, V., Aureliano, M., and Cancela, M.L. (2008) Vanadate effects on bone metabolism: Fish cell lines as an alternative to mammalian *in vitro* systems. In *Vanadium Biochemistry* (Aureliano, M., ed), in press. Research Signpost, Kerala, India.
[79] Canalis, E., Pash, J., and Varghese, S. (1993). Skeletal growth factors. *Crit Rev Eukaryot Gene Expr* 3, 155-66.
[80] McCarthy, T.L., Ji, C., and Centrella, M. (2000). Links among growth factors, hormones, and nuclear factors with essential roles in bone formation. *Crit Rev Oral Biol Med* 11, 409-22.
[81] Qin, X., Gysin, R., Mohan, S., and Baylink, D.J. (2001) Bone growth factors. In *Osteoporosis* (Marcus, R., Feldman, D. and Kelsey, J., eds), 405-31. Academic Press, San Diego.
[82] Thrailkill, K.M. et al. (2005). Bone formation is impaired in a model of type 1 diabetes. *Diabetes* 54, 2875-81.
[83] McCarthy, T.L., and Centrella, M. (2001). Local IGF-I expression and bone formation. *Growth Horm IGF Res* 11, 213-9.
[84] Thomas, D.M., Hards, D.K., Rogers, S.D., Ng, K.W., and Best, J.D. (1996). Insulin receptor expression in bone. *J Bone Miner Res* 11, 1312-20.
[85] Wang, E., Wang, J., Chin, E., Zhou, J., and Bondy, C.A. (1995). Cellular patterns of insulin-like growth factor system gene expression in murine chondrogenesis and osteogenesis. *Endocrinology* 136, 2741-51.
[86] Shinar, D.M., Endo, N., Halperin, D., Rodan, G.A., and Weinreb, M. (1993). Differential expression of insulin-like growth factor-I (IGF-I) and IGF-II messenger ribonucleic acid in growing rat bone. *Endocrinology* 132, 1158-67.
[87] Inzerillo, A.M., and Epstein, S. (2004). Osteoporosis and diabetes mellitus. *Rev Endocr Metab Disord* 5, 261-8.
[88] Goodman, W.G., and Hori, M.T. (1984). Diminished bone formation in experimental diabetes. Relationship to osteoid maturation and mineralization. *Diabetes* 33, 825-31.
[89] Shires, R., Teitelbaum, S.L., Bergfeld, M.A., Fallon, M.D., Slatopolsky, E., and Avioli, L.V. (1981). The effect of streptozotocin-induced chronic diabetes mellitus on bone and mineral homeostasis in the rat. *J Lab Clin Med* 97, 231-40.
[90] Rosen, C.J. et al. (2004). Congenic mice with low serum IGF-I have increased body fat, reduced bone mineral density, and an altered osteoblast differentiation program. *Bone* 35, 1046-58.
[91] Karsenty, G., and Wagner, E.F. (2002). Reaching a genetic and molecular understanding of skeletal development. *Dev Cell* 2, 389-406.
[92] Goldring, S.R., and Goldring, M.B. (2007). Eating bone or adding it: the Wnt pathway decides. *Nat Med* 13, 133-4.
[93] Blair, H.C., Zaidi, M., and Schlesinger, P.H. (2002). Mechanisms balancing skeletal matrix synthesis and degradation. *Biochem J* 364, 329-41.

[94] Murshed, M., Harmey, D., Millan, J.L., McKee, M.D., and Karsenty, G. (2005). Unique coexpression in osteoblasts of broadly expressed genes accounts for the spatial restriction of ECM mineralization to bone. *Genes Dev* 19, 1093-104.

[95] Grey, A., Chen, Q., Xu, X., Callon, K., and Cornish, J. (2003). Parallel phosphatidylinositol-3 kinase and p42/44 mitogen-activated protein kinase signaling pathways subserve the mitogenic and antiapoptotic actions of insulin-like growth factor I in osteoblastic cells. *Endocrinology* 144, 4886-93.

[96] Zhang, W., Lee, J.C., Kumar, S., and Gowen, M. (1999). ERK pathway mediates the activation of Cdk2 in IGF-1-induced proliferation of human osteosarcoma MG-63 cells. *J Bone Miner Res* 14, 528-35.

[97] Chihara, K., and Sugimoto, T. (1997). The action of GH/IGF-I/IGFBP in osteoblasts and osteoclasts. *Horm Res* 48 Suppl 5, 45-9.

[98] Hanai, Y. et al. (2006). Involvement of p44/p42 MAP kinase in insulin-like growth factor-I-induced alkaline phosphatase activity in osteoblast-like-MC3T3-E1 cells. *Mol Cell Endocrinol* 251, 42-8.

[99] Levy, J.R., Murray, E., Manolagas, S., and Olefsky, J.M. (1986). Demonstration of insulin receptors and modulation of alkaline phosphatase activity by insulin in rat osteoblastic cells. *Endocrinology* 119, 1786-92.

[100] Lu, H., Kraut, D., Gerstenfeld, L.C., and Graves, D.T. (2003). Diabetes interferes with the bone formation by affecting the expression of transcription factors that regulate osteoblast differentiation. *Endocrinology* 144, 346-52.

[101] Qutob, S., Dixon, S.J., and Wilson, J.X. (1998). Insulin stimulates vitamin C recycling and ascorbate accumulation in osteoblastic cells. *Endocrinology* 139, 51-6.

[102] Fulzele, K., DiGirolamo, D.J., Liu, Z., Xu, J., Messina, J.L., and Clemens, T.L. (2007). Disruption of the insulin-like growth factor type 1 receptor in osteoblasts enhances insulin signaling and action. *J Biol Chem* 282, 25649-58.

[103] Felsenfeld, A.J., Iida-Klein, A., and Hahn, T.J. (1992). Interrelationship between parathyroid hormone and insulin: effects on DNA synthesis in UMR-106-01 cells. *J Bone Miner Res* 7, 1319-25.

[104] Hickman, J., and McElduff, A. (1989). Insulin promotes growth of the cultured rat osteosarcoma cell line UMR-106-01: an osteoblast-like cell. *Endocrinology* 124, 701-6.

[105] Kream, B.E., Smith, M.D., Canalis, E., and Raisz, L.G. (1985). Characterization of the effect of insulin on collagen synthesis in fetal rat bone. *Endocrinology* 116, 296-302.

[106] Hill, P.A., Tumber, A., and Meikle, M.C. (1997). Multiple extracellular signals promote osteoblast survival and apoptosis. *Endocrinology* 138, 3849-58.

[107] Phornphutkul, C., Wu, K.Y., and Gruppuso, P.A. (2006). The role of insulin in chondrogenesis. *Mol Cell Endocrinol* 249, 107-15.

[108] Phornphutkul, C., Wu, K.Y., Yang, X., Chen, Q., and Gruppuso, P.A. (2004). Insulin-like growth factor-I signaling is modified during chondrocyte differentiation. *J Endocrinol* 183, 477-86.

[109] Hidaka, K., Kanematsu, T., Takeuchi, H., Nakata, M., Kikkawa, U., and Hirata, M. (2001). Involvement of the phosphoinositide 3-kinase/protein kinase B signaling pathway in insulin/IGF-I-induced chondrogenesis of the mouse embryonal carcinoma-derived cell line ATDC5. *Int J Biochem Cell Biol* 33, 1094-103.

[110] Hill, P.A., Reynolds, J.J., and Meikle, M.C. (1995). Osteoblasts mediate insulin-like growth factor-I and -II stimulation of osteoclast formation and function. *Endocrinology* 136, 124-31.
[111] DeChiara, T.M., Efstratiadis, A., and Robertson, E.J. (1990). A growth-deficiency phenotype in heterozygous mice carrying an insulin-like growth factor II gene disrupted by targeting. *Nature* 345, 78-80.
[112] Ogata, N. et al. (2000). Insulin receptor substrate-1 in osteoblast is indispensable for maintaining bone turnover. *J Clin Invest* 105, 935-43.
[113] Zhou, Y. et al. (1997). A mammalian model for Laron syndrome produced by targeted disruption of the mouse growth hormone receptor/binding protein gene (the Laron mouse). *Proc Natl Acad Sci U S A* 94, 13215-20.
[114] Meulenbelt, I. et al. (1998). A genetic association study of the IGF-1 gene and radiological osteoarthritis in a population-based cohort study (the Rotterdam Study). *Ann Rheum Dis* 57, 371-4.
[115] Rosen, C.J. et al. (1998). Association between serum insulin growth factor-I (IGF-I) and a simple sequence repeat in IGF-I gene: implications for genetic studies of bone mineral density. *J Clin Endocrinol Metab* 83, 2286-90.
[116] Canalis, E., McCarthy, T.L., and Centrella, M. (1989). Growth factors and the skeletal system. *J Endocrinol Invest* 12, 577-84.
[117] Canalis, E. (1985). Effect of sodium vanadate on deoxyribonucleic acid and protein synthesis in culture rat calvariae. *Endocrinology* 116, 855–62.
[118] Etcheverry, S.B., Apella, M.C., and Baran, E.J. (1984). A model study of the incorporation of vanadium in bone. *J Inorg Biochem* 20, 269-74.
[119] Anke, M., Groppel, B., Gruhn, K., Langer, M., and Arnhold, W. (1989) *The essentiality of vanadium for animals*, Fredrich-Jena. Jena.
[120] Fukui, K., Fujisawa, Y., OhyaNishiguchi, H., Kamada, H., and Sakurai, H. (1999). In vivo coordination structural changes of a potent insulin-mimetic agent, bis(picolinato)oxovanadium(IV), studied by electron spin-echo envelope modulation spectroscopy. *J Inorg Biochem* 77, 215-24.
[121] Setyawati, I.A. et al. (1998). Kinetic analysis and comparison of uptake, distribution, and excretion of 48V-labeled compounds in rats. *J Appl Physiol* 84, 569-75.
[122] Barrio, D.A., and Etcheverry, S.B. (2006). Vanadium and bone development: putative signaling pathways. *Can J Physiol Pharmacol* 84, 677-86.
[123] Lau, K.H., Tanimoto, H., and Baylink, D.J. (1988). Vanadate stimulates bone cell proliferation and bone collagen synthesis *in vitro*. *Endocrinology* 123, 2858-67.
[124] Sudo, H., Kodama, H.A., Amagai, Y., Yamamoto, S., and Kasai, S. (1983). *In vitro* differentiation and calcification in a new clonal osteogenic cell line derived from newborn mouse calvaria. *J Cell Biol* 96, 191-8.
[125] Cortizo, A.M., Salice, V.C., and Etcheverry, S.B. (1994). Vanadium compounds. Their action on alkaline phosphatase activity. *Biol Trace Elem Res* 41, 331-9.
[126] Cortizo, A.M., and Etcheverry, S.B. (1995). Vanadium derivatives act as growth factor--mimetic compounds upon differentiation and proliferation of osteoblast-like UMR106 cells. *Mol Cell Biochem* 145, 97-102.
[127] Etcheverry, S.B., Crans, D.C., Keramidas, A.D., and Cortizo, A.M. (1997). Insulin-mimetic action of vanadium compounds on osteoblast-like cells in culture. *Arch Biochem Biophys* 338, 7-14.

[128] Barrio, D.A., Braziunas, M.D., Etcheverry, S.B., and Cortizo, A.M. (1997). Maltol complexes of vanadium (IV) and (V) regulate in vitro alkaline phosphatase activity and osteoblast-like cell growth. *J Trace Elem Med Biol* 11, 110-5.
[129] Salice, V.C., Cortizo, A.M., Gomez Dumm, C.L., and Etcheverry, S.B. (1999). Tyrosine phosphorylation and morphological transformation induced by four vanadium compounds on MC3T3E1 cells. *Mol Cell Biochem* 198, 119-28.
[130] Etcheverry, S.B., Williams, P.A., Barrio, D.A., Salice, V.C., Ferrer, E.G., and Cortizo, A.M. (2000). Synthesis, characterization and bioactivity of a new VO2+/aspirin complex. *J Inorg Biochem* 80, 169-71.
[131] Etcheverry, S.B., Williams, P.A., Salice, V.C., Barrio, D.A., Ferrer, E.G., and Cortizo, A.M. (2002). Biochemical properties and mechanism of action of a vanadyl(IV)-aspirin complex on bone cell lines in culture. *Biometals* 15, 37-49.
[132] Barrio, D.A., Williams, P.A., Cortizo, A.M., and Etcheverry, S.B. (2003). Synthesis of a new vanadyl(IV) complex with trehalose (TreVO): insulin-mimetic activities in osteoblast-like cells in culture. *J Biol Inorg Chem* 8, 459-68.
[133] Cortizo, A.M., Molinuevo, M.S., Barrio, D.A., and Bruzzone, L. (2006). Osteogenic activity of vanadyl(IV)-ascorbate complex: Evaluation of its mechanism of action. *Int J Biochem Cell Biol* 38, 1171-80.
[134] McGonnell, I.M., and Fowkes, R.C. (2006). Fishing for gene function-endocrine modelling in the zebrafish. *J Endocrinol* 189, 425-39.
[135] Nissen, R.M., Amsterdam, A., and Hopkins, N. (2006). A zebrafish screen for craniofacial mutants identifies wdr68 as a highly conserved gene required for endothelin-1 expression. *BMC Dev Biol* 6, 28.
[136] Gavaia, P.J., Sarasquete, C., and and Cancela, M.L. (2000). Detection of mineralized structures in early stages of development of marine Teleostei using a modified alcian blue- alizarin red double staining technique for bone and cartilage. *Biotech Histochem* 75, 79-84.
[137] Simes, D.C., Williamson, M.K., Schaff, B.J., Gavaia, P.J., Ingleton, P.M., Price, P.A., and Cancela, M.L. (2004). Characterization of osteocalcin (BGP) and matrix Gla protein (MGP) fish specific antibodies: validation for immunodetection studies in lower vertebrates. *Calcif Tissue Int* 74, 170-80.
[138] Simes, D.C., Williamson, M.K., Ortiz-Delgado, J.B., Viegas, C.S., Price, P.A., and Cancela, M.L. (2003). Purification of matrix Gla protein from a marine teleost fish, Argyrosomus regius: calcified cartilage and not bone as the primary site of MGP accumulation in fish. *J Bone Miner Res* 18, 244-59.
[139] Pinto, J.P., Ohresser, M.C., and Cancela, M.L. (2001). Cloning of the bone Gla protein gene from the teleost fish *Sparus aurata*. Evidence for overall conservation in gene organization and bone-specific expression from fish to man. *Gene* 270, 77-91.
[140] Pinto, J.P., Conceição, N., Gavaia, P.J., and Cancela, M.L. (2003). Matrix Gla protein gene expression and protein accumulation co-localize with cartilage distribution during development of the teleost fish *Sparus aurata*. *Bone* 32, 201-10.
[141] Cancela, M.L., Williamson, M.K., and Price, P.A. (1995). Amino-acid sequence of bone Gla protein from the African clawed toad Xenopus laevis and the fish Sparus aurata. *Int J Pept Protein Res* 46, 419-23.
[142] Pombinho, A.R., Laize, V., Molha, D.M., Marques, S.M., and Cancela, M.L. (2004). Development of two bone-derived cell lines from the marine teleost

Sparus aurata; evidence for extracellular matrix mineralization and cell-type-specific expression of matrix Gla protein and osteocalcin. *Cell Tissue Res* 315, 393-406.

[143] Roy, M.E., and Nishimoto, S.K. (2002). Matrix Gla protein binding to hydroxyapatite is dependent on the ionic environment: calcium enhances binding affinity but phosphate and magnesium decrease affinity. *Bone* 31, 296-302.

[144] Chomczynski, P., and Sacchi, N. (1987). Single-step method of RNA isolation by acid guanidinium thiocyanate-phenol-chloroform extraction. *Anal Biochem* 162, 156-9.

[145] Livak, K.J., and Schmittgen, T.D. (2001). Analysis of relative gene expression data using real-time quantitative PCR and the $2^{(-\Delta\Delta C(T))}$ method. *Methods* 25, 402-8.

[146] Mosmann, T. (1983). Rapid colorimetric assay for cellular growth and survival: application to proliferation and cytotoxicity assays. *J Immunol Methods* 65, 55-63.

[147] Malich, G., Markovic, B., and Winder, C. (1997). The sensitivity and specificity of the MTS tetrazolium assay for detecting the *in vitro* cytotoxicity of 20 chemicals using human cell lines. *Toxicology* 124, 179-92.

[148] Bradford, M.M. (1976). A rapid and sensitive method for the quantitation of microgram quantities of protein utilizing the principle of protein-dye binding. *Anal Biochem* 72, 248-54.

[149] Tullberg-Reinert, H., and Jundt, G. (1999). *In situ* measurement of collagen synthesis by human bone cells with a Sirius red-based colorimetric microassay: effects of transforming growth factor-β2 and ascorbic acid 2-phosphate. *Histochem Cell Biol* 112, 271-6.

[150] Quarto, R., Campanile, G., Cancedda, R., and Dozin, B. (1992). Thyroid hormone, insulin, and glucocorticoids are sufficient to support chondrocyte differentiation to hypertrophy: a serum-free analysis. *J Cell Biol* 119, 989-95.

[151] Hock, J.M., Centrella, M., and Canalis, E. (1988). Insulin-like growth factor I has independent effects on bone matrix formation and cell replication. *Endocrinology* 122, 254-60.

[152] Duguay, S.J., Lai-Zhang, J., Steiner, D.F., Funkenstein, B., and Chan, S.J. (1996). Developmental and tissue-regulated expression of IGF-I and IGF-II mRNAs in *Sparus aurata*. *J Mol Endocrinol* 16, 123-32.

[153] Moriyama, S., Ayson, F.G., and Kawauchi, H. (2000). Growth regulation by insulin-like growth factor-I in fish. *Biosci Biotechnol Biochem* 64, 1553-62.

[154] Patthy, L. (1987). Intron-dependent evolution: preferred types of exons and introns. *FEBS Lett* 214, 1-7.

[155] Goldspink, G., and Yang, S.Y. (2004). The splicing of the IGF-I gene to yield different muscle growth factors. *Adv Genet* 52, 23-49.

[156] Etcheverry, S.B., and Cortizo, A.M. (1998) Bioactivity of vanadium compounds on cells in culture. In *Vanadium in the enviroment* (Nriagu, J.O., ed), 359-94. John Wiley & Sons, New York.

[157] Aureliano, M. (2000). Vanadate oligomer interactions with myosin. *J Inorg Biochem* 80, 141-3.

[158] Aureliano, M., and Madeira, V.M. (1994). Vanadate oligoanions interact with the proton ejection by the Ca2+ pump of sarcoplasmic reticulum. *Biochem Biophys Res Commun* 205, 161-7.

[159] Bracken, W.M., Sharma, R.P., and Elsner, Y.Y. (1985). Vanadium accumulation and subcellular distribution in relation to vanadate induced cytotoxicity in vitro. *Cell Biol Toxicol* 1, 259-68.
[160] Yang, X.G., Yang, X.D., Yuan, L., Wang, K., and Crans, D.C. (2004). The permeability and cytotoxicity of insulin-mimetic vanadium compounds. *Pharm Res* 21, 1026-33.
[161] Shisheva, A., and Shechter, Y. (1992). A cytosolic protein tyrosine kinase in rat adipocytes. *FEBS Lett* 300, 93-6.
[162] Cortizo, A.M., Bruzzone, L., Molinuevo, S., and Etcheverry, S.B. (2000). A possible role of oxidative stress in the vanadium-induced cytotoxicity in the MC3T3E1 osteoblast and UMR106 osteosarcoma cell lines. *Toxicology* 147, 89-99.
[163] Kono, S.J., Oshima, Y., Hoshi, K., Bonewald, L.F., Oda, H., Nakamura, K., Kawaguchi, H., and Tanaka, S. (2007). ERK pathways negatively regulate matrix mineralization. *Bone* 40, 68-74.
[164] Conover, C.A., Baker, B.K., and Hintz, R.L. (1989). Cultured human fibroblasts secrete insulin-like growth factor IA prohormone. *J Clin Endocrinol Metab* 69, 25-30.
[165] Tian, X.C., Chen, M.J., Pantschenko, A.G., Yang, T.J., and Chen, T.T. (1999). Recombinant E-peptides of pro-IGF-I have mitogenic activity. *Endocrinology* 140, 3387-90.
[166] Lin, W.W., and Oberbauer, A.M. (1999). Spatiotemporal expression of alternatively spliced IGF-I mRNA in the rat costochondral growth plate. *J Endocrinol* 160, 461-7.
[167] Lin, W.W., and Oberbauer, A.M. (1998). Alternative splicing of insulin-like growth factor I mRNA is developmentally regulated in the rat and mouse with preferential exon 2 usage in the mouse. *Growth Horm IGF Res* 8, 225-33.
[168] Yang, S., Alnaqeeb, M., Simpson, H., and Goldspink, G. (1996). Cloning and characterization of an IGF-1 isoform expressed in skeletal muscle subjected to stretch. *J Muscle Res Cell Motil* 17, 487-95.
[169] Tanaka, M., Taniguchi, T., Yamamoto, I., Sakaguchi, K., Yoshizato, H., Ohkubo, T., and Nakashima, K. (1998). Gene and cDNA structures of flounder insulin-like growth factor-I (IGF-I): multiple mRNA species encode a single short mature IGF-I. *DNA Cell Biol* 17, 859-68.
[170] Duguay, S.J., Park, L.K., Samadpour, M., and Dickhoff, W.W. (1992). Nucleotide sequence and tissue distribution of three insulin-like growth factor I prohormones in salmon. *Mol Endocrinol* 6, 1202-10.
[171] Duguay, S.J., Swanson, P., and Dickhoff, W.W. (1994). Differential expression and hormonal regulation of alternatively spliced IGF-I mRNA transcripts in salmon. *J Mol Endocrinol* 12, 25-37.
[172] Chun, C.Z., Tsai, H.J., and Chen, T.T. (2006). Trout Ea4- or human Eb-peptide of pro-IGF-I disrupts heart, red blood cell, and vasculature development in zebrafish embryos. *Mol Reprod Dev* 73, 1112-21.
[173] Chen, M.J., Kuo, Y.H., Tian, X.C., and Chen, T.T. (2002). Novel biological activities of the fish pro-IGF-I E-peptides: studies on effects of fish pro-IGF-I E-peptide on morphological change, anchorage-dependent cell division, and invasiveness in tumor cells. *Gen Comp Endocrinol* 126, 342-51.
[174] Wallis, A.E., and Devlin, R.H. (1993). Duplicate insulin-like growth factor-I genes in salmon display alternative splicing pathways. *Mol Endocrinol* 7, 409-22.

[175] Rasmussen, A.S., and Arnason, U. (1999). Molecular studies suggest that cartilaginous fishes have a terminal position in the piscine tree. *Proc Natl Acad Sci U S A* 96, 2177-82.
[176] Allendorf, F.W., and Thorgaard, G.H. (1984) *The evolutionary genetics of fishes* (Turner, B.J., ed), 1-53. Plembum Press, New York.
[177] Duguay, S.J., Chan, S.J., Mommsen, T.P., and Steiner, D.F. (1995). Divergence of insulin-like growth factors I and II in the elasmobranch, Squalus acanthias. *FEBS Lett* 371, 69-72.
[178] Funkenstein, B., and Cohen, I. (1996). Ontogeny of growth hormone protein and mRNA in the gilthead sea bream *Sparus aurata*. *Growth Regul* 6, 16-21.
[179] Falk-Petersen, I.B. (2005). Comparative organ differentiation during early life stages of marine fish. *Fish Shellfish Immunol* 19, 397-412.
[180] Ayala, M.D., Lopez-Albors, O., Gil, F., Ramirez-Zarzosa, G., Abellan, E., and Moreno, F. (1999). Red muscle development of gilthead sea bream *Sparus aurata* (L.): structural and ultrastructural morphometry. *Anat Histol Embryol* 28, 17-21.
[181] Ohlsson, C., Bengtsson, B.A., Isaksson, O.G., Andreassen, T.T., and Slootweg, M.C. (1998). Growth hormone and bone. *Endocr Rev* 19, 55-79.
[182] Suzuki, N., and Hattori, A. (2003). Bisphenol A suppresses osteoclastic and osteoblastic activities in the cultured scales of goldfish. *Life Sci* 73, 2237-47.
[183] Yang, S.Y., and Goldspink, G. (2002). Different roles of the IGF-I Ec peptide (MGF) and mature IGF-I in myoblast proliferation and differentiation. *FEBS Lett* 522, 156-60.
[184] Sakamoto, T., Hirano, T., Madsen, S.S., Nishioka, R.S., and Bern, H.A. (1995). Insulin-like growth factor-I gene expression during Parr-Smolt transformation of coho salmon. *Zool Sci* 12, 249-52.
[185] Mancera, J.M., and McCormick, S.D. (1998). Osmoregulatory actions of the GH/IGF axis in non-salmonid teleosts. *Comp Biochem Physiol B, Biochem Mol Biol* 121, 43-8.

Appendices

Appendix I – Medium and solutions compositions

Table AI.1 – Composition of DME medium used in cell culture.

DMEM (Invitrogen reference 21969-035)	
Inorganic salts:	Concentration (mM)
Calcium chloride	1.80
Ferric nitrate	2.48×10^{-4}
Magnesium sulfate	0.81
Potassium chloride	5.33
Sodium bicarbonate	44.05
Sodium chloride	110.34
Sodium phosphate monobasic	0.92
Amino acids:	
Glycine	0.40
L-Arginine HCl	0.40
L-Cystine 2HCl	0.20
L-Histidine HCl-H_2O	0.20
L-Isoleucine	0.80
L-Leucine	0.80
L-Lysine HCl	0.80
L-Methionine	0.20
L-Phenylalanine	0.40
L-Serine	0.40
L-Threonine	0.80
L-Tryptophan	7.84×10^{-2}
L-Tyrosine	0.40
L-Valine	0.80
Vitamins:	
Choline chloride	2.86×10^{-2}
D-Calcium pantothenate	8.39×10^{-3}
Folic acid	9.07×10^{-3}
i-Inositol	4.00×10^{-2}
Niacinamide	3.28×10^{-2}
Pyridoxine hydrochloride	1.96×10^{-2}
Riboflavin	1.06×10^{-3}
Thiamine hydrochloride	1.19×10^{-2}
Other components:	
D-Glucose	25.00
Phenol red	3.99×10^{-2}
Sodium pyruvate	1.00

Table AI.2 – Composition of solutions used in cell culture.

PBS 1X	
Component:	Concentration
Sodium chloride	137.00 mM
Potassium chloride	2.70 mM
Sodium phosphate dibasic	8.10 mM
Potassium phosphate monobasic	1.47 mM
pH	7.4
Solution T	
Component:	Concentration
Sodium chloride	137.00 mM
Potassium chloride	2.70 mM
Sodium phosphate dibasic	15.80 mM
Potassium phosphate monobasic	1.23 mM
EDTA	1.10 mM
Trypsin (Invitrogen)	0.2%
pH	7.4

Table AI.3 – Composition of RNA extraction buffers.

Trizol	
Component:	Quantity / final concentration
Guanidinium-HCl	4.00 M
Sodium acetate	0.05 M
Dithiothreitol	2.50×10^{-3} M
n-Lauryl-sarcosine (sodium salt)	0.25%
Saturated phenol pH 4.0	1 volume
Solution D	
Component:	Quantity
Guanidinium isothiocyanate	250 g
0.75 M Sodium citrate pH 7.0	17.6 ml
10% (w/v) n-Lauryl-sarcosine (sodium salt)	26.4 ml
RNase-free water	293.0 ml
β-mercaptoethanol	360 µl / 50 ml of solution D

Table AI.4 – Composition of ALP buffer.

ALP reaction buffer	
Component:	Concentration
Glycine	55.00 mM
Magnesium chloride	0.55 mM
pH	10.5

Table AI.5 – Composition of collagen staining solutions.

Bouin's fluid	
Component:	Volume
Saturated picric acid solution	15 ml
35% (w/v) formaldehyde	5 ml
Glacial acetic acid	1 ml
Sirius red staining solution	
Component:	Quantity
Sirius red dye (F3BA; Chroma)	10 mg
Saturated picric acid solution	10 ml

Table AI.6 – Composition of SSC solution.

SSC 10X	
Component:	Concentration
Sodium citrate	0.15 M
Sodium chloride	1.50 M
pH	7.0

Appendix II – Primers

Table AII.1 – PCR primers used in cloning of seabream IGF-1, identification of alternative splicing variants and gene expression analysis in development and adult tissues.

Primer names	Primer sequence (5' to 3')
Sparus aurata IGF-1 gene primers:	
IGF-1RV1	GCTAGACATCCCCACGGGTCTCCGCAAGA
IGF-1FW1	GTGACATTGCCCGCATCTCATCCTC
IGF-1FW2	TGGGGATGTCTAGCGCTCTTTCCTTTC
IGF-1RV2	TCCATTCGCTCCGTCCCTACATTC
IGF-1FW3	GGCATTGTGGACGAGTGCTGCTTCC
IGF-1FW4	TGTGAGCTGCGGCGTCTGGAGATGTAC
Commercial primers:	
oligo-d(T)-adapter	ACGCGTCGACCTCGAGATCGATG$(T)_{13}$
universal adapter	ACGCGTCGACCTCGAGATCGATG
MarAP1	CCATCCTAATACGACTCACTATAGGGC
MarAP2	ACTCACTATAGGGCTCGAGCGGC
GWAP1	GTAATACGACTCACTATAGGGC
GWAP2	ACTATAGGGCACGCGTGGT

Table AII.2 – Primers used in qPCR gene expression analysis in seabream development, adult tissues and VSa13 cells samples.

Primer names	Primer sequence (5' to 3')
Seabream IGF-1 gene primers:	
IGF-1ABC_FW	ACAGAATGTAGGGACGGAGCGAATGGAC
IGF-1A_FW	AGGACAGCACAGCAGCCAGACAAGAC
IGF-1AB_FW	AGTCATTCATCCTTCAAGGAAGTGCATCC
IGF-1ABC_RV	TTCGGACCATTGTTAGCCTCCTCTCTG
IGF1FW145	TCGACACGCTGCAGTTTGTGTGTGG
IGF1RV145	GCACAGTACATCTCCAGACGCCGCA
Seabream housekeeping genes primers:	
ActinFW	CTTCCTCGGTATGGAGTCCTGCGG
ActinRV	TCCTGCTTGCTGATCCACATCTGCT
RPL27aFW	AAGAGGAACACAACTCACTGCCCCAC
RPL27aRV	GCTTGCCTTTGCCCAGAACTTTGTAG

Appendix III – Methods complementary information

Table AIII.1 – Development stages and feeding calendar.

Development stage:															
UE	Embryo						Larvae						Juvenile		
Number of cells			HAF				DAH								
1	8	512	10	14	18	24	3	6	10	20	37	48	67	82	130
Feeding:															
Unfed							Rotifers				Artemia		Selco/dry food		

Note: UE means unfertilized eggs

Table AIII.2 – BSA standard stock solution, milliQ water, samples and Bradford reagent quantities used in protein quantification assay in each cuvette.

Protein quantity (µg)	Volume stock solution or sample (µl)	Volume milliQ water (µl)	Volume Bradford reagent (µl)
Standards (BSA 2 mg/ml stock solution)			
0	0	800	200
1	0.5	799.5	200
2	1	799	200
4	2	798	200
8	4	796	200
10	5	795	200
15	7.5	792.5	200
20	10	790	200
Sample (S) or extraction/purification buffer (B)			
S	10	790	200
B	10	790	200

Appendix IV – Results and discussion complementary information

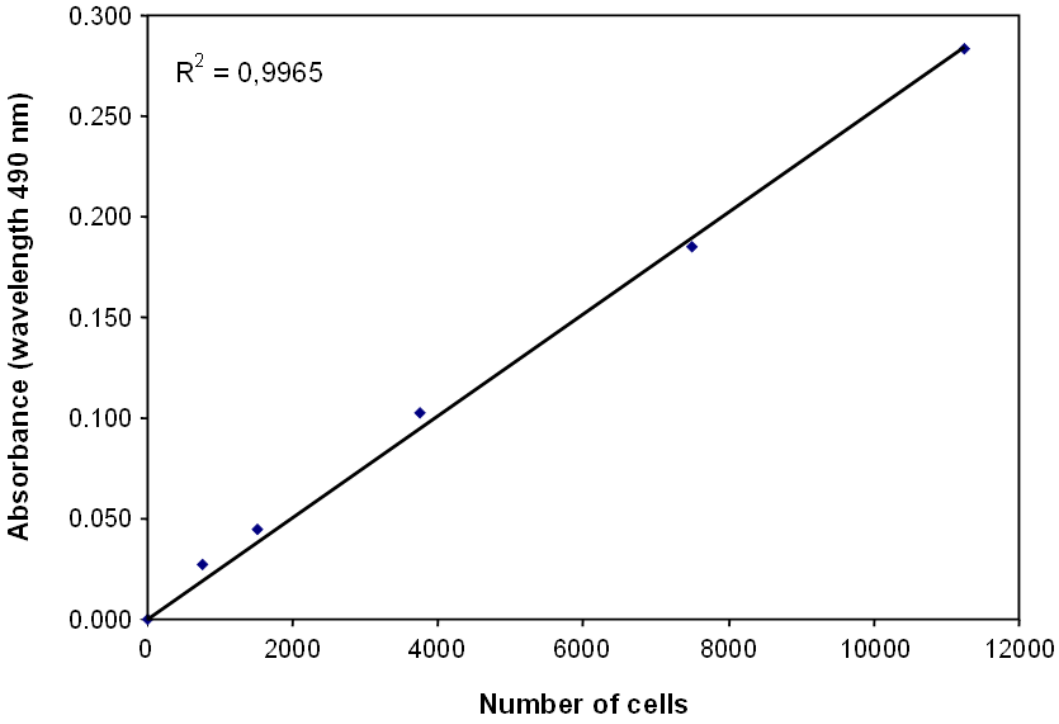

Figure AIV.1 – MTS assay linearity test in VSa13 cell line. Different quantities of cells were seeded in 96-well plates (150 µl cell suspension / well) and incubated approximately 6 hours at 37ºC and 5 % CO_2 for surface attaching; 20 µl of MTS/ phenazine methosulfate reagent mixture (see section 2.5) were added to cultures, incubated for 1 hour and absorbance measured at 490 nm wavelength in a Bio-rad Benchmark microplate reader; well culture medium and reagent was considered as blank and subtracted to measured absorbances.

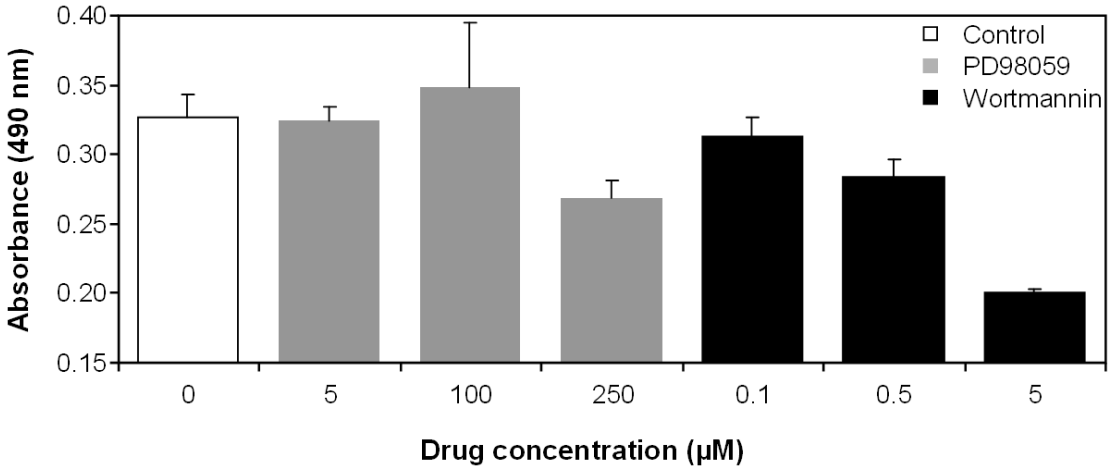

Figure AIV.2 - Viability of VSa13 cells after 8 days growth with wortmannin and PD98059. VSa13 cells were seeded in 96-well plates at 1.5×10^3 cells/well then either left untreated (control), treated with 5, 100 and 250 µM PD98059, or treated with 0.1, 0.5 and 5 µM wortmannin. Cell viability was evaluated at appropriate time using MTS assay. Values are the mean of at least three independent experiments.

Figure AIV.3 - IGF-1 sequences (cDNA/EST) retrieved from GenBank (in October 2006) using BLAST facilities at NCBI (www.ncbi.nih.gov).

1, *Pimephales promelas* IGF-1b from AY533140.
2, *Megalobrama amblycephala* IGF-1b from AF332865.
3, *Megalobrama terminalis* IGF-1b from AY247412.
4, *Gymnocypris przewalskii* IGF-1b from AY919608.
5, *Danio rerio* IGF-1b from BC114262, NM_131825, AF314545, AF268051, DT080649 and BF717691.
6, *Danio aequipinnatus* IGF-1b from DQ221105.
7, *Cyprinus carpio* IGF-1b from D83271, S82374 and D83272.
8, *Cirrhinus molitorella* IGF-1b from AY987045 and AY069945.
9, *Spinibarbus sinensis* IGF-1b from DQ449027.
10, *Ctenopharyngodon idella* IGF-1b from AF247658.
11, *Carassius auratus* IGF-1b from AF001005, AF001006 and AF216775
12, *Ictalurus punctatus* IGF-1b from AY353852.
13, *Clarias macrocephalus* IGF-1c from X79077 and X79244.
14, *Tetraodon nigroviridis* IGF-1a from CR653867.
15, *Mugil cephalus* IGF-1a from AY427954.
16, *Cottus kazika* IGF-1a from AB079539.
17, *Myoxocephalus scorpius* IGF-1a from Y12583.
18, *Paralichthys olivaceus* IGF-1a from AJ010603 and AF061278
19, *Paralichthys olivaceus* IGF-1b from AJ010602.
20, *Oreochromis mossambicus* IGF-1a from Y10830, Y18690 and AF033796.
21, *Siganus guttatus* IGF-1a from AY198184.
22, *Epinephelus coioides* IGF-1a from AY776159 and AY513719.
23, *Umbrina cirrosa* IGF-1a from AY941254.
24, *Perca flavescens* IGF-1a from AY332492.
25, *Perca fluviatilis* IGF-1a from AJ586907.
26, *Perca fluviatilis* IGF-1b from AJ586908.
27, *Dicentrarchus labrax* IGF-1a from AY800248, DQ105655, AJ579342 and AY847777.
28, *Micropterus salmoides* IGF-1a from DQ666526.
29, *Acanthopagrus latus* IGF-1a from AY608674.
30, *Acanthopagrus schlegeli* IGF-1a from AF030573.
31, *Salmo salar* IGF-1a from M81904.
32, *Oncorhynchus keta* IGF-1a from S70778 and AH004580.
33, *Oncorhynchus kisutch* IGF-1a from M81913.
34, *Oncorhynchus kisutch* IGF-1c from M81911.
35, *Oncorhynchus kisutch* IGF-1d from M81912 and M32792.
36, *Oncorhynchus mykiss* IGF-1a from CA381456.
37, *Oncorhynchus mykiss* IGF-1d from M95183.
38, *Oncorhynchus tschawytscha* IGF-1a from U15960 and U14536.
39, *Oncorhynchus tschawytscha* IGF-1b from U15961.
40, *Oncorhynchus tschawytscha* IGF-1c from U15962.
41, *Xenopus laevis* IGF-1c from M29857.
42, *Anser anser* IGF-1c from DQ662932 and DQ490222.
43, *Anas platyrhynchos* IGF-1c from AB061721 and DQ168593.
44, *Meleagris gallopavo* IGF-1c from AF074980.
45, *Struthio camelus* IGF-1c from AB035804.
46, *Gallus gallus* IGF-1c from NM_001004384, BU454475 and CT485883.
47, *Mus musculus* IGF-1-Ea (similar to IGF-1c) from X04480, AF440694, AK081019, AK165471, AK155435, AY878192, W96836, CN694804, CD241297, BI714882, BI440109, BF719517, BI441115, BG071465, BY732820, AA245300, AI526955, AA451360, BI144500, AA867155, AA690767, AA461866, BQ568928, BI714981, BI714874, BI715603, BI715465, BI715475, BI676839, DV043357, CF585817, CF585816, BI328661, AW493459, BQ567564, CB589117, BI731538, CA456022, AI326648, CA494190, AA277619, AA096666, AI573421, BI221656, AW413016 and AI314558.
48, *Mus musculus* IGF-1-Eb from NM_184052 and BY748273.
49, *Mus musculus* IGF-1-Ec (also lnown as MGF) from CT010364, NM_010512, X04482, AY878192, AW495481, AI503976, AI265629, AW146128, BF383724, CB846321, AI604642, CA491066 and AI119218.

50, *Homo sapiens* IGF-1-Ea (similar to IGF-1c) from X56773, CR541861, X00173, AB209184, M27544, M29644, NM_000618, M37484, BP423487, DB259587, AL599807, BY800109, AA542914, BM984670, AA913900, DR005306, AI248089 and CB959991.
51, *Homo sapiens* IGF-1-Eb from M11568, X56774 and AI401719.
52, *Homo sapiens* IGF-1-Ec (also kown as MGF) from U40870.

Appendix V – Submitted manuscripts

Cell Biol Toxicol
DOI 10.1007/s10565-007-9034-x

Impairment of mineralization by metavanadate and decavanadate solutions in a fish bone-derived cell line

Daniel M. Tiago · Vincent Laizé · M. Leonor Cancela · Manuel Aureliano

Received: 20 April 2007 / Accepted: 23 August 2007
© Springer Science + Business Media B.V. 2007

Abstract Vanadium, a trace metal known to accumulate in bone and to mimic insulin, has been shown to regulate mammalian bone formation using *in vitro* and *in vivo* systems. In the present work, short- and long-term effects of metavanadate (containing monomeric, dimeric, tetrameric and pentameric vanadate species) and decavanadate (containing decameric vanadate species) solutions on the mineralization of a fish bone-derived cell line (VSa13) were studied and compared to that of insulin. After 2 h of incubation with vanadate (10 μM in monomeric vanadate), metavanadate exhibited higher accumulation rates than decavanadate (6.85±0.40 versus 3.95± 0.10 μg V/g of protein, respectively) in fish VSa13 cells and was also shown to be less toxic when applied for short periods. In longer treatments with both metavanadate and decavanadate solutions, similar effects were promoted: stimulation of cell proliferation and strong impairment (75%) of extracellular matrix (ECM) mineralization. The effect of both vanadate solutions (5 μM in monomeric vanadate), on ECM mineralization was increased in the presence of insulin (10 nM). It is concluded that chronic treatment with both vanadate solutions stimulated fish VSa13 cells proliferation and prevented ECM mineralization. Newly developed VSa13 fish cells appeared to be appropriate in the characterization of vanadate effects on vertebrate bone formation, representing a good alternative to mammalian systems.

Keywords Bone-derived cell line · Vanadate · Decavanadate · Insulin-mimetic properties · Vertebrate bone formation · Teleost fish *Sparus aurata*

Abbreviations

DMEM	Dulbecco's modified Eagle medium
ECM	Extracellular matrix
ERK	Extracellular signal-regulated kinase
FBS	Fetal bovine serum
MAPK	Mitogen-activated protein kinase
MTS	(3-(4,5-dimethylthiazol-2-yl)-5-(3-carboxy-methoxyphenyl)-2-(4-sulfophenyl)-2H-tetrazolium
PBS	Phosphate-buffered saline
PI3-K	Phosphatidyl inositol-3 kinase

Daniel M. Tiago and Vincent Laizé1 contributed equally to this work.

D. M. Tiago · V. Laizé · M. L. Cancela · M. Aureliano
Centre of Marine Sciences (CCMAR),
University of Algarve, Campus Gambelas,
8005-139 Faro, Portugal

M. Aureliano (✉)
Faculdade de Ciências e Tecnologia (FCT),
Universidade do Algarve, Campus de Gambelas,
8005-139 Faro, Portugal
e-mail: maalves@ualg.pt

Introduction

Vanadium, an essential trace element found in animals and higher plants (Anke 2004) and described to be accumulated in mammalian bone (Etcheverry et al. 1984), has been shown to display important biological effects in association with its physicochemical properties, e.g. insulin-like activity and regulation of phosphatases and ATPases activity (Nielsen and Uthus 1990). Vanadium, which easily transitions between three oxidation states, namely, V(III), V(IV) and V(V), has been proposed to be potentially important for its role as a biometal (Rehder 1999, 2003). Vanadate (V(V)), which is the most stable oxidation state in aerobic conditions, forms in solution monomeric vanadate species with different states of protonation, such as HVO_4^{2-} or $H_2VO_4^-$, depending on pH value. However, at physiological pH values and at millimolar range of concentrations, several *n*-meric species ($n=1$ to 10), normally ascribed as vanadate oligomers, can occur simultaneously in equilibrium, such as monomeric (V_1), dimeric (V_2) and tetrameric (V_4) vanadate species (Amado et al. 1993). Eventually, even decameric (V_{10}) vanadate species can be formed upon medium acidification (Aureliano and Gândara 2005). These vanadate oligomers species have been shown to interact with several proteins, thus affecting many biological systems (Crans et al. 2004). For instance, monomeric vanadate as been described to behave as a phosphate analogue, inhibiting (or, in some cases, stimulating) several phosphatases (acid, alkaline and protein phosphatases), phosphorylases, ribonucleases and ATPases (Crans et al. 2004). Conversely, other vanadate oligomers, such as the decameric vanadate, has been described to inhibit non-competitively several enzymes, among others, proteins involved in muscle contraction and regulation such as myosin ATPase and sarcoplasmic reticulum calcium ATPase, thus contributing for the several biological processes influenced by vanadate (Aureliano and Madeira 1994; Tiago et al. 2004; Aureliano and Gândara 2005).

The most important clinical effect of vanadium is probably its ability to mimic or to enhance the effect of insulin, as demonstrated in various *in vivo* and *in vitro* studies using streptozocin-treated diabetic rats (Heyliger et al. 1985; Meyerovitch et al. 1987) and adipocyte cultures (Dubyak and Kleinzeller 1980; Shechter and Karlish 1980). Insulin, a peptide that binds to specific membrane tyrosine kinase receptors, initiates intracellular signalling that either results in the regulation of protein, lipid, carbohydrate and mineral metabolism, or cell differentiation and proliferation, depending on the involved pathways: phosphatidyl inositol-3 kinase (PI3-K) pathway for metabolic effects or mitogen-activated protein kinase (MAPK) pathway for cell proliferation and differentiation effects (Cheatham and Kahn 1995; Cohick and Clemmons 1993; LeRoith 2000). Vanadium insulin-mimetic properties have been associated to the activity of tyrosine phosphatases and consequent activation of tyrosine kinase receptors, including the insulin receptor (Goldwaser et al. 2000; Shechter et al. 1995; Shisheva and Shechter 1993). In vertebrates, a major process regulated by insulin (and insulin-like growth factor 1) is linear bone growth (McCarthy et al. 2000; Moriyama et al. 2000). Vanadate was also shown to exhibit strong metabolic and mitogenic effects, as demonstrated by *in vitro* studies using mammalian bone-derived cell lines (and also using rat calvaria and chondrocyte primary cultures) (Canalis 1985a; Kato et al. 1987; Lau et al. 1988). These effects have been extensively studied using two mammalian cell lines, MC3T3-E1 and UMR106, and important features, such as tyrosine phosphorylation and activation of signalling mechanisms, have been characterized (Barrio and Etcheverry 2006; Cortizo and Etcheverry 1995; Salice et al. 1999). Although repetitively studied in mammals, vanadate effects have not been investigated in marine vertebrates (e.g. fish and amphibians), despite being recognized as the second most abundant transition metal in seawater (Rehder 2003).

In this paper, we describe the effects of two different vanadate solutions on the growth and mineralization performances of a gilthead seabream bone-derived cell line (VSa13) recently developed in our laboratory (Pombinho et al. 2004) and capable of mineralizing its extracellular matrix.

Materials and methods

Dulbecco's modified Eagle medium (DMEM), fetal bovine serum (FBS), antibiotics (penicillin and streptomycin), antimycotic (fungizone), trypsin-EDTA solution and L-glutamine were purchased from Invitrogen. Tissue culture dishes were purchased from

Sarstedt or Nunc. CellTiter 96 non-radioactive proliferation assay kit was purchased from Promega. All other reagents were purchased from Sigma-Aldrich unless otherwise stated.

Cell culture maintenance

Cultured cells were maintained in DMEM supplemented with 1% penicillin-streptomycin, 1% fungizone, 2 mM L-glutamine and 10% FBS, and incubated at 33°C in a 10% CO_2 humidified atmosphere. Confluent cell cultures were divided (1:2) every 3–4 days using trypsin–EDTA solution.

Vanadate solution preparation

Metavanadate stock solution (50 mM, pH 6.7) was prepared from ammonium metavanadate (NH_4VO_3). Decavanadate stock solution was obtained by adjusting the pH of the former solution to 4.0, as described elsewhere (Aureliano and Madeira 1994). The acquired characteristic orange color in decavanadate solution upon acidification reveals the presence of decameric vanadate species (V_{10}). Decavanadate stock solution was always adjusted to pH 7.0 immediately before using it. Both vanadate solutions were stored at 4°C. Although total vanadate concentration does not change, note that in case of decavanadate solutions the concentration in decameric vanadate species was effectively reduced 10-fold, meaning that stock decavanadate solutions contain 5 mM decameric vanadate species. However, vanadate concentrations are always given for monomeric vanadate, i.e. total vanadate.

Characterization of vanadate solutions

The composition of both vanadate solutions was analysed by ^{51}V Nuclear Magnetic Resonance (NMR) spectroscopy, as described elsewhere (Aureliano and Madeira 1994). Briefly, the composition of vanadate solutions upon dilution into DMEM was analysed in a Bruker AM-400 spectrometer at 105.2 MHz equipped with a 5-mm multinuclear inverse probe, using a 90° pulse Fourier transform technique. Spectra were acquired at room temperature using 0.5 ml of vanadate samples in the medium, containing at least 10% D_2O, under the following conditions: spectral width 45,455 Hz, accumulation time 0.05 s and relaxation delay 0.01 s. ^{51}V NMR chemical shifts are reported relative to an external reference of $VOCl_3$ (0 ppm). The relative areas of the several free or/and bound vanadate resonances were integrated and the line widths were obtained after subtracting the value (20 Hz) used in line broadening. The concentration of each vanadate oligomer V_x was calculated from the fractions of the total integrated areas observed in the recorded spectra as described (Equation 1). The symbol A corresponds to the area measured for the x vanadate species with the n aggregation number (number of vanadium atoms), A_t, the sum of measured areas and $[V_t]$ corresponds to total vanadate concentration.

$$[V_x] = \frac{A_x}{A_t} \times \frac{[V_t]}{n} \quad (1)$$

The calculated concentrations of vanadate oligomers were reproducible within 2–4%. For quantitative measurements, all spectra parameters were kept constant. Vanadate concentrations are always given for monomeric vanadate, i.e. total vanadium.

Unlike metavanadate, decavanadate solutions are unstable. The partial deoligomerization of decameric vanadate species present at the decavanadate solutions upon dilution in DMEM medium was analysed by ultraviolet/visible spectroscopy at 400 nm, as described elsewhere (Soares et al. 2006).

Cell viability measurement

Cytotoxic and proliferative effects of vanadate oligomers on VSa13 cells were assessed through cell viability analysis using the CellTiter 96 non-radioactive proliferation assay kit according to the manufacturer's instructions. Tetrazolium reagent (3-(4,5-dimethylthiazol-2-yl)-5-(3-carboxy-methoxyphenyl)-2-(4-sulfophenyl)-2H-tetrazolium; inner salt, MTS) and the electron-coupling reagent, phenazine methosulfate, were mixed in solution in a 20:1 proportion. Once added to cell culture, MTS is reduced into formazan by the dehydrogenase enzyme found in metabolically active cells. Formazan formation, which is proportional to the number of living cells (Malich et al. 1997), was followed at 490 nm in 96-well tissue culture dishes. Incubation with 20 μl of reagent mixture during 1 h was determined to be the optimal conditions for VSa13 cell viability measurement. Vanadate cytotoxic effects were studied in confluent cell cultures (approximately 1.7×10^4 cells/well) while effects on cell proliferation were investi-

gated in low-density cell cultures (starting from 1.5×10^3 cells/well).

Vanadium accumulation measurement

Cells were cultured for 0, 1, 2, 4, 8 and 24 h in the presence of 10 μM metavanadate or decavanadate. At appropriate times, cell cultures were washed three times with phosphate-buffered saline (PBS), supplemented with 1 ml of MilliQ water (Millipore) and placed at −80°C for 10 h. Frozen cells were thawed at room temperature for 15 min, collected using a cell scraper and transferred into a 2-ml microcentrifuge tube. Cell culture dishes were washed once with 1 ml of MilliQ water and washing solution was transferred into the microcentrifuge tube containing the initial cell extract. Total protein content was quantified from cell extracts using Bradford reagent. Samples were then digested at 100°C with 30 μl of 65% HNO_3 and final solid residues dissolved in 5% HCl solution. Vanadium concentration was determined by atomic absorption spectrometry analysis using a GBC Avanta atomic absorption spectrometer equipped with a GBC GF 3000 graphite furnace system and a GBC PAL 3000 auto sampler working at a furnace program of 63 s with an argon gas flow of 3.0 L/min. The vanadium lamp was operated at 318.2 nm, with slit width of 0.2 nm, and the instrument was calibrated against a series of solutions containing 12.5, 25, 37.5 and 50 ppb of vanadium. Calibrating standards were obtained by successive dilutions of a standard solution of vanadium 1002±2 mg/L (Merck). The detection and quantification limits of the instrument for these analysis conditions, determined according to ISO 8466-1, were 5 and 11 ppb, respectively.

Extracellular matrix mineralization and nodule detection

Cells were seeded in 24-well plates at 2×10^4 cells/well and cultured in DMEM supplemented with 10% FBS. To induce ECM mineralization, confluent cultures received medium supplemented with 50 μg/mL of L-ascorbic acid (vitamin C), 10 mM β -glycerophosphate and 4 mM $CaCl_2$ up to 4 weeks. Wherever appropriate, cells were washed three times with PBS at 4°C, fixed with 10% formaldehyde (in PBS) for 1 h at 4°C, washed three times with distilled water, then incubated with 5% silver nitrate for 30 min under ultraviolet light. Relative levels of ECM mineralization were determined by densitometric methods using Quantity 1 software (Bio-Rad).

Statistical analysis

The data were presented as average and standard deviation of measurements taken at least in three separate experiments. Statistical significance of data was analysed wherever indicated by Student *t* test or analysis of variance (ANOVA) analysis. Differences were considered to be significant at $P<0.05$.

Results

Vanadate solutions characterization in DMEM

^{51}V-NMR spectroscopy of 1 and 5 mM decavanadate solutions in DMEM, at pH 7.0, revealed three signals attributed to three specific vanadium atoms in V10 structure: V10A at −515 ppm, V10B at −498 ppm and V10C at −425 ppm (Fig. 1a). Conversely, in 1 and 5 mM metavanadate solutions (Fig. 1a), detected signals ascribed to mono- (V1), di- (V2), tetra- (V4) and pentameric (V5) vanadate species, respectively, at −556 ppm, −571 ppm, −579 ppm and at 587 ppm (Fig. 1a). Monomeric NMR signal is clearly broadened, with a half line-width value (270 Hz) approx. 3.4-fold of normal value (80 Hz), probably caused by vanadate interactions with compounds present in DMEM such as glucose (25 mM) and piruvate (1 mM), or even interactions with several proteins also present in the medium. For each metavanadate concentration in DMEM (1 and 5 mM), different amounts of mono (V1), di (V2), tetra (V4) and pentameric (V5) species have been observed, that corresponded to different species profiles (Fig. 1b). While tetrameric species were predominant at 5 mM metavanadate, monomeric vanadate was the major specie in the lower concentration (Fig. 1b). Conversely, decameric vanadate species present in the decavanadate solutions increased linearly with total vanadate concentration (Fig. 1c).

Although ^{51}V-NMR spectroscopy is an essential technique for the analysis of vanadate oligomers composition and interactions, approximately 1 h acquisition time was necessary to obtain a clear spectrum of 1 mM decavanadate solution (Fig. 1a).

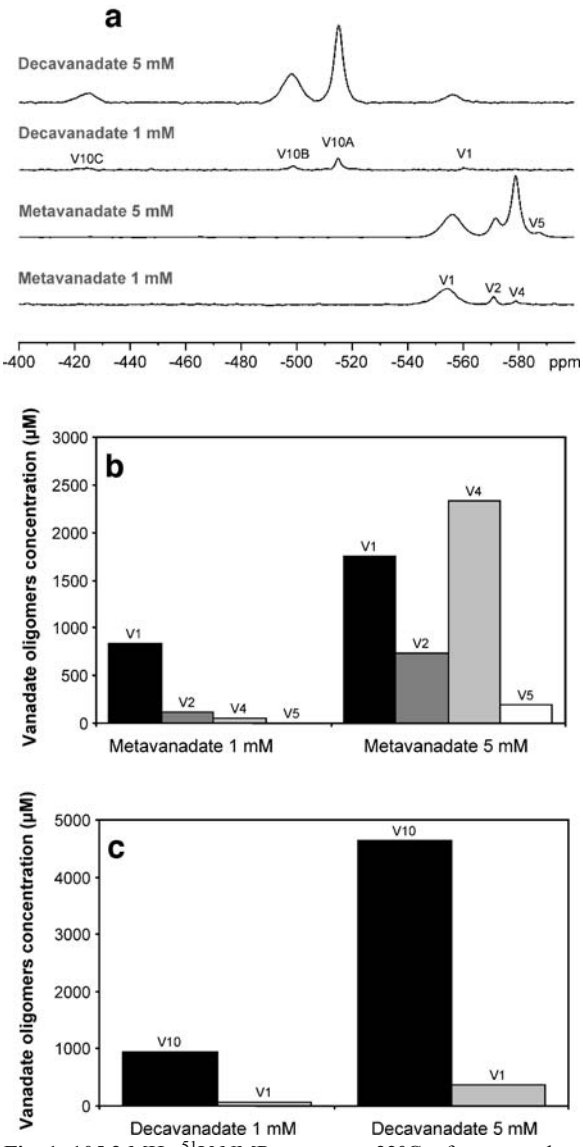

Fig. 1 105.2 MHz ^{51}V NMR spectra, at 22°C, of two vanadate concentrations (total vanadate), namely, 1 and 5 mM of decavanadate and metavanadate in DMEM, pH 7.1. (**a**) V1 and V2 signals correspond to monomeric ($H_2VO_4^-$) and dimeric ($HV_2O_7^{3-}$ and $H_2V_2O_7^{2-}$) vanadate species, respectively, irrespective of the protonation state, whereas V4 and V5 correspond to cyclic tetrameric ($V_4O_{12}^{4-}$) and pentameric ($V_5O_{15}^{5-}$) vanadate species. V10A, V10B and V10C signals correspond, respectively, to the V(2), V(1) and V(3) vanadium atoms in the decameric vanadate specie ($V_{10}O_{28}^{6-}$). The concentrations of each vanadium (V) species for metavanadate (**b**) and decavanadate (**c**) solutions were calculated from the fractions of the total integrated areas observed in the spectra. For quantitative measurements, spectral parameters were kept constant and the spectra were normalized regarding 5 mM decavanadate spectra

In this sense, ^{51}V-NMR spectroscopy is not adequate to follow the decomposition kinetics of decavanadate, in particular for vanadate concentrations lower than 1 mM. However, the disappearance of decameric vanadate species can be easily followed by ultraviolet/visible (UV/Vis) spectroscopy. Therefore, the stability of decameric species in DMEM was analysed by UV/Vis, at 33°C, using a 250 μM decavanadate solution (total vanadium concentration, meaning 25 μM decameric vanadate species). It was observed that in DMEM, decameric species decompose through a first-order kinetic, with a half-life time of 150 min (not shown).

Long- and short-term exposure to meta- and decavanadate

Cytotoxicity of vanadate oligomers on VSa13 cells was tested in confluent cultures for either 15 days using concentrations ranging from 0 to 250 μM (chronic toxicity) or 4 h using a concentration of 1 mM (acute toxicity). Prolonged exposure to meta- or decavanadate similarly affected VSa13 cell viability (Fig. 2): treatments with concentrations up to 7.5 μM did not decrease cell viability (a slight increase was even observed after 15 days), while treatments with concentrations from 10 to 250 μM seriously affected cell viability, killing most of the cells at highest concentrations. On the contrary, short-term exposure to meta- and decavanadate differentially affected VSa13 cell viability (Fig. 3): While 1 mM decavanadate significantly reduced cell viability after 2 hours, 1 mM metavanadate showed no effects. After 4 hours, both solutions significantly (according to ANOVA analysis) reduced the cell viability to levels approximate to 50%. This observation suggests that decameric vanadate species, still present in culture medium after 2 h, are likely to induce more toxicity effects than monomeric vanadate species, certainly the most abundant vanadate form found in culture medium after 4 h (half-life time of decavanadate in DMEM was estimated at 2.5 h) upon decameric vanadate disintegration.

Stimulation of cell proliferation by vanadate

Vanadate effect on VSa13 cell proliferation rate was also investigated in dividing cultures (Fig. 4), and both metavanadate and decavanadate exhibited similar effects (thus, only metavanadate results are shown), *i.e.* a significant stimulation of proliferation rate was observed for 7.5 μM concentration (accord-

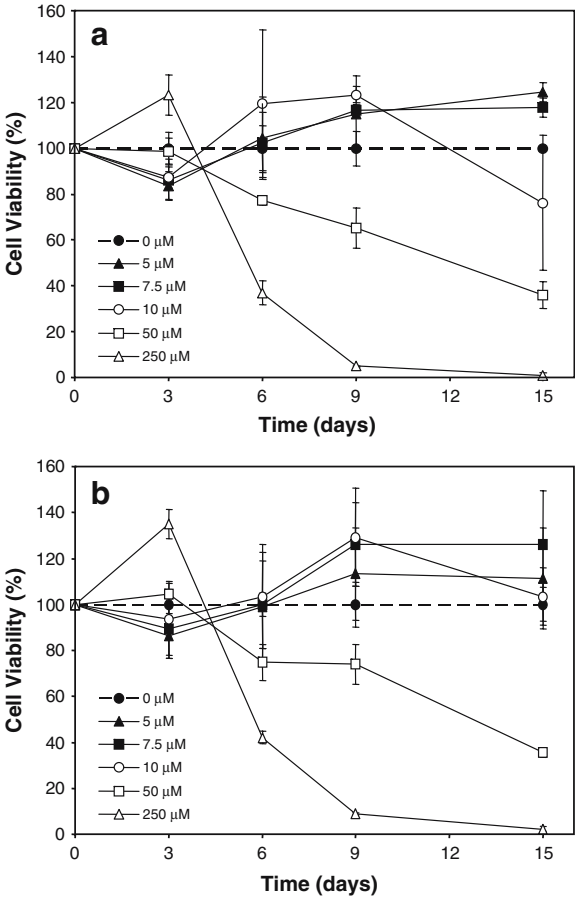

Fig. 2 Long-term effect of metavanadate and decavanadate on VSa13 cell viability. VSa13 cells were seeded in 96-well plates, grown in DMEM until confluence then treated with metavanadate (**a**) and decavanadate (**b**) using concentrations ranging from 5 to 250 μM. Cell viability was evaluated at appropriate times using MTS assay and is presented as the percentage of control value (set to 100%). Values are the mean of at least three independent experiments

ing to ANOVA analysis). On the contrary, 10 nM insulin (concentration used in mammalian bone-derived cell line, Quarto et al. 1992), had no effect on cell proliferation (Fig. 4) suggesting that vanadate, despite proven insulin-mimetic properties, stimulates cell proliferation. Nevertheless, no effects were observed in cell proliferation using insulin concentrations up to 100 nM (not shown).

Metavanadate and decavanadate exhibit different rates of accumulation in cells

The amount of vanadium accumulated within VSa13 cells was determined in confluent cultures treated with 10 μM meta- or decavanadate for 0, 1, 2, 4, 8 and 24 h after subtraction of vanadium content measured in non-treated cells (2.54±0.43 μg V/g of protein) (Fig. 5). After 1 h of treatment, vanadium accumulation was higher in cells treated with metavanadate (4.61±0.29 μg V/g of protein) than in cells treated with decavanadate (3.24±0.24 μg V/g of protein), being the effect statistically significant (according to Student's *t* test). A similar, but more pronounced, difference between meta- and decavanadate-related vanadium accumulations was observed after 2 h of treatment (6.85±0.4 μg and 3.95±0.1 μg V/g of protein, respectively). Longer incubation times resulted in a higher accumulation of vanadium (approximately 18-fold increase above control value after 24 h), but no significant differences were observed between metavanadate and decavanadate treated cells, as expected. These results suggest that monomeric species enter VSa13 cells and accumulate more easily than decameric species and that accumulation rates become similar only when most of decameric molecules are decomposed (half-life time of decavanadate in DMEM was estimated at 2.5 h).

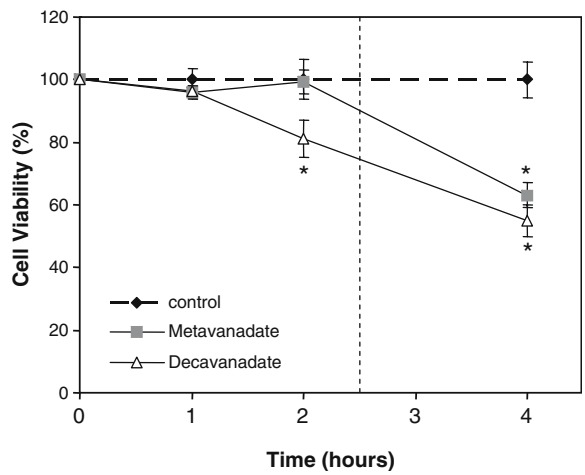

Fig. 3 Short-term effect of metavanadate and decavanadate on VSa13 cell viability. VSa13 cells were seeded in 96-microwell plates, grown in DMEM until confluence then treated with 1 mM metavanadate and decavanadate. Cell viability was evaluated at appropriate times using MTS assay and is presented as the percentage of control value (set to 100%). Values are the mean of at least three independent experiments. *Asterisk* indicates that values are statistically different in comparison to the respective control ($P<0.05$ one-way ANOVA). *Dashed line* indicates the half-life of decavanadate in DMEM estimated at 2.5 h

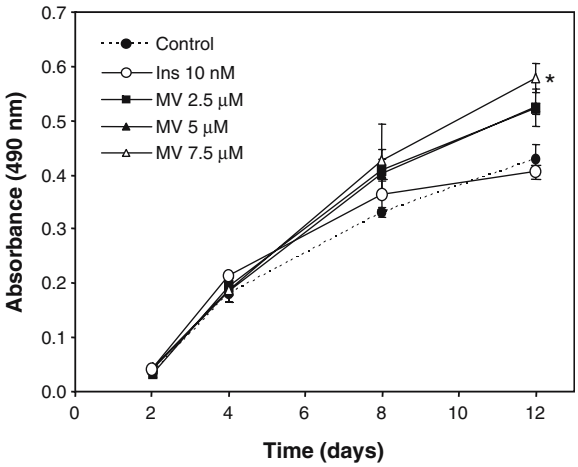

Fig. 4 Effect of metavanadate and insulin on VSa13 cell proliferation. VSa13 cells were seeded in 96-well plates at 1.5×10^3 cell/well then treated with metavanadate using concentrations ranging from 2.5 to 7.5 μM or 10 nM insulin. Cell proliferation was evaluated at appropriate times using MTS assay. Values are the mean of at least three independent experiments. *Asterisk* indicates that values are statistically different in comparison to the respective control ($P<0.05$ one-way ANOVA)

Discussion

The effects of vanadium on bone biology have been extensively studied in several mammalian *in vivo* and *in vitro* systems (Etcheverry and Cortizo 1998; Shechter 1990), but, to our knowledge, no studies have been performed using bone-derived systems of aquatic vertebrate origin. In this study, we analyse, for the first time, the effects different vanadate oligomers have on bone-derived cell line mineralization. However, the composition of vanadate solutions is very sensitive to vanadate concentration, pH, buffer and other compounds used in biochemical studies. Therefore, it is of primary importance to precisely characterise the species that can interact with a system before attempting to understand the effects promoted by vanadate solutions. Unlike metavanadate containing several oxovanadates, decavanadate solutions contain decameric vanadate species (V10). However, V10 is unstable and decomposes into monomeric vanadate with a half-life time of above 2 h in DMEM. In this regard, effects of decavanadate were always compared with those of metavanadate.

Vanadate and insulin decrease ECM mineralization

Vsa13 cells were cultured under mineralizing conditions for 4 weeks. Then, extracellular matrix mineralization was evaluated by densitometric analysis of von Kossa staining. The effects of vanadate (5 μM) and insulin (10 nM) on ECM mineralization were tested separately or in combination (Fig. 6). Vanadate 7.5 μM concentration was excluded from this experiment because of cytotoxic effects observed after 4 weeks of treatment (data not shown). Insulin, metavanadate and decavanadate significantly decreased ECM mineralization (according to ANOVA analysis), although to different extents: 31%, 74% and 78% decrease for insulin, meta- and decavanadate, respectively. The combination of insulin with any of the vanadate oligomers resulted in a more pronounced decrease (88% and 86%, respectively), although not significant (according to ANOVA analysis), suggesting an additive effect. A lower concentration of vanadate (2.5 μM) was also tested and shown to exhibit a similar, but less pronounced, decrease (data not shown) indicating a dose-dependent inhibition of ECM mineralization by vanadate oligomers.

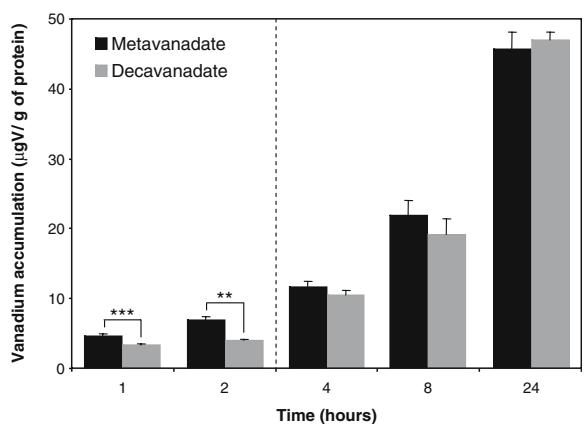

Fig. 5 Vanadium accumulation in VSa13 cells upon vanadate solutions exposure. VSa13 cells were seeded in 100-mm plates, grown in DMEM until confluence then treated with 10 μM metavanadate or decavanadate. At appropriate times, vanadium content was determined by atomic absorption from cellular extract and normalized with protein content. Vanadium content measured in non-treated samples (2.54±0.43 μg V/g of protein) was subtracted from each value. *Asterisks* indicate statistically significant differences between metavanadate and decavanadate according to Student's test (**$p<0.005$ and ***$p<0.001$). Values are the mean of at least three independent experiments. *Dashed line* indicates the half-life of decavanadate in DMEM estimated at 2.5 h

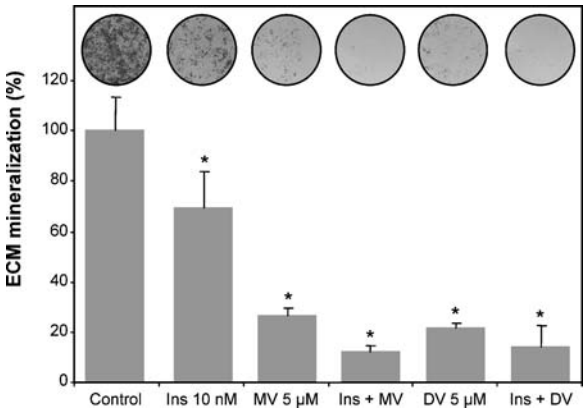

Fig. 6 Effect of metavanadate, decavanadate and insulin on extracellular matrix mineralization. VSa13 cells were seeded in 24-well plates, grown in DMEM until confluence then treated for mineralization. Mineralizing cultures were subsequently treated with 10 nM insulin (Ins), 5 μM metavanadate (MV), 5 μM decavanadate (DV), metavanadate and insulin (Ins+MV), decavanadate and insulin (Ins+DV) or left untreated. Mineral deposition was revealed by von Kossa staining and evaluated by densitometric analysis. Pictures of von Kossa-stained VSa13 cells are presented above each treatment. Values are the mean of at least three independent experiments. *Asterisk* indicates that values are statistically different in comparison to the respective control ($P<0.05$ one-way ANOVA)

Monomeric and decameric vanadate species affect VSa13 cells differently

Prolonged exposure to low levels of meta- and decavanadate similarly affected VSa13 cell viability and proliferation, whereas short-term exposure to high levels of decavanadate was more toxic than that of metavanadate. In DMEM, decavanadate decomposes into monomeric species with a half-life time of ~150 min, suggesting that its long-term effects are most probably caused by newly formed monomeric species (as for metavanadate), whereas short-term effects are likely caused by decameric vanadate species. Considering that decavanadate solution contains 10 times less molecules (particularly in shorter exposure times, in which decameric species are predominant) than metavanadate (in which monomeric species are predominant), short-term toxicity of decavanadate is even more remarkable. This result is consistent with previous observations that decavanadate and metavanadate produce different oxidative stress levels in cardiac muscle in toadfish and gilthead seabream (Aureliano et al. 2002; Soares et al. 2007) and interact differently *in vitro* with specific proteins such as myosin and sarcoplasmic reticulum Ca^{2+}-ATPase (Aureliano and Madeira 1994; Tiago et al. 2004; Aureliano and Gândara 2005). Prolonged exposure to low levels of vanadate resulted in an apparent increase in cell viability/number, an effect that was previously observed in mammalian bone-derived cell cultures (MC3T3E1 and UMR106) (Barrio et al. 1997; Cortizo et al. 2000; Etcheverry et al. 1997; Salice et al. 1999) and attributed to its ability to increase phosphotyrosine protein levels and to inhibit phosphotyrosine phosphatases, thus regulating growth signalling pathways.

Although cellular accumulation of metavanadate has been previously demonstrated in mammalian systems, *e.g.* bovine kidney and Caco-2 cells (Bracken et al. 1985; Yang et al. 2004), this process has never been analysed in a comparative study with decavanadate. We present evidences that vanadium differently accumulates in VSa13 cells treated with metavanadate or decavanadate solutions (decavanadate treatments resulted in significantly lower vanadium accumulation at 1 and 2 h; Fig. 5), which was probably caused by an inexistent or a less efficient uptake mechanism for decameric species.

Vanadate stimulates VSa13 cell proliferation

Both vanadate oligomers exhibited a similar effect on VSa13 growth rate, *i.e.* a stimulation of cell proliferation. A similar effect has been reported in mammalian bone-derived cell lines and associated with the activation of the insulin receptor. Insulin was shown not to affect VSa13 cell proliferation, indicating that either insulin receptor/signalling pathway is absent in VSa13 cells (this hypothesis was later ruled out after insulin was shown to affect ECM mineralization) or vanadate stimulating effect is not mediated through insulin signalling pathway. Several studies have already proposed cytosolic tyrosine kinase receptor as a mediator of vanadate proliferative effect (Shisheva and Shechter 1992, 1993), and we propose that a similar mechanism could occur in VSa13 cells.

Inhibition of ECM mineralization by vanadate

Mineralization of VSa13 extracellular matrix was mildly reduced by insulin, strongly inhibited by vanadate, regardless of its oligomerization (monomeric or decameric), and even more strongly inhibited

when both insulin and vanadate were present. Two important regulatory effects have been associated with vanadium osteogenic action in mammalian bone-derived cells: the inhibition of alkaline phosphatase activity and the stimulation of type I collagen synthesis (Barrio and Etcheverry 2006; Canalis 1985b; Lau et al. 1988). Both processes are essential to the correct mineralization of the extracellular matrix of bone cells (Murshed et al. 2005), and it is likely that vanadium effect on vertebrate bone depends on the equilibrium between its stimulatory and inhibitory properties. Vanadium derivatives were previously shown to specifically activate insulin-associated pathways (i.e. MAPK and PI-3K pathways) through phosphorylation of common intermediates such as extracellular signal-regulated kinase (ERK) (Barrio and Etcheverry 2006). Moreover, vanadium proliferative effect was reverted by specific inhibitors of insulin-associated pathways. In one of those studies, vanadyl (IV)-ascorbate, a vanadium complex, significantly increased the rate and extent of mineral deposition within the ECM of mouse MC3T3-E1 bone-derived cells and stimulated type I collagen synthesis (Cortizo et al. 2006). These effects were apparently related to both MAPK and PI-3K pathways activation and ERK increased phosphorylation. In another study, it was described that the alkaline phosphatase activity is inhibited in MC3T3-E1 cells by a trehalose vanadyl complex independently of regular insulin-associated pathways. Based on published results, we suggest that vanadate inhibitory effect on VSa13 ECM mineralization could be associated with either direct interference of vanadium into key processes such as alkaline phosphatase activity, or indirect interference of vanadium into insulin-associated pathways. Recently, it was shown that the ECM mineralization of MC3T3-E1 cells is inhibited by platelet-derived growth factor through ERK activation (Kono et al. 2007). This result is, on one hand, contradictory to a previous observation where ECM mineralization of MC3T3-E1 cells was stimulated by vanadium through ERK activation (Cortizo et al. 2006), but, on the other hand, in total agreement with the inhibition of VSa13 ECM mineralization by vanadate, possibly through ERK activation. The characterisation of the mechanisms involved in vanadate inhibitory effect in VSa13 cell line will need to be investigated in future studies.

Conclusion

Vanadate was shown here to accumulate within VSa13 bone-derived cells, stimulating growth performance through insulin-independent mechanisms and preventing ECM mineralization probably through multiple processes involving regulation that may or may not depend on the activation of insulin-stimulated pathways. The presence of decameric vanadate species was also shown to produce differences (accumulation and cytotoxicity) between meta- and decavanadate in short-term exposure while acting similarly in prolonged exposure caused eventually by the decomposition of decavanadate into other oligomers. VSa13 cells were shown to be a suitable model to study vanadium mechanisms of action in vertebrate bone development and to be a good alternative to mammalian systems.

Acknowledgements The authors thank Dr. Hélio Martins from the Faculty of Sciences and Technology (FCT) of the University of Algarve for his technical help in the course of atomic absorption spectrometry experiments. Thanks also to J.J.G. Moura, REQUIMTE, New University of Lisbon, for the esteemed collaboration in the NMR studies. DMT was the recipient of a Ph.D. fellowship (BD/12773/2003) from the Portuguese Science and Technology Foundation.

References

Amado AM, Aureliano M, Ribeiro-Claro PJA, Teixeira-Dias JJ. Combined Raman and V-51 NMR spectroscopic study of vanadium (V) oligomerization in aqueous alkaline-solutions. J Raman Spectrosc 1993;24:699–703.

Anke M. Vanadium – An element both essential and toxic to plants, animals and humans? Anal Real Acad Nac Farm 2004;70:961–99.

Aureliano M, Madeira VM. Interactions of vanadate oligomers with sarcoplasmic reticulum Ca(2+)-ATPase. Biochim Biophys Acta 1994;1221:259–71.

Aureliano M, Gandara RM. Decavanadate effects in biological systems. J Inorg Biochem 2005;99:979–85.

Aureliano M, Joaquim N, Sousa A, Martins H, Coucelo JM. Oxidative stress in toadfish (Halobactrachus didactylus) cardiac muscle. Acute exposure to vanadate oligomers. J Inorg Biochem 2002;90:159–65.

Barrio DA, Etcheverry SB. Vanadium and bone development: putative signaling pathways. Can J Physiol Pharmacol 2006;84:677–86.

Barrio DA, Braziunas MD, Etcheverry SB, Cortizo AM. Maltol complexes of vanadium (IV) and (V) regulate in vitro alkaline phosphatase activity and osteoblast-like cell growth. J Trace Elem Med Biol 1997;11:110–5.

Bracken WM, Sharma RP, Elsner YY. Vanadium accumulation and subcellular distribution in relation to vanadate induced cytotoxicity in vitro. Cell Biol Toxicol 1985;1:259–68.

Canalis E. Effect of sodium vanadate on deoxyribonucleic acid and protein synthesis in culture rat calvariae. Endocrinology 1985a;116:855–62.

Canalis E. Effect of sodium vanadate on deoxyribonucleic acid and protein syntheses in cultured rat calvariae. Endocrinology 1985b;116:855–62.

Cheatham B, Kahn CR. Insulin action and the insulin signaling network. Endocr Rev 1995;16:117–42.

Cohick WS, Clemmons DR. The insulin-like growth factors. Annu Rev Physiol 1993;55:131–53.

Cortizo AM, Etcheverry SB. Vanadium derivatives act as growth factor-mimetic compounds upon differentiation and proliferation of osteoblast-like UMR106 cells. Mol Cell Biochem 1995;145:97–102.

Cortizo AM, Bruzzone L, Molinuevo S, Etcheverry SB. A possible role of oxidative stress in the vanadium-induced cytotoxicity in the MC3T3E1 osteoblast and UMR106 osteosarcoma cell lines. Toxicology 2000;147:89–99.

Cortizo AM, Molinuevo MS, Barrio DA, Bruzzone L. Osteogenic activity of vanadyl(IV)-ascorbate complex: evaluation of its mechanism of action. Int J Biochem Cell Biol 2006;38:1171–80.

Crans DC, Smee JJ, Gaidamauskas E, Yang L. The chemistry and biochemistry of vanadium and the biological activities exerted by vanadium compounds. Chem Rev 2004;104:849–902.

Dubyak GR, Kleinzeller A. The insulin-mimetic effects of vanadate in isolated rat adipocytes. Dissociation from effects of vanadate as a (Na+-K+) ATPase inhibitor. J Biol Chem 1980;255:5306–12.

Etcheverry SB, Cortizo AM. Bioactivity of vanadium compounds on cells in culture. In: Nriagu JO, editor. Vanadium in the environment. New York: John Wiley & Sons; 1998.

Etcheverry SB, Apella MC, Baran EJ. A model study of the incorporation of vanadium in bone. J Inorg Biochem 1984;20:269–74.

Etcheverry SB, Crans DC, Keramidas AD, Cortizo AM. Insulin-mimetic action of vanadium compounds on osteoblast-like cells in culture. Arch Biochem Biophys 1997;338:7–14.

Goldwaser I, Gefel D, Gershonov E, Fridkin M, Shechter Y. Insulin-like effects of vanadium: basic and clinical implications. J Inorg Biochem 2000;80:21–5.

Heyliger CE, Tahiliani AG, McNeill JH. Effect of vanadate on elevated blood glucose and depressed cardiac performance of diabetic rats. Science 1985;227:1474–7.

Kato Y, Iwamoto M, Koike T, Suzuki F. Effect of vanadate on cartilagematrix proteoglycan synthesis in rabbit costal chondrocyte cultures. J Cell Biol 1987;104:311–9.

Kono SJ, Oshima Y, Hoshi K, Bonewald LF, Oda H, Nakamura K, et al. Erk pathways negatively regulate matrix mineralization. Bone 2007;40:68–74.

Lau KH, Tanimoto H, Baylink DJ. Vanadate stimulates bone cell proliferation and bone collagen synthesis in vitro. Endocrinology 1988;123:2858–67.

LeRoith D. Insulin-like growth factor I receptor signaling-overlapping or redundant pathways? Endocrinology 2000; 141:1287–8.

Malich G, Markovic B, Winder C. The sensitivity and specificity of the MTS tetrazolium assay for detecting the in vitro cytotoxicity of 20 chemicals using human cell lines. Toxicology 1997;124:179–92.

McCarthy TL, Ji C, Centrella M. Links among growth factors, hormones, and nuclear factors with essential roles in bone formation. Crit Rev Oral Biol Med 2000;11:409–22.

Meyerovitch J, Farfel Z, Sack J, Shechter Y. Oral administration of vanadate normalizes blood glucose levels in streptozotocin-treated rats. Characterization and mode of action. J Biol Chem 1987;262:6658–62.

Moriyama S, Ayson FG, Kawauchi H. Growth regulation by insulin-like growth factor-I in fish. Biosci Biotechnol Biochem 2000;64:1553–62.

Murshed M, Harmey D, Millan JL, McKee MD, Karsenty G. Unique coexpression in osteoblasts of broadly expressed genes accounts for the spatial restriction of ECM mineralization to bone. Genes Dev 2005;19:1093–104.

Nielsen FH, Uthus EO. The essentiality and metabolism of vanadium. In: Chasteen ND, editor. Vanadium in biological systems. Boston: Kluwer Academic Publishers; 1990.

Pombinho AR, Laize V, Molha DM, Marques SM, Cancela ML. Development of two bone-derived cell lines from the marine teleost Sparus aurata; evidence for extracellular matrix mineralization and cell-type-specific expression of matrix Gla protein and osteocalcin. Cell Tissue Res 2004;315:393–406.

Quarto R, Campanile G, Cancedda R, Dozin B. Thyroid hormone, insulin and glucocorticoids are sufficient to support chondrocyte differentiation to hypertrophy: a serum-free analysis. J Cell Biol 1992;119:989–95.

Rehder D. The coordination chemistry of vanadium as related to its biological functions. Coord Chem Rev 1999;182:297–322.

Rehder D. Biological and medicinal aspects of vanadium. Inorg Chem Commun 2003;6:604–17.

Salice VC, Cortizo AM, Gomez Dumm CL, Etcheverry SB. Tyrosine phosphorylation and morphological transformation induced by four vanadium compounds on MC3T3E1 cells. Mol Cell Biochem 1999;198:119–28.

Shechter Y. Perspective in diabetes: insulin-mimetic effects of vanadate. Possible implications for future treatment of diabetes. Diabetes 1990;39:1–5.

Shechter Y, Karlish SJ. Insulin-like stimulation of glucose oxidation in rat adipocytes by vanadyl (IV) ions. Nature 1980;284:556–8.

Shechter Y, Li J, Meyerovitch J, Gefel D, Bruck R, Elberg G, et al. Insulin-like actions of vanadate are mediated in an insulin-receptor-independent manner via non-receptor protein tyrosine kinases and protein phosphotyrosine phosphatases. Mol Cell Biochem 1995;153:39–47.

Shisheva A, Shechter Y. A cytosolic protein tyrosine kinase in rat adipocytes. FEBS Lett 1992;300:93–6.

Shisheva A, Shechter Y. Role of cytosolic tyrosine kinase in mediating insulin-like actions of vanadate in rat adipocytes. J Biol Chem 1993;268:6463–9.

Soares SS, Martins H, Aureliano M. Vanadium distribution following decavanadate administration. Arch Environ Contam Toxicol 2006;50:60–4.

Soares SS, Martins H, Duarte RO, Moura JJG, Coucelo J, Gutiérrez-Merino C, et al. Vanadium distribution, lipid peroxidation and oxidative stress markers upon decavanadate *in vivo* administration. J Inorg Biochem 2007; 101:80–8.

Tiago T, Aureliano M, Gutierrez-Merino C. Decavanadate binding to a high affinity site near the myosin catalytic centre inhibits F-actin-stimulated myosin ATPase activity. Biochemistry 2004;43:5551–61.

Yang XG, Yang XD, Yuan L, Wang K, Crans DC. The permeability and cytotoxicity of insulin-mimetic vanadium compounds. Pharm Res 2004;21:1026–33.

Research Signpost
37/661 (2), Fort P.O., Trivandrum-695 023, Kerala, India

Vanadium Biochemistry, 2007: 269-283 ISBN: 978-81-308-0184-1
Editor: Manuel Aureliano Alves

14

Vanadate effects on bone metabolism: Fish cell lines as an alternative to mammalian *in vitro* systems

Daniel M. Tiago, Vincent Laizé, Manuel Aureliano Alves and M. Leonor Cancela
Centre of Marine Sciences (CCMAR), University of Algarve, Faro, Portugal

Abstract

Vanadate, one of the most relevant forms of vanadium in solution, has been associated with the regulation of various enzyme activities (e.g. phosphatases, ribonucleases, ATPases, etc.) and shown to exhibit important biological effects. Several in vivo and in vitro studies have clearly demonstrated that any deficiency or excess of vanadium can seriously affect bone formation and its metabolism. Bone-related effects result largely from vanadium insulin-mimetic capabilities mediated by specific inhibition of protein tyrosine phosphatases

Correspondence/Reprint request: Dr. M. Leonor Cancela, CCMAR, University of Algarve, Campus de Gambelas 8005-139 Faro, Portugal. E-mail: lcancela@ualg.pt

(PTPases) and consequent activation of tyrosine kinase receptors (e.g. insulin receptor). Although mammals have been repetitively shown to be appropriate models to study vanadate mechanisms of action, fish have recently emerged as alternative models. Fish has been recognized as suitable model to study vertebrate bone formation and the natural presence of high quantities of vanadium in water makes it even more suitable to investigate vanadium effect on bone formation. Recent data obtained using fish bone-derived cells revealed that micromolar concentrations (5 μM) of monomeric and decameric vanadate slightly stimulate growth performances while strongly inhibiting extracellular matrix mineralization through mechanisms involving both alkaline phosphatase and MAPK pathways. Recent data obtained in fish cells will be discussed here and further compared to results obtained in mammalian systems.

1. Introduction

Vanadium is a trace element that has been shown to be essential for biological activity in various organisms [1-3]. In plants and algae, vanadium is directly involved in enzyme activity, acting as a cofactor in vanadium nitrogenases and vanadate-dependent haloperoxidases. In mammals, reduced doses of vanadium have been associated with poorly developed animals and higher rates of spontaneous abortion or mortality [4].

Biological effects of vanadium in vertebrates, in particular in mammals, essentially come from its capacity to interfere with several key enzymes, such as ATPases, phosphorylases, phosphatases (alkaline, acid and protein phosphatases) and ribonucleases [2]. This interference has been attributed to vanadium oxidation states V^{V} and V^{IV} (vanadate and vanadyl, respectively), which exhibit some analogy with phosphate, although to different extents (strong for vanadate and weak for vanadyl). Inhibition of phosphatases by vanadate was attributed to the formation of good transition state analogues during enzymatic catalysis [2,5] and a similar mechanism was proposed for vanadyl although its geometry of coordination is somewhat different to that of phosphate [2].

An important feature of vanadate resides in its capacity to promote distinct effects depending on its oligomerization (monomeric to decameric species according to pH and concentration [6]) as shown using *in vitro* and *in vivo* models [7-9]. For example, decameric species were shown, in fish, to induce higher oxidative stress, haemoglobin oxidation, stimulate antioxidant enzyme activities and generate more tissue damages than other oligomeric species [10-12], while monomeric species apparently accumulated at higher rates and doses in cardiac muscle, red blood cells and plasma [13]. Aspects related with decavanadate *in vivo* effects are reviewed in Chapter 9 of this book. Decameric

species also revealed stronger inhibition and affinity for ATPases, in particular myosin ATPase and sarcoplasmic reticulum (SR) Ca^{2+}- ATPase [9,14-16]. Decavanadate effects in the contractile system and in SR calcium pump are reviewed in Chapters 5 and 7 of this book, respectively.

The most important biological effect of vanadium is probably insulin mimicking. It was first demonstrated in the early 80's, when vanadate and vanadyl treatments applied to isolated rat adipocytes [17,18] were shown to stimulate hexose transport, glucose oxidation and lipogenesis, as insulin [19]. Additional *in vivo* studies showed that oral administration of vanadate to streptozocin-treated diabetic rats (STZ rats) resulted in decreased blood glucose to normal levels [20,21], confirming its action as a substitute of insulin. Vanadate was consequently proposed as a possible therapeutic agent for diabetes mellitus (insulin-dependent). However, the therapeutic use of vanadate has been seriously hampered by its relatively high toxicity [22,23]. Recent efforts have therefore focused on the discovery of chelators, which would reduce vanadyl and vanadate toxicity while preserving its insulin-mimetic properties [24].

Insulin-mimetic properties of vanadium have been associated to specific inhibition of protein tyrosine phosphatases (PTPases) and consequent activation of receptor-associated protein tyrosine kinase (PTK), including that of insulin receptor [23,25,26]. Alternatively, non-receptor PTK, *e.g.* insulin receptor substrate 1 (IRS-1), or cytosolic PTK can be activated [27]. Two pathways involved in vanadate intracellular signalling have been identified, both resulting in distinct effects (Figure 1). A common feature of both pathways is the activation of PTK domain in IRS-1 through phosphorylation of tyrosines. While metabolic effects are mediated by phosphatidylinositol-3 kinase (PI-3K) activation, effects on cell proliferation and differentiation result from the activation of mitogen-responsive protein kinases (MAPK) [28]. Alternatively, specific insulin-like effects, *e.g.* glycogen synthase activation, have been associated to PI-3K/Ras/ERK activation [27].

While most studies investigating vanadium effects have been performed in adipose tissue, bone has recently emerged as a system of interest after its regulation by insulin and IGF1 was demonstrated [1,29-31] and after vanadium was shown to accumulate in mammalian bones [32] and affect bone formation when absent from diet [4,33]. Accumulation of vanadium within bone, was first proposed to be related to a detoxification process [34,35]. Severe malformations occurring in bone of animals lacking vanadium however suggested that it could interact with specific growth factor-dependent signalling, in particular those known to control bone development: platelet-derived growth factor (PDGF), fibroblast growth factors (FGF1 and 2), insulin, insulin-like growth factors (IGF1 and 2), transforming growth factors beta (TGF-β1, 2 and 3), and bone morphogenetic proteins (BMP) [30,36]. Because

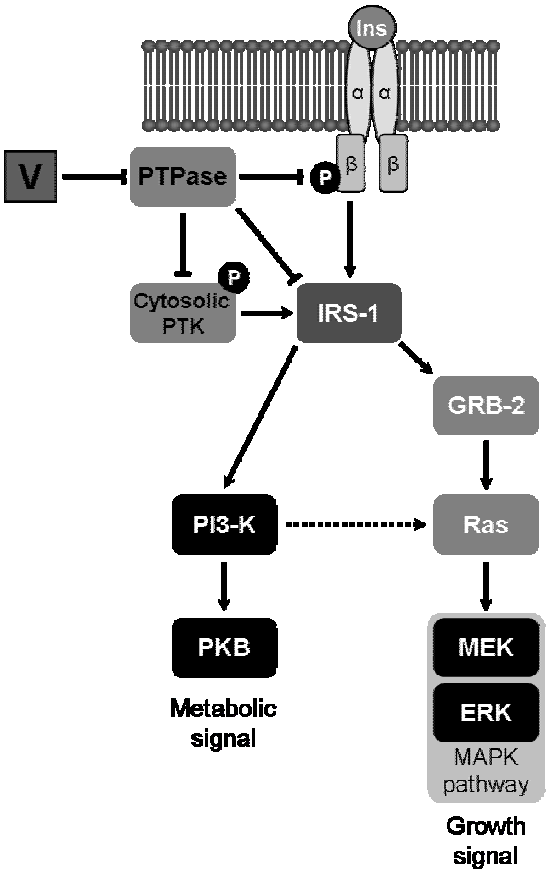

Figure 1. Insulin signalling pathways and putative regulation by vanadium. Ins indicates insulin peptide; V indicates vanadium; α and β represent the subunits of insulin tyrosine kinase receptor; circled P represents phosphorylation of tyrosines in PTK domain within the β subunit of insulin receptor; PKB indicates protein kinase B, the activated intermediate in PI-3K pathway. GRB-2, Ras, MEK and ERK indicate intermediate adaptor proteins in MAPK pathways.

insulin, IGFs and TGF-β bind to specific tyrosine kinase receptors and are involved in osteoblast differentiation, they have been therefore considered as putative targets for vanadium. Effects due to insulin and IGF mimicking action of vanadium, were first demonstrated *in vitro* by Canalis and colleagues, who showed that concentrations below 15 μM of sodium vanadate increased DNA synthesis and mitotic index of rat calvaria primary cultures [31]. Since then,

two mammalian cell lines, MC3T3-E1 (developed from newborn mouse calvaria, composed of pre-osteoblasts and able to mineralize extracellular matrix (ECM) [37]) and UMR106 (developed from rat osteosarcoma, composed of differentiated osteoblasts and unable to mineralize the ECM [38]) were shown to be particularly useful in understanding insulin and IGF mimicking effects of vanadium in bone and important features like tyrosine kinase receptors phosphorylation (with consequent activation) and activation of signalling mechanisms have been characterized [39].

Until recently, effects of vanadate on bone metabolism have been exclusively characterized *in vitro* using these two mammalian bone-derived cell lines [39]. The recent contribution of a fish-bone derived cell line to this characterization is hereby described and results obtained compared to those derived from studies on mammalian cell lines and its suitability as an *in vitro* model system to study these effects is further discussed.

2. Mammalian cell lines as *in vitro* models to study vanadium mechanisms of action in bone

Primary cell cultures of rat and chicken calvaria were the first *in vitro* systems used to investigate vanadium insulin-like effects in bone [31,40] and have contributed to the characterization of osteogenic action of vanadium in mammals including the inhibition of alkaline phosphatase (ALP) activity and the stimulation of type-I collagen synthesis [39], two mechanisms essential to the correct mineralization of the extracellular matrix of bone cells [41]. Osteogenic actions of vanadate are also described in Chapter 13 of this book. The key role of growth factors, *e.g.* IGF1, and tyrosine protein phosphorylation in the mediation of vanadium action was later demonstrated using mouse MC3T3-E1 and rat UMR106 cell lines [39]. Osteoblastic differentiation of these cells, monitored through the measurement of ALP activity, was show to be inhibited by vanadate, vanadyl, hydroperoxo- and peroxo-vanadium, in agreement with previous observations in primary bone-derived cultures [42]. Interestingly, enzymatic activity of PTPases was also shown to be inhibited in treated cells, suggesting a probable signalling interference with insulin and other growth factors that bind to tyrosine kinase receptors. In more recent experiments, vanadate, vanadyl and pervanadate were shown to stimulate cell proliferation at low doses, while higher doses severely arrested growth [43]. Primitive vanadium complexes (vanadium oxalate, citrate, tartrate and nitrilotriacetate) tested in mammalian MC3T3-E1 and UMR106 bone-derived cell lines revealed effects similar to those of vanadate: stimulation of cell proliferation, glucose consumption and protein content. It is worth to note that both vanadate and vanadium nitriloacetate exhibited a stronger inhibition of UMR106 cells differentiation [44]. However, complex toxicity was still high.

The new generation of vanadium complexes (*e.g.* bis(maltolato)oxovanadium (IV) - BMOV - and bis(maltolato)dioxovanadium(V) - BMV) also exhibited effects similar to those of vanadium but revealed lower toxicity rates (BMV). All treatments with these complexes promoted cell growth in a biphasic manner, as well as increased phosphorylation of tyrosine residues, consistent with previous observation of strong inhibition of PTPases. In addition, BMOV, like vanadate, strongly inhibited ALP activity [45,46]. Similar results have been observed when using vanadyl/aspirin complex [47,48]. Relevant information concerning vanadium regulatory mechanisms associated to insulin signalling pathways were obtained only recently. Involvement of MAPK and PI-3K pathways in vanadium osteogenic effects was investigated using two complexes, trehalose vanadyl (TreVO) and vanadyl ascorbate (VOAsc) [49,50] and specific inhibitors of these pathways. While stimulation of cell proliferation and type-I collagen synthesis were shown to be mediated by an insulin-dependent mechanism, stimulation of glucose consumption and inhibition of ALP activity were apparently mediated by an insulin-independent mechanism. Another important observation was the increased phosphorylation of key intermediates of these cascades upon vanadium treatments. One of the major subfamilies of the MAP kinases, the extracellular signal-regulated kinase (ERK), has been shown to be phosphorylated / activated in UMR106 and MC3T3-E1 cells after vanadium treatments. This effect is apparently mediated by a PI-3K/ras/ERK (extracellular signal-regulated kinase) pathway [39]. This mechanism is probably essential to explain vanadium effect in bone and will be further discussed.

Although vanadium insulin-dependent and insulin-independent actions have been already described in mammalian bone-derived *in vitro* systems, there is a lack of information concerning other vertebrate bone-derived systems, in particular those derived from marine vertebrate species.

3. Teleost fish bone-derived cell lines as an alternative to mammalian systems to study vanadium effects in bone

VSa13 bone-derived cell line has been recently developed from the vertebra of *Sparus aurata*, a marine teleost fish, and fully characterized [51]. This cell line is capable of mineralizing its extracellular matrix under appropriate culture conditions and has been associated to the chondrocyte lineage, as suggested by a relatively high expression of matrix gla protein (a calcification inhibitor normally produced by chondrocytes in cartilage), no expression of osteocalcin (an osteoblastic marker) and strong alcian blue staining (normally associated with cartilage extracellular matrix). The suitability of VSa13 cells to study *in vitro* vanadium insulin-like action on

bone was confirmed by its responsiveness to insulin treatments (10 nM insulin was shown to decrease by 25% the degree of ECM mineralization in VSa13 cell [52]). To date, only vanadate oligomeric solutions have been tested in VSa13 cells. Metavanadate (containing n-meric species with n = 1-5) and decavanadate (n = 1 or 10) effects on VSa13 cells viability, growth, vanadium accumulation and ECM mineralization have been investigated [52]. Vanadate oligomerization did not originate differences in toxicity levels after prolonged exposures (metavanadate and decavanadate solutions were shown to be non-toxic at concentrations below 10 μM during 15 days). However, decameric species exhibited higher toxicity after 2 h of treatment using 1 mM concentration (acute toxicity). Similarly, accumulation of vanadium in VSa13 cells was oligomerization-independent from 4 to 24 h but much slower for decavanadate within the first 2 h of treatment. These results were shown to be coherent with decameric species decomposition rate into monomeric species (half-life time of approximately 150 min), suggesting that decavanadate long-term effects resulted mainly from monomeric species. However, in short-term treatments in which decameric species were still present in solution, vanadate was shown to accumulate much slower in cells, and to induce higher toxicities. These results reinforced the hypothesis of the higher toxicity of species highly oligomerized, which are probably formed in specific cellular environments (*e.g.* in which the pH is low). Merged results of long-term treatments by monomeric and decameric vanadate indicate that cell proliferation was stimulated (Figure 2) in a dose-dependent manner. The observation that insulin did not stimulate VSa13 cell proliferation (inset of Figure 2) suggested that mitogenic pathways may not be controlled by this hormone in these cells. It also suggested that vanadate effects on cell proliferation were not mediated through insulin signalling pathways, and possibly involving other PTK.

However, mineralization of VSa13 ECM was later shown to be negatively regulated by insulin [52] (Figure 3), demonstrating the presence of insulin receptors and signalling pathways in these cells. ECM mineralization was also inhibited by vanadate in VSa13 cells, and combined treatments with insulin and vanadate resulted in stronger inhibition (31%, 76% and 87% inhibition in cells treated with insulin, vanadate and insulin + vanadate, respectively; Figure 3). Effect of vanadium on ECM mineralization in mammals has been reported in a recent study [50]. Surprisingly, vanadyl(IV)-ascorbate complex strongly increased mineral deposition within ECM of MC3T3-E1 (up to 20-fold using concentrations from 5 to 25 μM). This result, at the opposite of that observed in fish bone-derived cells, was even more surprising considering the mild effects of vanadium on bone markers: ALP activity was maintained or slightly decreased and type-I collagen synthesis was only slightly increased (approximately 10%). The opposite effect of vanadium on ECM mineralization observed in VSa13 and MC3T3- E1 cells may be related to the species studied

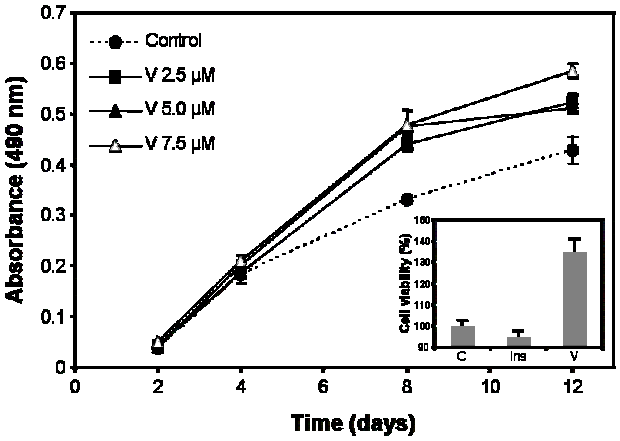

Figure 2. Vanadate and insulin effects on VSa13 cell proliferation. VSa13 cells were seeded in 96-well plates at 1.5×10^3 cell/well then treated with metavanadate and decavanadate using concentrations ranging from 2.5 to 7.5 µM. Cell viability was evaluated at appropriate times using MTS assay. Inset indicates vanadate (5 µM) effect on VSa13 cell proliferation compared with that of insulin (10 nM) after 12 days of treatment. Vanadate values are the mean of metavanadate and decavanadate merged data resulting from at least six independent experiments. Insulin values are the mean of at least 3 independent experiments.

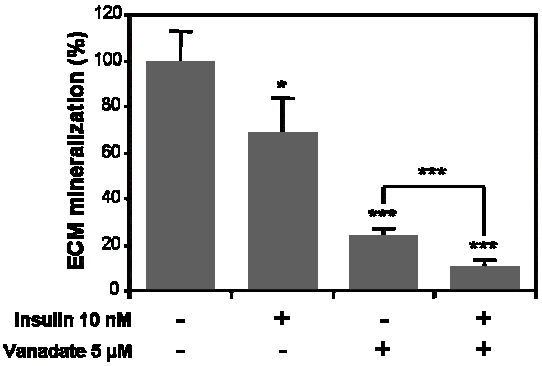

Figure 3. Effect of vanadate and insulin on VSa13 extracellular matrix (ECM) mineralization. Mineral deposition was revealed by von Kossa staining and evaluated by densitometric analysis. Values are the mean of metavanadate and decavanadate merged data resulting from at least six independent experiments. Asterisks indicate statistically significant differences compared to control (or between conditions) according to Student's test (* $p < 0.05$, *** $p < 0.001$).

(fish *versus* mammal) or the cell types used (osteoblast *versus* chondrocyte) and will require additional studies in the future.

Data obtained from VSa13 cells suggested that vanadate effect on ECM mineralization probably involves insulin-signalling pathways, but the contribution of other mechanisms must also be considered. In that aspect, preliminary data obtained in VSa13 cells indicated a strong decrease in ALP activity in vanadate-treated cells during ECM mineralization (Figure 4; our unpublished results). ALP activity in VSa13 cells was demonstrated to be up regulated during ECM mineralization [51], which is consistent with a differentiation process, but treatments with 5 µM monomeric vanadate have shown to massively decrease this activity. Specific inhibitors should be tested, in order to evaluate to what extent, and which insulin signalling pathways are mediating vanadate inhibition of ECM mineralization. Preliminary data from experiments using MAPK and PI-3K inhibitors (PD98059 and wortmannin, respectively) have involved mitogenic pathways (possibly through PI-3K/ras/MAPK signalling pathways). This issue will be further discussed in the next section of this chapter.

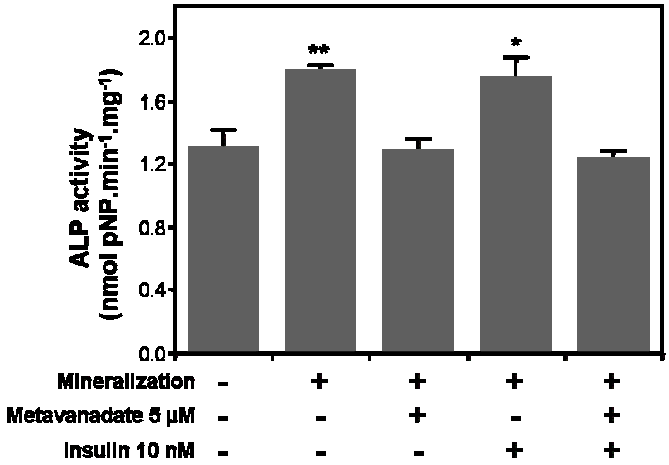

Figure 4. Effect of vanadate and insulin on alkaline phosphatase (ALP) activity of VSa13 cells during extracellular matrix (ECM) mineralization. Extracts from ECM mineralized cells alternatively treated with either insulin alone or metavanadate alone, or both, were collected in 0,1% (v/v) Triton X-100; samples ALP activity was evaluated in 50 mM glycine plus 0.5 mM $MgCl_2$ reaction buffer using 0.5 mM pNP-P (p-nitrophenyl-phosphate) as substrate. Values are the mean of at least three independent experiments. Asterisks indicate statistically significant differences compared to control according to Student's test (* $p < 0.05$, ** $p < 0.01$).

4. Mechanisms of action of vanadium in bone-derived cell lines

Different *in vitro* systems (different species and cell type) have been used to investigate proliferative and mineralogenic effects of vanadium. Available data (summarized in Table 1) suggest that vanadium may promote distinct effects depending on the system used. Although similar toxic and proliferative effects have been recognized in both systems (*i.e.* mammalian and fish), effects on ECM mineralization were contradictory (*i.e.* stimulation in mammalian cells and inhibition in fish cells). Interestingly, vanadium-treated MC3T3-E1 cells exhibited increased ERK phosphorylation. ERK activation by vanadium salts was previously demonstrated in experiments using Chinese hamster ovary cells overexpressing insulin receptor [27]. Stimulation of ras/ERK pathway mediated by PI-3K activation (resulting in the PI-3K/ras/ERK pathway) promoted important insulin-mimetic effects, *e.g.* glycogen synthesis and glucose homeostasis. Nevertheless, this pathway is commonly associated to growth promotion effects [53]. Recently, the ECM mineralization of MC3T3-E1 cells was show to be significantly inhibited by PDGF, also through the activation of ERK pathway. This result is, on one hand, in contradiction with the ERK-dependent mineralogenic effect of vanadium in MC3T3-E1, but, on the other hand,

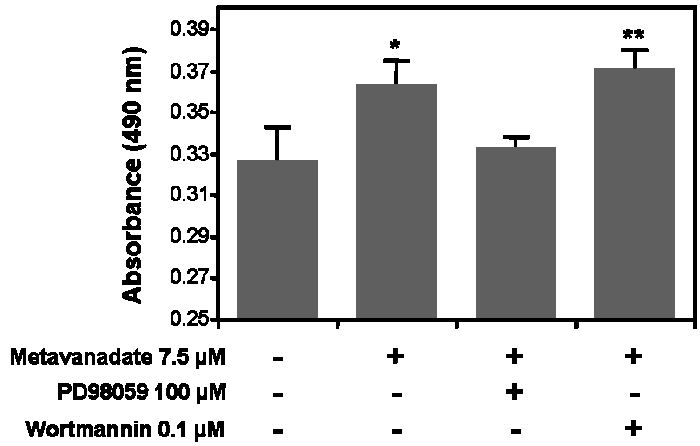

Figure 5. Effect of MAPK and PI-3K inhibitors on vanadate stimulation of VSa13 cells proliferation. VSa13 cells were seeded in 96-well plates at 1.5×10^3 cell/well then treated with 7.5 µM metavanadate Cell viability was evaluated at 8 days using MTS assay. Values are the mean of at least three independent experiments. Asterisks indicate statistically significant differences compared to control according to Student's test (* $p < 0.05$, ** $p < 0.01$).

Table 1. Effects of vanadium on vertebrate bone-derived cell systems.

Effects	Mammalian		Non-mammalian
Cell line			
Name	MC3T3-E1	UMR106	VSa13
Origin	Mouse calvaria	Rat osteosarcoma	Seabream vertebra
Cell type	Pre-osteoblastic	Differentiated osteoblast	Chondrocyte-like
Vanadate acute toxicity (1 mM during 4 h)			
	↓↓ [54]	↓ [54]	↓ [52]
Phenotype			
Proliferation	↑ * [44,46,49,50,55,56]	↑ [44,49,50,55,56]	↑↑ ** [52]
ECM mineralization	↑↑↑ [50]	NT	↓↓↓ [52]
Protein content	↑↑ [44]	↑ [44]	↑↑↑ [UR]
Cell differentiation			
ALP activity	↔ [50]	↓↓↓ [44,49,50,54,56]	↓↓↓ ** [UR]
Type-I collagen synthesis	↑ * [50]	↑↑↑ * [50]	NT
Other activities			
Glucose consumption	↑↑ ** [44]	↑↑↑ ** [44,49,56]	NT
PTPase	↓↓↓ [46]	↓↓↓ [50]	NT
ERK activation	↑ * [50]	↑ * [49,50]	NT

* indicates insulin-like effect; ** indicates non-insulin-like effect; NT indicates not tested; UR indicates unpublished result

in total agreement with the anti-mineralogenic effect of vanadium in VSa13. It also suggests that vanadium effect could be mediated in VSa13 through ERK/MAPK pathway, an hypothesis which is strengthened by preliminary data showing the reversion of vanadium effect on cell proliferation by PD98059, a specific inhibitor of MAPK pathway early events (Figure 5; our unpublished results). However, increased ERK phosphorylation in VSa13 cells is still to be confirmed.

Alkaline phosphatase (ALP) activity (and cell differentiation) was shown to be similarly affected by vanadium in all systems. Preliminary data suggest that

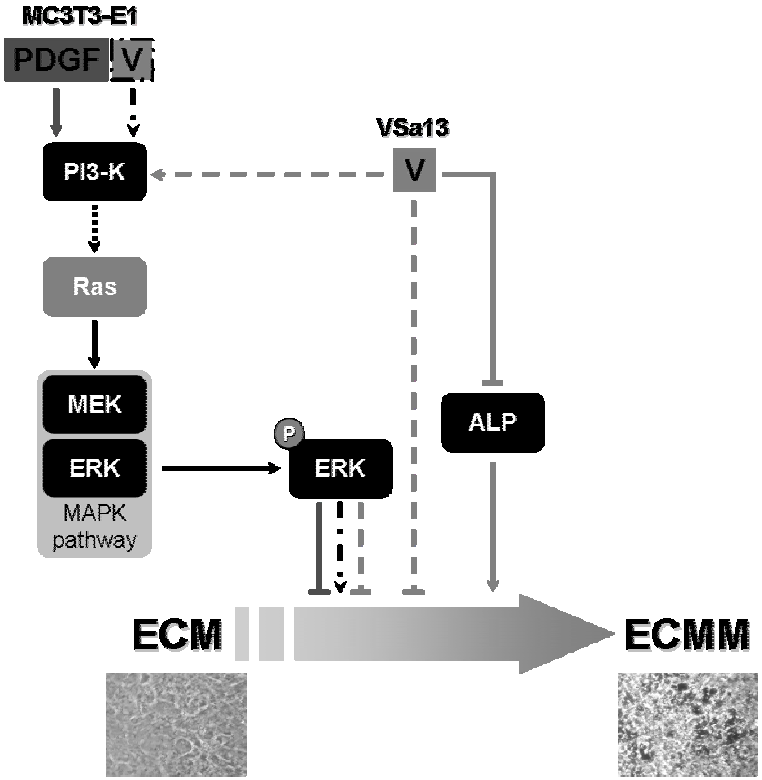

Figure 6. Vanadium putative regulation mechanisms for extracellular matrix (ECM) mineralization in VSa13 and MC3T3-E1 cells. ECMM indicates mineralized ECM; P indicates phosphorylation of ERK; V indicates vanadium; light grey arrows and dashed lines indicate vanadium putative effects in VSa13 cells; dark grey arrows and lines indicate PDGF effect in MC3T3-E1 cells; black dashed/dotted arrows indicate vanadium putative effects in MC3T3-E1 cells; dotted arrow indicates PI-3K/ras/MAPK pathway; below are represented micrographs of non-mineralized and mineralized VSa13 cells.

vanadate may not directly inhibit ALP activity in VSa13 cells (our unpublished result). We hypothesize that vanadate may affect indirectly the levels of ALP activity during ECM mineralization by down-regulating gene expression. A putative model for vanadium action during ECM mineralization is presented in Figure 6.

5. Concluding remarks

This chapter presents a comprehensive collection of *in vitro* data regarding the effects of vanadium on bone metabolism in mammals. It also describes the recent work performed in fish bone-derived cells shown to respond to insulin, but also to be finely regulated by vanadate. In these cells, like in mammalian bone-derived cell lines, vanadate behaves as a growth factor, stimulating VSa13 cell proliferation through an insulin-independent mechanism. On the contrary, ECM mineralization of VSa13 cells is negatively regulated by insulin and vanadium, with a stronger inhibition resulting from the combination of both treatments. Based on previous studies, it is suggested that this effect may be mediated through activation of ERK pathway and consequent down-regulation of mineralization. However, in order to confirm specific involvement of this pathway further investigation will be necessary. Preliminary results in VSa13 cells have so far indicated (1) the involvement of MAPK pathways in the vanadate effects on cell proliferation through a non-insulin related mechanism, and (2) the vanadate-dependent inhibition of cell differentiation through an effect on ALP activity. In general, it is important to notice that full characterization of vanadium effects in bone-derived systems will require further investigation, such as the analysis of: a) combined action of vanadium and other growth factors (*e.g.* IGF1, TGF-β); b) general gene expression during vanadium treatments (using microarray technology); c) specific bone-related gene expression; d) specific bone-related protein synthesis. The development of non-mammalian *in vitro* systems is likely to bring new insights on vanadium mechanisms of action in bone.

Acknowledgements

Daniel M. Tiago was the recipient of a Ph.D. fellowship (BD/12773/2003) from the Portuguese Science and Technology Foundation.

References

1. Nielsen, F.H., and Uthus, E.O. 1990, Vanadium in biological systems, N.D. Chasteen (Ed.), Kluwer Academic Publishers, Boston, 51.
2. Crans, D.C., Smee, J.J., Gaidamauskas, E., and Yang, L. 2004, Chem Rev, 104, 849.
3. Rehder, D. 2003, Inorg. Chem. Commun., 6, 604.

4. Anke, M. 2004, Anal. Real Acad. Nac. Farm., 70, 961.
5. Chasteen, N.D. 1983, Structure and Bonding, 53, 105.
6. Amado, A.M., Aureliano, M., Ribeiro-Claro, P.J.A., and Teixeira-Dias, J.J. 1993, J Raman Spectrosc, 24, 699.
7. Crans, D.C., Mahroof-Tahir, M., and Keramidas, A.D. 1995, Mol Cell Biochem, 153, 17.
8. Aureliano, M., and Madeira, V.M.C. 1998, Vanadium in the environment: Chemistry and Biochemistry, J.O. Nriagu (Ed.), J. Wiley, New York, 333.
9. Aureliano, M., and Gandara, R.M. 2005, J Inorg Biochem, 99, 979.
10. Borges, G., Mendonca, P., Joaquim, N., Coucelo, J., and Aureliano, M. 2003, Arch Environ Contam Toxicol, 45, 415.
11. Aureliano, M., Joaquim, N., Sousa, A., Martins, H., and Coucelo, J.M. 2002, J Inorg Biochem, 90, 159.
12. Soares, S.S., Aureliano, M., Joaquim, N., and Coucelo, J.M. 2003, J Inorg Biochem, 94, 285.
13. Soares, S.S., Martins, H., and Aureliano, M. 2006, Arch Environ Contam Toxicol, 50, 60.
14. Tiago, T., Aureliano, M., and Gutierrez-Merino, C. 2004, Biochemistry, 43, 5551.
15. Aureliano, M., and Madeira, V.M. 1994, Biochim Biophys Acta, 1221, 259.
16. Tiago, T., Aureliano, M., and Moura, J.J. 2004, J Inorg Biochem, 98, 1902.
17. Shechter, Y., and Karlish, S.J. 1980, Nature, 284, 556.
18. Dubyak, G.R., and Kleinzeller, A. 1980, J Biol Chem, 255, 5306.
19. Shechter, Y., and Ron, A. 1986, J Biol Chem, 261, 14945.
20. Heyliger, C.E., Tahiliani, A.G., and McNeill, J.H. 1985, Science, 227, 1474.
21. Meyerovitch, J., Farfel, Z., Sack, J., and Shechter, Y. 1987, J Biol Chem, 262, 6658.
22. Shechter, Y. 1998, Lett Pept Sci, 5, 319.
23. Goldwaser, I., Gefel, D., Gershonov, E., Fridkin, M., and Shechter, Y. 2000, J Inorg Biochem, 80, 21.
24. Thompson, K.H., and Orvig, C. 2000, J Chem Soc Dalton, 2885.
25. Shechter, Y., Li, J., Meyerovitch, J., Gefel, D., Bruck, R., Elberg, G., Miller, D.S., and Shisheva, A. 1995, Mol Cell Biochem, 153, 39.
26. Shisheva, A., and Shechter, Y. 1993, J Biol Chem, 268, 6463.
27. Pandey, S.K., Anand-Srivastava, M.B., and Srivastava, A.K. 1998, Biochemistry, 37, 7006.
28. Cheatham, B., and Kahn, C.R. 1995, Endocr Rev, 16, 117.
29. Canalis, E. 1993, Bone, 14, 273.
30. Canalis, E., McCarthy, T.L., and Centrella, M. 1989, J Endocrinol Invest, 12, 577.
31. Canalis, E. 1985, Endocrinology, 116, 855.
32. Etcheverry, S.B., Apella, M.C., and Baran, E.J. 1984, J Inorg Biochem, 20, 269.
33. Anke, M., Groppel, B., Gruhn, K., Langer, M., and Arnhold, W. 1989, S.I.T.E. Symposium (Ed.), Fredrich- Jena, Schiller Universität, Jena, 17.
34. Fukui, K., Fujisawa, Y., OhyaNishiguchi, H., Kamada, H., and Sakurai, H. 1999, J Inorg Biochem, 77, 215.
35. Setyawati, I.A., Thompson, K.H., Yuen, V.G., Sun, Y., Battell, M., Lyster, D.M., Vo, C., Ruth, T.J., Zeisler, S., McNeill, J.H., and Orvig, C. 1998, J Appl Physiol, 84, 569.

36. Canalis, E., Pash, J., and Varghese, S. 1993, Crit Rev Eukaryot Gene Expr, 3, 155.
37. Sudo, H., Kodama, H.A., Amagai, Y., Yamamoto, S., and Kasai, S. 1983, J. Cell Biol., 96, 191.
38. Ituarte, E.A., Halstead, L.R., Iida-Klein, A., Ituarte, H.G., and Hahn, T.J. 1989, Calcif Tissue Int, 45, 27.
39. Barrio, D.A., and Etcheverry, S.B. 2006, Can J Physiol Pharmacol, 84, 677.
40. Lau, K.H., Tanimoto, H., and Baylink, D.J. 1988, Endocrinology, 123, 2858.
41. Murshed, M., Harmey, D., Millan, J.L., McKee, M.D., and Karsenty, G. 2005, Genes Dev, 19, 1093.
42. Cortizo, A.M., Salice, V.C., and Etcheverry, S.B. 1994, Biol Trace Elem Res, 41, 331.
43. Cortizo, A.M., and Etcheverry, S.B. 1995, Mol Cell Biochem, 145, 97.
44. Etcheverry, S.B., Crans, D.C., Keramidas, A.D., and Cortizo, A.M. 1997, Arch Biochem Biophys, 338, 7.
45. Barrio, D.A., Braziunas, M.D., Etcheverry, S.B., and Cortizo, A.M. 1997, J Trace Elem Med Biol, 11, 110.
46. Salice, V.C., Cortizo, A.M., Gomez Dumm, C.L., and Etcheverry, S.B. 1999, Mol Cell Biochem, 198, 119.
47. Etcheverry, S.B., Williams, P.A., Barrio, D.A., Salice, V.C., Ferrer, E.G., and Cortizo, A.M. 2000, J Inorg Biochem, 80, 169.
48. Etcheverry, S.B., Williams, P.A., Salice, V.C., Barrio, D.A., Ferrer, E.G., and Cortizo, A.M. 2002, Biometals, 15, 37.
49. Barrio, D.A., Williams, P.A., Cortizo, A.M., and Etcheverry, S.B. 2003, J Biol Inorg Chem, 8, 459.
50. Cortizo, A.M., Molinuevo, M.S., Barrio, D.A., and Bruzzone, L. 2006, Int J Biochem Cell Biol, 38, 1171.
51. Pombinho, A.R., Laizé, V., Molha, D.M., Marques, S.M., and Cancela, M.L. 2004, Cell Tissue Res, 315, 393.
52. Tiago, D.M., Laizé, V., Cancela, M.L., and Aureliano, M. 2007, Submitted to J Inorg Biochem,
53. Kitagawa, D., Tanemura, S., Ohata, S., Shimizu, N., Seo, J., Nishitai, G., Watanabe, T., Nakagawa, K., Kishimoto, H., Wada, T., Tezuka, T., Yamamoto, T., Nishina, H., and Katada, T. 2002, J Biol Chem, 277, 366.
54. Cortizo, A.M., Bruzzone, L., Molinuevo, S., and Etcheverry, S.B. 2000, Toxicology, 147, 89.
55. Cortizo, A.M., Caporossi, M., Lettieri, G., and Etcheverry, S.B. 2000, Eur J Pharmacol, 400, 279.
56. Williams, P.A., Barrio, D.A., Etcheverry, S.B., and Baran, E.J. 2004, J Inorg Biochem, 98, 333.

FEBS Letters 582 (2008) 1381–1385

Vanadate proliferative and anti-mineralogenic effects are mediated by MAPK and PI-3K/Ras/Erk pathways in a fish chondrocyte cell line

Daniel M. Tiago, M. Leonor Cancela, Manuel Aureliano, Vincent Laizé*

Centre of Marine Sciences (CCMAR), University of Algarve, 8005-139 Faro, Portugal

Received 22 January 2008; revised 6 March 2008; accepted 13 March 2008

Available online 25 March 2008

Edited by Lukas Huber

Abstract **We recently reported proliferative and anti-mineralogenic effects of vanadate on fish chondrocytes and here we investigate the signalling pathways associated with these effects. Our data show that vanadate stimulates chondrocyte proliferation through the MAPK pathway, using signalling mechanisms similar to those used by IGF-1, while it inhibits chondrocyte differentiation/mineralization through a putative PI-3K/Ras/Erk signalling, a pathway shared with insulin. Our data also suggest that vanadate impairs ECM mineralization not only by interfering with regulatory pathways but also by inhibiting enzymatic activity of ALP. Finally, this work provides additional evidence for the conservation, throughout evolution, of mechanisms regulating chondrocyte proliferation and differentiation.**

© 2008 Published by Elsevier B.V. on behalf of the Federation of European Biochemical Societies.

Keywords: Vanadium; Insulin-like activity; Intracellular signalling; In vitro mineralization; Bony fish; Bone-derived cell line

1. Introduction

Vanadium, mostly known for enhancing mechanical properties of alloy steels in the metal industry, has also been recognized as an essential trace element for biological activity in most living animals [1]. In mammals, vanadium has been associated to a variety of insulin-like effects [2] and its action associated to the specific regulation of protein tyrosine phosphatases and consequent activation of tyrosine kinase receptors, including the insulin receptor [2,3]. A role for vanadium in bone formation has been demonstrated [4,5] but mechanisms of action have remained largely unexplored. In vitro studies, using calvaria primary cultures [6,7] and bone-derived cell lines [5,8,9], have evidenced the regulation of bone-related enzymes activity (e.g. alkaline phosphatase (ALP) and protein tyrosine phosphatases), the stimulation of bone-related protein synthesis (e.g. type I collagen), the alteration of bone-related cell proliferation and extracellular matrix (ECM) mineralization, and the activation of insulin and insulin-like growth factor 1 (IGF-1) signalling mechanisms [5,9] by vanadium compounds. However, there is still much to unveil in order to understand vanadium mechanisms of action in bone.

In this study, wortmannin, a specific inhibitor of phosphatidyl inositol-3 kinase (PI-3K) pathway, and PD98059, a specific inhibitor of mitogen-activated protein kinase (MAPK) have been tested for their effects on vanadium-associated alteration of growth performances, ECM mineralization, ALP activity, collagen synthesis in VSa13 cells.

2. Materials and methods

2.1. Cell culture and ECM mineralization

VSa13 cells were cultured as described previously [10]. ECM mineralization was induced in confluent cultures by supplementing medium with 50 μg/ml of L-ascorbic acid, 10 mM β-glycerophosphate and 4 mM $CaCl_2$. At appropriate times, mineral deposition was revealed using the von Kossa staining method and quantified by densitometric analysis [10]. Culture medium was renewed every 2 days in proliferation experiments and every 3.5 days in mineralization experiments. Insulin (1–100 nM), IGF-1 (1–100 nM) and vanadate (2.5–7.5 μM) treatments were applied at the time of medium renewal.

2.2. Preparation of vanadate, PD98059, wortmannin, insulin and IGF-1 stock solutions

Vanadate solution (50 mM, pH 6–7) was prepared as described previously [8]. PD98059 and wortmannin were solubilised in DMSO at 6 and 10 mg/ml, respectively. Bovine insulin (Sigma–Aldrich) and *Pagrus auratus* IGF-1 (Novozymes GroPep) were solubilised in pH 2 water at 10 μM and in pH 6 water at 0.1 mg/ml, respectively. Milli-Q water (Millipore) was used to prepare vanadate, insulin and IGF-1 solutions.

2.3. Measurement of cell proliferation

VSa13 cell proliferation was determined from cultures seeded in 96-well plates at 1.5×10^3 cells/well using the CellTiter 96 non-radioactive proliferation assay kit (Promega). At appropriate times, cells were incubated for 1 h with 20 μl of reagent mixture then cell proliferation was determined from absorbance at 490 nm.

2.4. Measurement of ALP activity

VSa13 cells grown for 4 weeks under mineralizing conditions were washed three times with phosphate-buffered saline (PBS), scrapped off the plate into 500 μl of 0.1% Triton X-100 then centrifuged for 1 min at 16000 × *g*. ALP activity was determined at 37 °C from initial rates of *p*-nitrophenyl phosphate (*p*-NPP) hydrolysis into *p*-nitrophenol (*p*-NP). Formation of *p*-NP was monitored at 405 nm from the following reaction mixture: 800 μl of reaction buffer (55 mM glycine and 0.55 mM $MgCl_2$ at pH 10.5), 100 μl of 5 mM *p*-NPP and 100 μl of cell extract supernatant. ALP activity was normalized with protein content determined using Bradford reagent (Bio-Rad).

*Corresponding author. Fax: +351 289 800069.
E-mail address: vlaize@ualg.pt (V. Laizé).

Abbreviations: ALP, alkaline phosphatase; ECM, extracellular matrix; IGF-1, insulin-like growth factor 1; MAPK, mitogen-activated protein kinase; PI-3K, phosphatidyl inositol-3 kinase

0014-5793/$34.00 © 2008 Published by Elsevier B.V. on behalf of the Federation of European Biochemical Societies.
doi:10.1016/j.febslet.2008.03.025

2.5. Measurement of collagen content

VSa13 cells grown for 4 weeks under mineralizing conditions were washed three times with PBS then stained with Sirius red dye (F3BA; Chroma) as described previously [11]. Bound dye was solubilised into 200 μl of 0.1 N NaOH and collagen content was determined from absorbance at 550 nm.

2.6. Statistical analysis

Values are the mean of at least three separate experiments and are presented with their standard deviation. Differences upon treatment were analyzed by one-way ANOVA and considered significant at $P < 0.05$.

3. Results and discussion

In vitro studies investigating vanadium insulin-like effects and specific targets in bone have been largely restricted to a particular taxonomic group (i.e. mammals) and to particular cell types (i.e. osteoblast-like and osteosarcoma cells). This work evidences, for the first time in a non-mammalian in vitro system and using a chondrocyte-like cell line, the role of MAPK and PI-3K pathways in the mediation of vanadate effects on proliferation and mineralization.

3.1. MAPK pathway mediates vanadate stimulation of VSa13 cell proliferation

Vanadate (2.5–7.5 μM), insulin (1–100 nM) and IGF-1 (1–100 nM) were tested for their effect on VSa13 cell growth. Both vanadate and IGF-1, but not insulin, stimulated cell proliferation to a similar extent (strongest stimulation at 7.5 μM and 10 nM, respectively; Supplementary Figures 1 and 2 and Fig. 1). Wortmannin and PD98059, known inhibitors of PI-3K and MAPK pathways, respectively, were then tested for their effect on VSa13 cell proliferation and for their capacity of reverting IGF-1 and vanadate stimulatory effects. Dividing cultures of VSa13 cells were treated for 8 days with 0.1 μM wortmannin, 100 μM PD98059 (non-toxic concentrations, data not shown) in the presence or absence of insulin, vanadate or IGF-1 (Fig. 1). PD98059, but not wortmannin, totally abolished vanadate and IGF-1 stimulation of cell proliferation (inhibitors alone had no effect) suggesting that proliferation of VSa13 cells is stimulated by vanadate through the activation of the MAPK pathway. A similar contribution of the MAPK pathway in the transduction of vanadate proliferative effect has been reported in mammalian osteoblast-like cells [12,13], suggesting a conservation of mechanisms of action throughout evolution and across bone cell types. The inability of insulin to enhance VSa13 cell proliferation suggests that the activation of MAPK pathway by vanadate would occur through an insulin receptor-independent manner. Similarly, the stimulation of VSa13 cell proliferation by IGF-1 through MAPK pathway and to a similar extent, suggest that the activation of MAPK pathway by vanadate could occur through IGF-1 receptor and/or signalling pathway, although we cannot exclude that other tyrosine kinase receptors (e.g. platelet-derived growth factor (PDGF) receptor) may be involved [5]. Similar mechanisms (i.e. those related to the proliferative effect of IGF-1) have been recently reported in the mouse chondrocyte ATDC5 cell line [14] and thus, based on those results as well as our data reported in this study, we propose the existence of a mechanism involving MAPK pathway that would regulate chondrocyte proliferation and transduce vanadate effect (Fig. 5A).

3.2. Putative PI-3K/Ras/Erk pathway mediates vanadate impairment of VSa13 ECM mineralization

Wortmannin and PD98059 were then tested for their effect on VSa13 ECM mineralization and for their capacity of reverting vanadate and insulin inhibitory effects previously demonstrated [8] and further confirmed here. Mineralizing VSa13

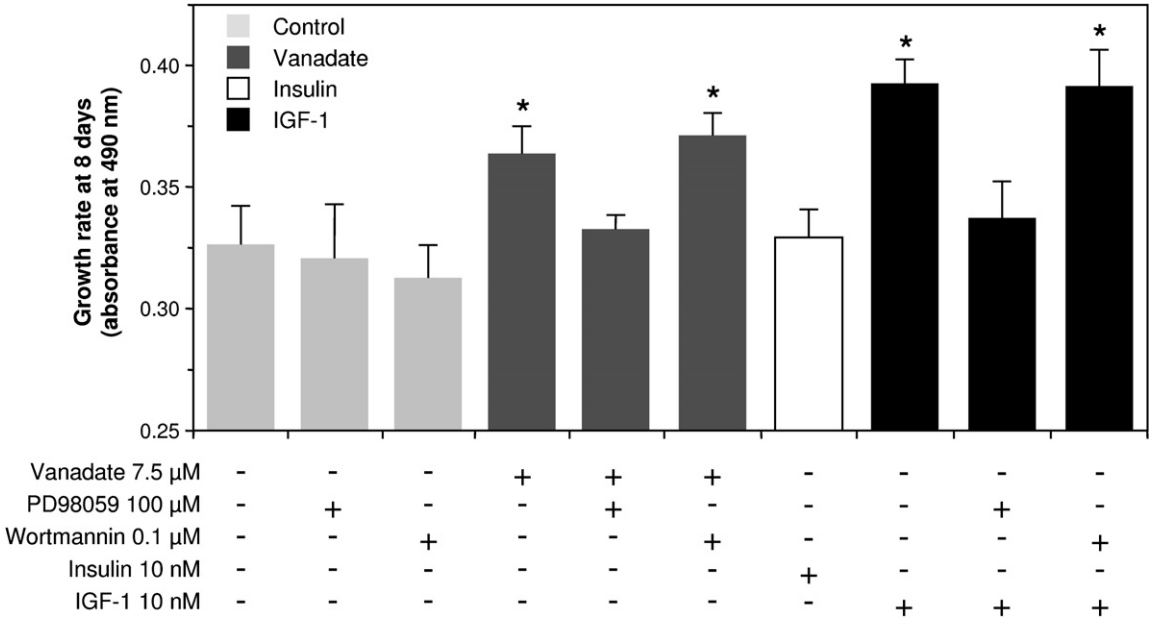

Fig. 1. Effect of vanadate, insulin, IGF-1, wortmannin and PD98059 on VSa13 cell proliferation. VSa13 cells were seeded in 96-well plates at 1.5×10^3 cells/well then either left untreated or treated with PD98059, wortmannin, vanadate, insulin or IGF-1, alone or in combinations. Cell proliferation was evaluated after 8 days using MTS assay. Asterisk indicates values statistically different from corresponding controls ($n \geqslant 3$; $P < 0.05$; one-way ANOVA).

cultures were treated for 4 weeks with 0.1 μM wortmannin, 100 μM PD98059, 10 nM IGF-1, 10 nM insulin, and/or 5 μM vanadate, then evaluated for mineralization. While unaltered by IGF-1, mineral deposition was increasingly impaired by insulin (1.4-fold), vanadate (8-folds) and almost abolished by a combination of both agents (Fig. 2). Apparent synergy between vanadate and insulin could suggest that different signalling pathways are involved in both mechanisms of action, or that vanadate potentiates insulin action during mineralization, e.g. by inhibiting PTPases, therefore increasing sensitivity of insulin pathway as previously suggested [15]. Interestingly, ECM of PD98059-treated cells, but not that of wortmannin-treated cells, exhibited a significant increase in mineral deposition (3.2-folds), suggesting a down-regulation of ECM mineralization by MAPK pathway. We propose, in agreement with recent results obtained in mouse ATDC5 chondrocyte cells [14,16], that MAPK pathway may affect ECM mineralization of VSa13 cells by inhibiting cell differentiation. The role of MAPK pathway in regulating VSa13 ECM mineralization was further confirmed by the reversion (100% and 72.5%, respectively) of insulin and vanadate anti-mineralogenic effects with PD98059. Surprisingly, wortmannin also reverted (100% and 57.5%, respectively) insulin and vanadate anti-mineralogenic effects, suggesting a role for PI-3K pathway in regulating VSa13 ECM mineralization. As expected, impairment of mineralization by the combined effects of insulin and vanadate was reverted to an extent similar to that observed for vanadate alone. Altogether, these results suggest that both MAPK and PI-3K pathways could mediate vanadate and insulin anti-mineralogenic effects. We propose that regulation of VSa13 cell differentiation/mineralization is exerted through the PI-3K/Ras/Erk pathway (a combination of MAPK and PI-3K pathways), a finding that is in agreement with recent results obtained for mouse MC3T3-E1 cells [17]. We further propose, based on overall available data as well as results reported in this study, that a similar mechanism is responsible for transducing vanadate effects (Fig. 5B). However, incomplete reversion of vanadate anti-mineralogenic effect by both PD98059 and wortmannin (83.2% reversion, result not shown) suggests that other differentiation/mineralization-related mechanisms are affected by vanadate. ALP, by cleaving pyrophosphate, an inhibitor of ECM mineralization [18], and collagen, an essential structural component of ECM [19], were considered as putative targets for vanadate action and further investigated.

3.3. ALP activity is inhibited while collagen content is increased by micromolar concentrations of vanadate

Enzymatic activity of ALP was first determined in mineralized cell cultures treated with 5 μM vanadate and/or 10 nM insulin. Interestingly, a 40% increase in ALP activity was observed following ECM mineralization, while activity remained similar to non-mineralizing control cells upon vanadate treatment (Fig. 3). In similar experiments, collagen content was shown to increase by 57% in mineralized cultures and by an additional 17% when those cultures were also treated with vanadate (Fig. 4). The stimulation of both ALP activity and collagen production in mineralized cultures is consistent with their role in mineralization mechanisms. The inability of insulin to affect ALP activity and collagen production suggests that vanadate action occurs through an insulin receptor-independent manner. ALP activity was then measured in cellular extracts of mineralized cultures (4 weeks) in the presence of increasing concentrations of vanadate: activity was stimulated at low concentration (5 μM) while strongly inhibited at higher concentrations (from 25 to 500 μM) of vanadate. We propose, in

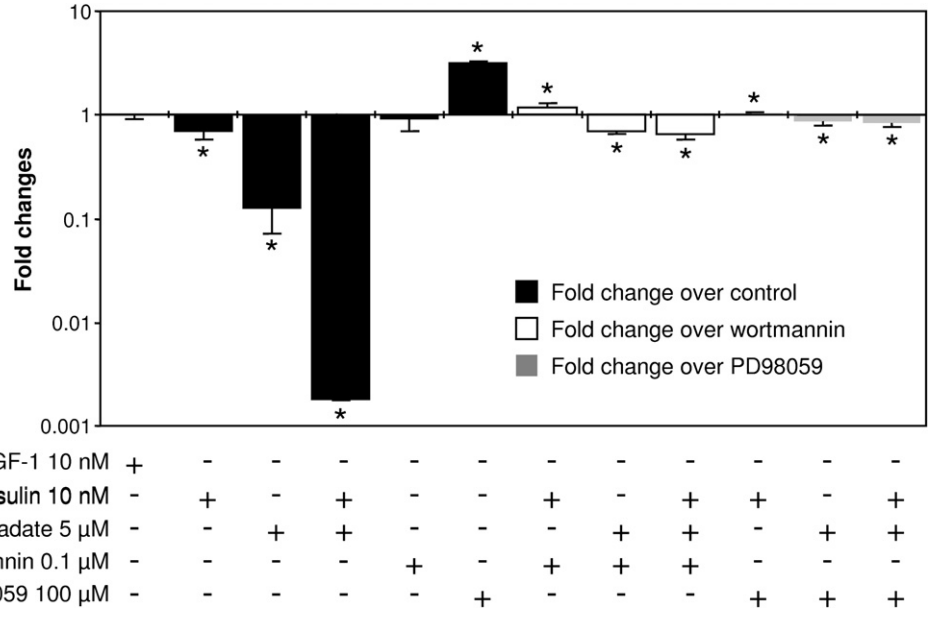

Fig. 2. Effect of IGF-1, vanadate, insulin, wortmannin and PD98059 on VSa13 ECM mineralization. VSa13 cells were seeded in 24-well plates at 2×10^4 cells/well, grown until confluence then treated for mineralization. Mineralizing cultures were then left untreated or treated with IGF-1, insulin, vanadate, PD98059, or wortmannin, alone or in combinations. Mineral deposition was revealed after 4 weeks by von Kossa staining and evaluated by densitometry analysis. Mineralization data are presented as the ratio between individual values and their corresponding controls (non-treated, treated with wortmannin and treated with PD98059). Asterisk indicates values statistically different from corresponding controls ($n \geqslant 3$; $P < 0.05$; one-way ANOVA).

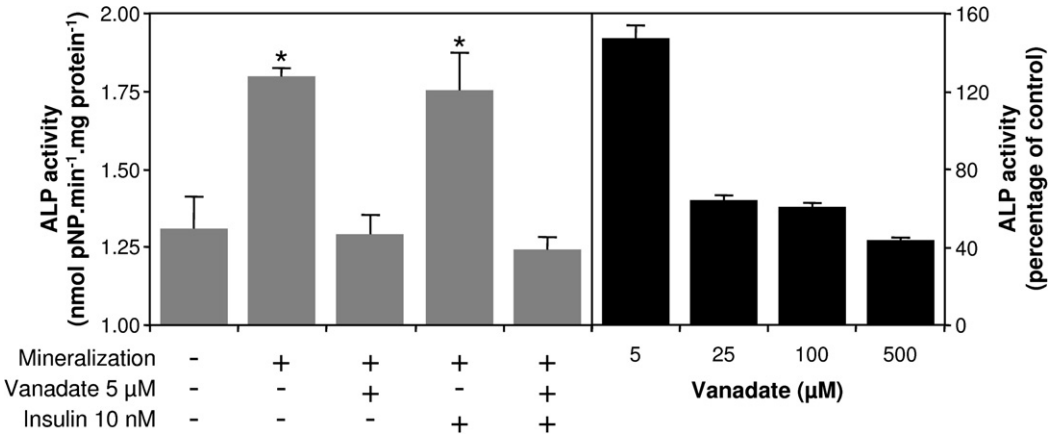

Fig. 3. ALP activity in mineralized cell cultures treated with insulin and vanadate. VSa13 cells were seeded in 24-well plates at 2×10^4 cells/well, grown until confluence then treated for mineralization. Mineralizing cultures were then left untreated (control) or treated with insulin and/or vanadate. ALP activity was measured in cell extracts after 4 weeks of treatment (left panel) or assayed in the presence of increasing concentration of vanadate (right panel; values are normalized with ALP activity measured in the absence of vanadate). Asterisk indicates values statistically different from corresponding controls ($n \geqslant 3$; $P < 0.05$; one-way ANOVA).

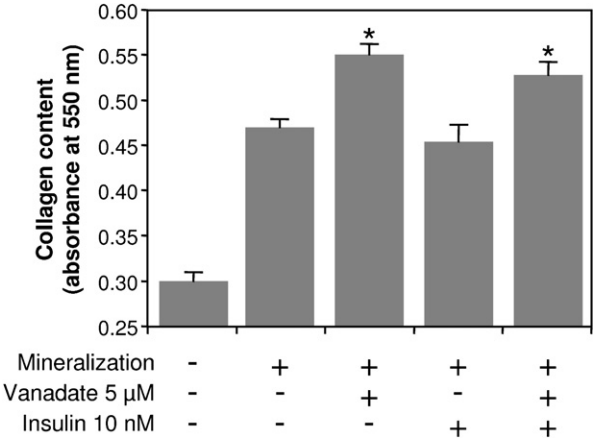

Fig. 4. Collagen content in mineralized cell cultures treated with insulin and/or vanadate. VSa13 cells were seeded in 24-well plates at 2×10^4 cells/well, grown until confluence then treated for mineralization. Mineralizing cultures were then left untreated (control) or treated with insulin and/or vanadate. Total collagen content was determined after 4 weeks of treatment through Sirius red staining. Asterisk indicates values statistically different from corresponding controls ($n \geqslant 3$; $P < 0.05$; one-way ANOVA).

agreement with recent result demonstrating the accumulation of vanadium in VSa13 cells [8], that although cultures were treated with non-inhibitory concentrations of vanadate, these may accumulate intracellularly and reach concentrations inhibitory for ALP activity therefore affecting mechanisms of ECM mineralization. On the contrary, the increase of total collagen content in vanadate-treated mineralized cultures (most probably the result of increased type X collagen as observed in differentiating ATDC5 chondrocyte cells [16]) can hardly explain the decrease of ECM mineralization since increased collagen production is rather likely to benefit ECM mineralization. Similar results (i.e. inhibition of ALP activity and/or stimulation of collagen synthesis) have been reported in chicken [7] and mouse [6,12,20] bone-derived systems, suggesting once again a conservation of mechanisms throughout evolution and across bone cell types.

4. Conclusions

Various evidences have been collected during this work towards the involvement of MAPK and PI-3K/Ras/Erk path-

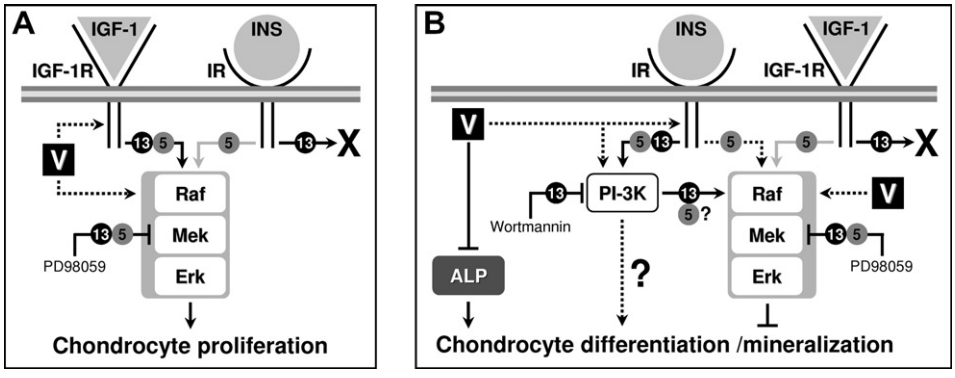

Fig. 5. Putative mechanisms of action for insulin, IGF-1 and vanadate in vertebrate chondrocyte cells. Circled 5 and 13 indicate pathways related to ATDC5 and VSa13 cell lines, respectively. Black, gray and dashed arrows indicate activated, moderately activated and putatively activated pathways, respectively. X indicates an absence of effect. V, vanadate. Raf, Mek and Erk are intermediates in the MAPK pathway.

ways in vanadate proliferative and anti-mineralogenic effects, respectively, using a fish bone-derived cell line of the chondrocyte lineage. We propose that vanadate shares with IGF-1 the signalling pathway regulating chondrocyte proliferation, while it shares with insulin the signalling pathway regulating chondrocyte differentiation/mineralization. We also propose that vanadate not only affects ECM mineralization by activating the PI-3K/Ras/Erk pathway but also inhibits the enzymatic activity of ALP. Finally, this work provides strong evidence for the conservation, throughout evolution, of those mechanisms regulating chondrocyte proliferation and differentiation, emphasizing the suitability of fish to investigate vertebrate development, in particular mechanisms related to chondrogenesis.

Acknowledgement: This work was partially funded by CCMAR and EU-FP6 MGE network of excellence (GOCE-CT-2004-505403). D.M.T. was the recipient of a Ph.D. fellowship (BD/12773/2003) from the Portuguese Science and Technology Foundation.

Appendix A. Supplementary material

Supplementary data associated with this article can be found, in the online version, at doi:10.1016/j.febslet.2008.03.025.

References

[1] Crans, D.C., Smee, J.J., Gaidamauskas, E. and Yang, L. (2004) The chemistry and biochemistry of vanadium and the biological activities exerted by vanadium compounds. Chem. Rev. 104, 849–902.
[2] Shechter, Y. (1998) Insulin-like effects of vanadium: mechanisms of action, clinical and basic implications. Lett. Pept. Sci. 5, 319–322.
[3] Shisheva, A. and Shechter, Y. (1993) Role of cytosolic tyrosine kinase in mediating insulin-like actions of vanadate in rat adipocytes. J. Biol. Chem. 268, 6463–6469.
[4] Anke, M. (2004) Vanadium – an element both essential and toxic to plants, animals and humans? Anal. Real Acad. Nac. Farm. 70, 961–999.
[5] Barrio, D.A. and Etcheverry, S.B. (2006) Vanadium and bone development: putative signaling pathways. Can. J. Physiol. Pharmacol. 84, 677–686.
[6] Canalis, E. (1985) Effect of sodium vanadate on deoxyribonucleic acid and protein synthesis in cultured rat calvariae. Endocrinology 116, 855–862.
[7] Lau, K.H., Tanimoto, H. and Baylink, D.J. (1988) Vanadate stimulates bone cell proliferation and bone collagen synthesis in vitro. Endocrinology 123, 2858–2867.
[8] Tiago, D.M., Laizé, V., Cancela, M.L. and Aureliano, M. (2008) Impairment of mineralization by metavanadate and decavanadate solutions in a fish bone-derived cell line. Cell Biol. Toxicol., doi:10.1007/s10565-007-9034-x.
[9] Tiago, D.M., Laizé, V., Aureliano, M. and Cancela, M.L. (2008) Vanadate effects on bone metabolism: fish cell lines as an alternative to mammalian in vitro systems. in: Vanadium Biochemistry (Aureliano, M., Ed.), pp. 269–283. Research Signpost, Kerala, India.
[10] Pombinho, A.R., Laizé, V., Molha, D.M., Marques, S.M. and Cancela, M.L. (2004) Development of two bone-derived cell lines from the marine teleost *Sparus aurata*; evidence for extracellular matrix mineralization and cell-type-specific expression of matrix Gla protein and osteocalcin. Cell. Tissue Res. 315, 393–406.
[11] Tullberg-Reinert, H. and Jundt, G. (1999) *In situ* measurement of collagen synthesis by human bone cells with a Sirius red-based colorimetric microassay: effects of transforming growth factor-β2 and ascorbic acid 2-phosphate. Histochem. Cell Biol. 112, 271–276.
[12] Cortizo, A.M., Molinuevo, M.S., Barrio, D.A. and Bruzzone, L. (2006) Osteogenic activity of vanadyl(IV)-ascorbate complex: evaluation of its mechanism of action. Int. J. Biochem. Cell Biol. 38, 1171–1180.
[13] Barrio, D.A., Williams, P.A., Cortizo, A.M. and Etcheverry, S.B. (2003) Synthesis of a new vanadyl(IV) complex with trehalose (TreVO): insulin-mimetic activities in osteoblast-like cells in culture. J. Biol. Inorg. Chem. 8, 459–468.
[14] Phornphutkul, C., Wu, K.Y., Yang, X., Chen, Q. and Gruppuso, P.A. (2004) Insulin-like growth factor-I signaling is modified during chondrocyte differentiation. J. Endocrinol. 183, 477–486.
[15] Fantus, I.G., Ahmad, F. and Deragon, G. (1994) Vanadate augments insulin-stimulated insulin receptor kinase activity and prolongs insulin action in rat adipocytes. Evidence for transduction of amplitude of signaling into duration of response. Diabetes 43, 375–383.
[16] Phornphutkul, C., Wu, K.Y. and Gruppuso, P.A. (2006) The role of insulin in chondrogenesis. Mol. Cell Endocrinol. 249, 107–115.
[17] Kono, S.J., Oshima, Y., Hoshi, K., Bonewald, L.F., Oda, H., Nakamura, K., Kawaguchi, H. and Tanaka, S. (2007) ERK pathways negatively regulate matrix mineralization. Bone 40, 68–74.
[18] Blair, H.C., Zaidi, M. and Schlesinger, P.H. (2002) Mechanisms balancing skeletal matrix synthesis and degradation. Biochem. J. 364, 329–341.
[19] Murshed, M., Harmey, D., Millan, J.L., McKee, M.D. and Karsenty, G. (2005) Unique coexpression in osteoblasts of broadly expressed genes accounts for the spatial restriction of ECM mineralization to bone. Genes Dev. 19, 1093–1104.
[20] Cortizo, A.M., Salice, V.C. and Etcheverry, S.B. (1994) Vanadium compounds. Their action on alkaline phosphatase activity. Biol. Trace Elem. Res. 41, 331–339.

General and Comparative Endocrinology xxx (2008) xxx–xxx

Contents lists available at ScienceDirect

General and Comparative Endocrinology

journal homepage: www.elsevier.com/locate/ygcen

Alternatively spliced transcripts of *Sparus aurata* insulin-like growth factor 1 are differentially expressed in adult tissues and during early development

Daniel M. Tiago, Vincent Laizé, M. Leonor Cancela *,[1]

Centre of Marine Sciences (CCMAR), University of Algarve, Campus de Gambelas, 8005-139 Faro, Portugal

ARTICLE INFO

Article history:
Received 9 October 2007
Revised 2 April 2008
Accepted 14 April 2008
Available online xxxx

Keywords:
Pro-insulin-like growth factor 1 (proIGF-1)
Alternative splicing
E domain
Gilthead seabream (*Sparus aurata*)

ABSTRACT

Spliced variants of insulin-like growth factor 1 (IGF-1), a small peptide with a critical role in metabolism and growth, have been identified in various vertebrate species. However, despite recent functional data in mammalian systems suggesting specific roles (e.g. in muscle formation) for their pro-peptides and/or E domains, their function remains unclear. In this study, three alternatively spliced variants of *Sparus aurata* proIGF-1 (1a, 1b, and 1c) were identified and their expression analyzed. In adult fish, IGF-1 gene expression was observed in various soft tissues (highest levels in liver) and calcified tissues, with IGF-1c being always the most expressed isoform. In developing larvae, each isoform presented a specific pattern of expression, characterized by different onset and extent and consistent with a possible role of IGF-1a and 1b during early post-hatching events (e.g. bone or muscle formation), while IGF-1c would be rather involved in early larvae formation but probably acts in concerted action with other isoforms at later stages. We also propose that, in adults, IGF-1a and 1b isoforms may have a local action, while isoform 1c would assume a systemic action, as its mammalian counterpart. This hypothesis was further supported by *in silico* analysis of isoform distribution, revealing that only IGF-1c/Ea isoform has been conserved throughout evolution and that other fish isoforms (i.e. 1a and 1b) may be associated with mechanisms of osmoregulation. We finally propose that IGF-1 variants may exhibit different modes of action (systemic or local) and may be involved in different developmental and adaptive mechanisms.
© 2008 Published by Elsevier Inc.

1. Introduction

In vertebrates, body size and linear bone growth are regulated by numerous and complex cellular signaling pathways controlled by various growth factors and hormones (Canalis et al., 1993; Efstratiadis, 1998; Qin et al., 2001). In this regulatory network, insulin-like growth factor 1 (IGF-1) plays an essential role, regulating processes such as tissue homeostasis (e.g. bone), metabolism (e.g. glucose) and organogenesis (including cell differentiation and proliferation) (Powell-Braxton et al., 1993; D'Ercole et al., 1996; McCarthy and Centrella, 2001) but it can also act in an autocrine/paracrine manner, regulating local processes (Schmid, 1995). IGF-1 is mainly produced in liver, under the control of growth hormone (GH) (Duguay et al., 1996; Ohlsson et al., 1998), but also occurs in other tissues, e.g. brain, muscle, kidney, gut, and bone (Moriyama et al., 2000). It is synthesized as a prepro-peptide containing a signal peptide and five domains named B, C, A, D, and E. Mature peptide is formed after the proteolytic cleavage of signal peptide and E domain (Dupont and Holzenberger, 2003). Multiple forms of proIGF-1 have been detected in mammals (Goldspink and Yang, 2004) and teleost fish (Duguay et al., 1992; Shamblott and Chen, 1993; Wallis and Devlin, 1993; Tanaka et al., 1998), all resulting from alternative splicing in the region coding for the E domain. A generally accepted view on IGF-1 was that the E domain had little or no biological activity other than its potential role in the biosynthesis of mature peptides (Kuo and Chen, 2002). However, recent works have clearly demonstrated the specificity of proIGF-1 isoforms for particular tissues or cell types (Goldspink and Yang, 2004) suggesting otherwise. In human, isoform Ea assumes a systemic role and is mostly expressed in the liver whereas isoform Ec, also known as the mechano growth factor (MGF), is mostly expressed in muscle in response to mechanical stimuli and assumes an autocrine/paracrine role. Functional analysis of these variants showed that isoform Ec was more effective in promoting muscle tissue repair and growth than IGF-1Ea (Goldspink and Yang 2004). In teleost fish (i.e. Salmonids and Japanese flounder), four different isoforms have been identified, shown to be either tissue-specific or differentially stimulated by GH (Cao et al., 1989; Duguay et al., 1992; Wallis and Devlin, 1993; Tanaka et al., 1998) and associated (i.e. the recombinant E peptides) to cell proliferation/differentiation, angiogenesis and tumor growth (Tian et al., 1999; Chen et al., 2002; Chun et al., 2006). However, despite an increasing interest in understanding the physiological role of proIGF-1 and E peptides, basic data such as a comprehensive

* Corresponding author. Fax: +351 289 800069.
E-mail address: lcancela@ualg.pt (M.L. Cancela).
[1] *URL:* http://www.ualg.pt/fcma/edge/web/ (M.L. Cancela).

0016-6480/$ - see front matter © 2008 Published by Elsevier Inc.
doi:10.1016/j.ygcen.2008.04.006

Please cite this article in press as: Tiago, D.M. et al., Alternatively spliced transcripts of *Sparus aurata* insulin-like growth factor 1 are differentially expressed in adult tissues and during early development ..., Gen. Comp. Endocrinol. (2008), doi:10.1016/j.ygcen.2008.04.006

description of existing forms and characterization of their expression patterns are still lacking. In this paper, we report the existence of three alternatively spliced IGF-1 transcripts in the gilthead seabream (*Sparus aurata*) and characterize the expression patterns of each variant in a wide selection of adult tissues and throughout fish development. Furthermore, available E domain structures from various vertebrates were compared from an evolutionary point of view.

2. Materials and methods

2.1. Materials

Moloney murine leukemia virus reverse transcriptase (MMLV-RT), *Taq* DNA polymerase and TOPO TA Cloning kit were purchased from Invitrogen (Carlsbad, CA); [α-^{32}P]dCTP, GFX PCR DNA and Gel Band Purification kit, Rediprime II kit, MicroSpin G-50 columns, Quick Prep Micro mRNA Purification kit and Hybond-XL nylon membrane were purchased from Amersham Biosciences (Piscataway, NJ); RQ1 RNase-free DNase was purchased from Promega (Madison, WI); Advantage, Marathon and GenomeWalker Universal kits were purchased from Clontech BD Biosciences (Mountain View, CA); Real-time PCR iQ SYBR Green Supermix was purchased from Bio-Rad (Hercules, CA). All other reagents were purchased from Sigma-Aldrich (St. Louis, MO), unless otherwise stated.

2.2. Larvae, juvenile, and adult fish

Eggs collected from natural spawning of *S. aurata* (from January to March 2006) were placed at 16 °C in a closed recirculating system with 35 ppt salinity water. Light was controlled with fluorescent lamps, maintaining a 12:12 h light–dark photoperiod. Hatching took place 48–56 h after fertilization (HAF; size of larvae was approximately 3 mm). Developing larvae were fed with rotifers from 96 HAF to 20 days after hatching (DAH; approx. size 7–8 mm) and with newly hatched *Artemia nauplii* from 20 to 50 DAH (approx. size 15 mm). Rotifers and *A. nauplii* were fed with microalgae *Tetraselmis suecica* and *Isochrysis galbana*. Selco (INVE, Dendermond, Belgium) was introduced into larval diet between 35 and 45 DAH through the use of Selco-enriched *A. nauplii*. Dry food was introduced into larval diet between 45 and 70 DAH (approx. size 20 mm) through the use of Selco/dry food mixture (50:50). After 70 DAH, larvae were maintained on a dry food diet. Definitive morphology was reached at 90 DAH (approx. size 30 mm). Juvenile and adult fish were reared at 16–20 °C in 100-L tanks with a 12:12 h light–dark photoperiod, aeration of 100 ml/min, and renewal flow of 1 tank/day and fed with artificial food (Sorgal, Porto, Portugal). When sampled for RNA preparation, eggs, larvae (in pools of at least 10) and juvenile fish were washed in phosphate-buffered saline solution and stored at −80 °C in 5 ml of Trizol reagent. Tissues for RNA preparation were removed from anesthetized (using 2-phenoxyethanol at 1:10,000 in seawater) then decapitated adult fish, and stored at −80 °C in 5 ml of guanidine thiocyanate solution.

2.3. RNA preparation

Total RNA was extracted from selected tissues of adult seabream (3 males of approx. 0.5 kg and 1 female of approx. 2 kg; equal amount of male and female tissues were mixed), and from eggs, larvae and juvenile using Trizol. Total RNA concentration was determined by spectrophotometry at 260 nm (GeneQuant, Pharmacia Biotech, Sweden).

2.4. Construction of cDNA and genomic DNA libraries

Full-length cDNA library and genomic DNA libraries used in this work have been previously developed in our laboratory using the Marathon cDNA Amplification kit and a pool of poly(A$^+$) RNA from *S. aurata* liver, kidney, brain, and pituitary, and using the GenomeWalker Universal kit and genomic DNA from *S. aurata* digested with PvuII and ScaI, respectively. Libraries were constructed according to manufacturer's instructions.

2.5. DNA amplification and cloning

Rapid amplification of cDNA ends (RACE) and amplification of full-length cDNAs were performed by PCR using a 1:50 dilution of the Marathon cDNA library, Advantage *Klen Taq* Polymerase mix and primers listed in Table 1. Amplification of genomic fragments was performed by PCR using GenomeWalker libraries, Advantage *Klen Taq* Polymerase mix and primers listed in Table 1. PCR amplifications were performed according to manufacturer's instructions. PCR products were size-separated by agarose gel electrophoresis, purified using the GFX PCR DNA and Gel Band Purification kit, and cloned into pCRII-TOPO vector. Final fragment identification was achieved by DNA sequencing (Macrogen, Seoul, South Korea) and comparative analysis using BLAST facilities at NCBI (http://www.ncbi.nih.gov).

Table 1
PCR primers used in this study

Primer names	Primer sequence (5′–3′)
Sparus aurata IGF-1 gene primers	
IGF-1RV1	GCTAGACATCCCCACGGGTCTCCGCAAGA
IGF-1FW1	GTGACATTGCCCGCATCTCATCCTC
IGF-1FW2	TGGGGATGTCTAGCGCTCTTTCCTTTC
IGF-1RV2	TCCATTCGCTCCGTCCCTACATTC
IGF-1FW3	GGCATTGTGGACGAGTGCTGCTTCC
IGF-1FW4	TGTGAGCTGCGGCGTCTGGAGATGTAC
IGF-1ABC_FW	ACAGAATGTAGGGACGGAGCGAATGGAC
IGF-1A_FW	AGGACAGCACAGCAGCCAGACAAGAC
IGF-1AB_FW	AGTCATTCATCCTTCAAGGAAGTGCATCC
IGF-1ABC_RV	TTCGGACCATTGTTAGCCTCCTCTCTG
Sparus aurata housekeeping gene primers	
ActinFW	CTTCCTCGGTATGGAGTCCTGCGG
ActinRV	TCCTGCTTGCTGATCCACATCTGCT
RPL27aFW	AAGAGGAACACAACTCACTGCCCCAC
RPL27aRV	GCTTGCCTTTGCCCAGAACTTTGTAG
Commercial primers	
Oligo-d(T)-adapter	ACGCGTCGACCTCGAGATCGATG(T)$_{13}$
Universal adapter	ACGCGTCGACCTCGAGATCGATG
MarAP1	CCATCCTAATACGACTCACTATAGGGC
MarAP2	ACTCACTATAGGGCTCGAGCGGC
GWAP1	GTAATACGACTCACTATAGGGC
GWAP2	ACTATAGGGCACGCGTGGT

2.6. Sequence reconstruction

GenBank database was searched using BLAST facilities at NCBI for sequences showing similarities to IGF-1 transcripts. Species-specific sequences were first clustered then assembled using ContigExpress module of Vector NTI Suite 10 (Invitrogen) to generate, after manual correction, accurate consensus sequences. Virtual transcripts and alternative splicing events were deduced from consensus sequences using stringent overlap criteria.

2.7. Genomic Southern analysis

Aliquots (10 μg) of *S. aurata* genomic DNA, prepared using DNeasy Tissue kit (QIAGEN, Hilden, Germany), were digested with 25 units of selected endonucleases (BglI, BglII, EcoRI, HindIII, PstI, and ScaI) and DNA fragments were size-separated on a 0.8% agarose gel for 10 h at 50 V. DNA was then transferred onto a Hybond-XL nylon membrane by capillarity blotting with 10× standard saline citrate buffer (SSC; 1× SSC is 0.15 M NaCl and 15 mM sodium citrate, pH 7.0). IGF-1 cDNA probe (199 bp corresponding to cDNA positions 357–555 bp) was radiolabeled with [α-^{32}P]dCTP (3000 Ci/ml) using the Rediprime II kit and purified from unincorporated nucleotides using MicroSpin G-50 columns. The hybridization was performed overnight at 42 °C in ULTRAhyb solution (Ambion, Austin, TX). Blots were washed 2 × 5 min in low stringency solution (2× SSC, 0.1% SDS) and 3 × 15 min in high stringency solution (0.1× SSC, 0.1% SDS) at 60 °C, then autoradiographed.

2.8. Analysis of gene expression levels by quantitative real-time PCR

Quantitative real-time PCR was performed using iCycler iQ system (Bio-Rad). Total RNA (1 μg) from *S. aurata* unfertilized eggs, embryos, larvae, juveniles or adult tissues was treated with RQ1 RNase-free DNase (Promega) then reverse-transcribed at 37 °C according to manufacturer's instruction using MMLV-RT and specific reverse primers (Table 1). PCR amplification of cDNA fragments was performed using the iQ SYBR Green I mix, specific primers (Table 1) and 10 ng of reverse-transcribed RNA. The following PCR conditions were used: an initial denaturation step at 95 °C for 4 min then 40–50 cycles of amplification (each cycle is 30 s at 95 °C, 30 s at 68 °C). Fluorescence was measured at the end of each extension cycle in the FAM-490 channel. Levels of IGF-1 gene expression were calculated using the $\Delta\Delta C_t$ method and normalized using expression levels of β-actin or ribosomal protein L27a (RPL27a) housekeeping genes in developmental samples and in adult samples, respectively.

3. Results

3.1. Cloning of seabream IGF-1 transcripts

A 155-bp fragment was first amplified by two rounds of RACE-PCR using Marathon primers AP1 and AP2 combined with reverse primer IGF-1RV1 (Table 1), designed according to the partial sequence published by Duguay et al. (1996). This fragment was se-

UNCORRECTED P

quenced, identified as the 5′ end of seabream IGF-1 cDNA, and then used to design the forward specific primer IGF-1FW1 (Table 1). Using this primer and Marathon primer AP1, two fragments of 2204 and 2285 bp were amplified by PCR. Both fragments were sequenced and identified as full-length IGF-1 cDNAs, then termed IGF-1a (longer transcript; Accession No. AY996779) and IGF-1b (shorter transcript; Accession No. EF688015). The comparison of both sequences identified a region of 81 bp present in IGF-1a but absent in IGF-1b (Fig. 1) and localized in the sequence coding for E domain (from nt 492 to nt 572). Specific primers were designed in order to detect additional IGF-1 transcripts. Using primer sets IGF-1FW1/AP1 and IGF-1FW2/IGF-1RV2 (Table 1), a third fragment was amplified and termed IGF-1c (Accession No. EF688016). The comparison of IGF-1c sequence with that of IGF-1a identified a region of 117 bp present in IGF-1a but absent in IGF-1c (Fig. 1) and localized in the sequence coding for E domain (from nt 492 to nt 608). No polyadenylation signal has been clearly identified but a putative one has been underlined in Fig. 1. All transcripts identified in this study as *S. aurata* IGF-1 encode peptides containing the six canonical domains (Moriyama et al., 2000) but exhibiting different sizes for the E domain: 74, 47, and 35 aa for IGF-1a, 1b, and 1c, respectively.

3.2. IGF-1 gene occurrence and structure

In order to determine whether the identified transcripts originated from alternative splicing of a single IGF-1 gene or from several genes, *S. aurata* genome was analyzed by Southern blot. Probe was designed within putative exon 3 (determined by comparison of seabream cDNA with zebrafish, salmon and flounder IGF-1

```
cggaatattgagatgtgacattgcccgcatctcatcctctttctccccgtttttaatgacttcaaacaagttcat   75
                                        M  S  S  A  L  S  F  Q  W  H  L  C  D   13
tttcgccgggctttgtcttgcggagacccgtgggg ATGTCTAGCGCTCTTTCCTTTCAGTGGCATTTATGTGAT  149
 V  F  K  S  A  M  C  C  I  S  C  S  H  T  L  S  L  L  L  C  V  L  T  L  T   38
GTCTTCAAGAGTGCGATGTGCTGTATCTCCTGTAGCCACACCCTCTCACTACTGCTGTGCGTCCTCACCCTGACT  224
 P  T  A  T  G  A  S  P  E  T  L  C  G  A  E  L  V  D  T  L  Q  F  V  C  G   63
CCGACGGCAACAGGGGCGAGCCCAGAGACCCTGTGCGGGGCGGAGCTGGTCGACACGCTGCAGTTTGTGTGTGGA  299
 E  R  G  F  Y  F  S  K  P  G  Y  G  P  N  A  R  R  S  R  G  I  V  D  E  C   88
GAGAGAGGCTTTTATTTCAGTAAACCTGGCTACGGCCCCAATGCACGGCGGTCACGTGGCATTGTGGACGAGTGC  374
 C  F  Q  S  C  E  L  R  R  L  E  M  Y  C  A  P  A  K  T  S  K  A  A  R  S  113
TGCTTCCAAAGCTGTGAGCTGCGGCGTCTGGAGATGTACTGTGCACCTGCCAAGACTAGCAAGGCTGCTCGCTCT  449
 V  R  A  Q  R  H  T  D  M  P  R  A  P  K  V  S  T  A  G  H  K  V  D  K  G  138
GTGCGTGCACAGCGCCACACAGACATGCCAAGAGCACCCAAGGTTAGTACCGCAGGGCACAAAGTGGACAAGGGC  524
 T  E  R  R  T  A  Q  Q  P  D  K  T  K  N  K  K  R  P  L  P  G  H  S  H  S  163
ACAGAGCGTAGGACAGCACAGCAGCCAGACAAGACAAAAAACAAGAAGAGACCTTTACCTGGACATAGTCATTCA  599
 S  F  K  E  V  H  P  K  N  S  S  R  G  N  A  G  G  R  N  Y  R  M  ***       185
TCCTTCAAGGAAGTGCATCCGAAAAACTCAAGTCGAGGCAACGCGGGGGGCAGAAATTACAGAATGTAG ggacg  673

gagcgaatggacaaatgcccagcgacttgggaagagagaagggagtggccttacctggtacccctgtggaatggt  748
tcactgtaaaacaaaacagagaggaggctaacaatggtccgaaacgctcttcagaatgattgaacgctgagagct  823
aagtggtgtttaagggttttgatgagggatcttgtgattattttatacactgcaccattccatatcgggaggaat  898
tctttgttaatgcaatgtaacagactagtttagctgctgagacacgaaacaagagcttattatacctccatgtgt  973
gagctgcagcaacccctggctccaggaaaggtgggaacggatctgggcttcagccaatcagagagctgcaggctg 1048
cgttttcttgtttttgctaacgagcgatccgtcccgtcccttgaactctgcggaggtaaatccttttttctctg 1123
agagagtggactcgttcgctctgtccgtaagacaggatatttcttcaccggtcacatattacagttaaaatcaga 1198
tcatcttaccgtcgagcgtttgttttcatgcaccgtgcgttactgaggatatttttaacaagtaaaaaaagttcg 1273
ctttaaagcacaaagaccaggtggttcattctcagactttaaacattgtagttatttttacataaaatcccttcgt 1348
ctcattgactgaaggcagcgttcttctgtctaagtggagtcagtcgaaggcttcagtccaatccaaatccctcct 1423
aagctgcaggaagtgttgagaacctgagatctgagtctacaatccaaacacctctgtaacaacagatcaagcacc 1498
attagaggggattttaaggaacagtaggtactccaaaaaacaagactgtgctttttgcctatttttccaaaacaga 1573
gaatcaaattaaccagaagctcaattgaatcaaagtttctttggccgctcgttgcgtggtgcttgtttggttgtc 1648
agaaatgggtcattcagtggattcaaagtgcatttggcataagccagtggaataagtcaaatagcgacaatcagg 1723
caaaatgtttgtcgtctgcatccttttcacatgtcaccgccgctgccaaatcagattttctgtcaacaatccagt 1798
cggcgctgatcaacatttgagtctgagtggaggcctgtgttcaaggttaaacacaagtcatgaaagtttagtggc 1873
agaaagagccaagagctcgaagagaagtatcaaatacggtcaaatctttcctcgtgctctcttgaagaactagcg 1948
atgtgcccccaagtcttcgtaaagttggagaggctcgaacaattgccgctccacagatgtgaagtttaacaatcg 1923
atcgatctcggcgtgtaatattttgtcagttaacgttgcaacttcggtcgttgcttgtgctgccgtcgttacgag 2098
agcgcaacggaactcaaagtccaacaaagaaactgaatgatttggtaaatagaacaaagtgactcgtcctcttgc 2173
ggatgtgagatacggcacgcaatttaacagcgcacaaacacacatgcaaaaaaaaaaaaaaaaaaaaaaaaaa   2245
```

Fig. 1. *Sparus aurata* IGF-1 full-length cDNA and deduced amino acid sequences. Light gray box and black letters indicate the signal peptide; dark gray box and black letters indicate the B domain; dark gray box and white letters indicate the C domain; white box indicates the A domain; light gray box and white letters indicate the D domain; black box and white letters indicate the E domain; asterisks indicate the stop codon; black arrows set the boundaries of the 81-bp alternatively spliced region present in IGF-1a transcript but absent in transcripts IGF-1b and IGF-1c (alternative GT donor splice site is bold-underlined); gray arrows set the boundaries of the 36-bp alternatively spliced region present in transcripts IGF-1a and IGF-1b but absent in transcript IGF-1c; putative polyadenylation signal sequence is underlined.

Please cite this article in press as: Tiago, D.M. et al., Alternatively spliced transcripts of *Sparus aurata* insulin-like growth factor 1 are differentially expressed in adult tissues and during early development ..., Gen. Comp. Endocrinol. (2008), doi:10.1016/j.ygcen.2008.04.006

genes), which is present in all three transcripts, and found to contain no restriction sites for the endonucleases used in this work to digest genomic DNA. Accordingly, a single signal was detected in each lane of the Southern blot (Fig. 2), suggesting the presence of only one copy of IGF-1 gene in *S. aurata* genome and that IGF-1 transcripts were spliced variants. Using primer IGF-1FW3 and IGF-1FW4, designed immediately upstream of the spliced regions, in combination with GenomeWalker AP1 and AP2 primers, respectively (Table 1), a genomic fragment of approximately 4600-bp was amplified, sequenced and identified as partial seabream IGF-1 gene (Accession No. DQ118098). This genomic fragment was compared with each of the transcripts using the Spidey mRNA-to-genomic alignment tool at NCBI, allowing the reconstruction of partial IGF-1 gene structure (Fig. 3). Exon 3 (partial), exon 4, and exon 5 (containing 3′UTR) were identified, coding for domains A (partial), D and E, respectively (Fig. 3A). Spliced regions were localized within exon 3 and exon 4 and shown to be removed through two different splicing mechanisms: (1) alternative donor site (two functional GT donor sites were localized 81 bp from each other) at the 3′ extremity of exon 3, and (2) alternative skipping of the entire exon 4. In all cases, the phase of intron insertion was conserved (phase 0 according to (Patthy, 1987) thus maintaining the same reading frame.

3.3. Expression of IGF-1 transcripts during development and in adult seabream

Relative expression of alternatively spliced transcripts was measured by real-time PCR in developing and adult seabream using three sets of variant-specific primers (Table 1 and Fig. 3): set 1 (IGF-1ABC) to amplify all isoforms, set 2 (IGF-1A) to amplify IGF-1a, and set 3 (IGF-1AB) to amplify simultaneously IGF-1a and IGF-1b (Fig. 3B). IGF-1b relative gene expression was determined by subtracting values from set 2 to those from set 3 while relative levels of IGF-1c gene expression were determined by subtracting values from set 3 to those of set 1 (Figs. 4 and 5). IGF-1c was expressed at basal levels in unfertilized eggs and during early development (embryo) while strongly up-regulated (around 30-fold) in hatched larvae. Levels of IGF-1c expression remained high in juvenile fish. IGF-1a transcript was first detected in larvae at 20 DAH, exhibiting intermediate levels of expression that remained stable throughout larval and juvenile development. IGF-1b transcript was detected soon after hatching but the levels remained low throughout larval and juvenile development. All three transcripts clearly exhibited different patterns of gene expression during development (different onset and extent), suggesting different roles during this particular process in fish. Differential expression of spliced variants was also observed in adult tissues. IGF-1c was by far the most expressed transcript in all adult tissues, exhibiting highest levels of expression in liver, adipose tissue and pancreas, and moderate levels in brain, gall bladder, spleen and most of the calcified tissues, including poorly calcified branchial arches and gills. Both IGF-1a and IGF-1b were poorly expressed in most tissues analyzed, with the exception of liver.

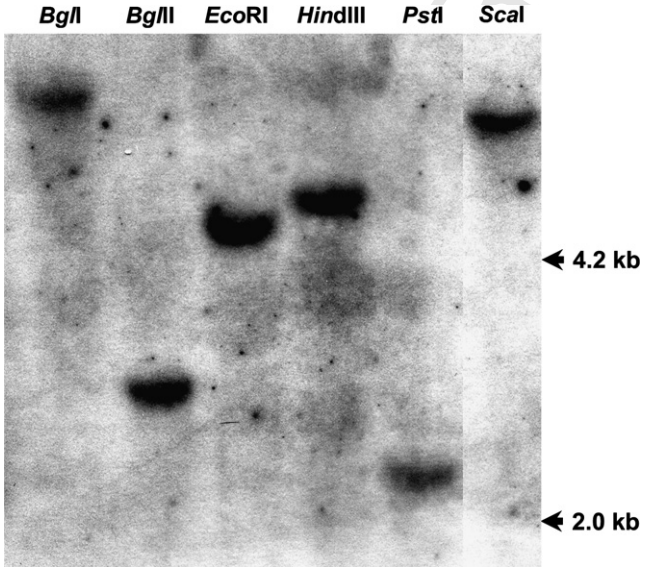

Fig. 2. Southern blot analysis of *S. aurata* genomic DNA. A 199-bp radiolabeled probe specific for exon 3 was used for hybridization; restriction enzymes used to digest genomic DNA (BglI, BglII, EcoRI, HindIII, PstI, and ScaI) are indicated above each lane; DNA marker sizes are indicated in the right.

4. Discussion

Recent reports on the existence of multiple forms of IGF-1 propeptides (or E peptides) in vertebrates have increased the interest of the scientific community in understanding its biological role, which remains largely controversial (Duguay et al., 1992, 1994; Tian et al., 1999; Chen et al., 2002; Goldspink and Yang, 2004; Chun et al., 2006).

4.1. Seabream IGF-1: one gene, several transcripts

Three alternatively spliced IGF-1 transcripts (IGF-1a, 1b, and 1c) have been identified in gilthead seabream. A transcript similar to seabream IGF-1a was already available (Duguay et al., 1996), but with what appears to have been an error in termination codon identification and a partial 3′UTR. Alternative splicing mechanisms identified in seabream IGF-1 (alternative donor sites in exon 3 and entire skipping of exon 4) are consistent with those previously observed in Salmonids and flounder (Wallis and Devlin, 1993; Tanaka et al., 1998), as well as in mammals (Goldspink and Yang, 2004). Based on these similarities, a fourth transcript was predicted in seabream (IGF-1d; Fig. 3). IGF-1d has however never been detected yet and is, therefore, either weakly or not expressed in seabream, or its expression is restricted to sites not explored in this work. IGF-1d variant could also be related to the existence of a second IGF-1 gene as in Salmonids (note that existing data in Salmonids does not allow the association of any of the variants to a specific gene), and consequently be absent in seabream where available evidence does not support the existence of two genes.

4.2. Expression of IGF-1 spliced variants is tightly regulated during seabream development

Seabream IGF-1 variants have been shown in this study to exhibit different onset and extent of expression during development. A similar analysis, although not quantitative, has been performed in Coho salmon (Duguay et al., 1992): IGF-1b, IGF-1c, and IGF-1d isoforms were detected in 6-week-old embryos and thereafter, and shown to be mainly expressed in liver, muscle, and brain. Expression patterns of seabream IGF-1 variants during development suggest that either pro-peptides or E domains may be involved in specific organ formation and/or development. The early development of the endocrine system in seabream (Funkenstein and Cohen, 1996; Falk-Petersen, 2005) and the known regulation of IGF-1 gene expression (through growth hormone) by the endocrine system in vertebrates (Duguay et al., 1994; Ohlsson et al., 1998) may be related, in part, to the expression patterns of IGF-1b and IGF-1c transcripts during seabream early development. Similarly, the early onset of calcification in seabream and the later amplification of tissue mineralization (Pinto et al., 2001, 2003) and the pro-

CORRECTED PROOF

Please cite this article in press as: Tiago, D.M. et al., Alternatively spliced transcripts of *Sparus aurata* insulin-like growth factor 1 are differentially expressed in adult tissues and during early development ..., Gen. Comp. Endocrinol. (2008), doi:10.1016/j.ygcen.2008.04.006

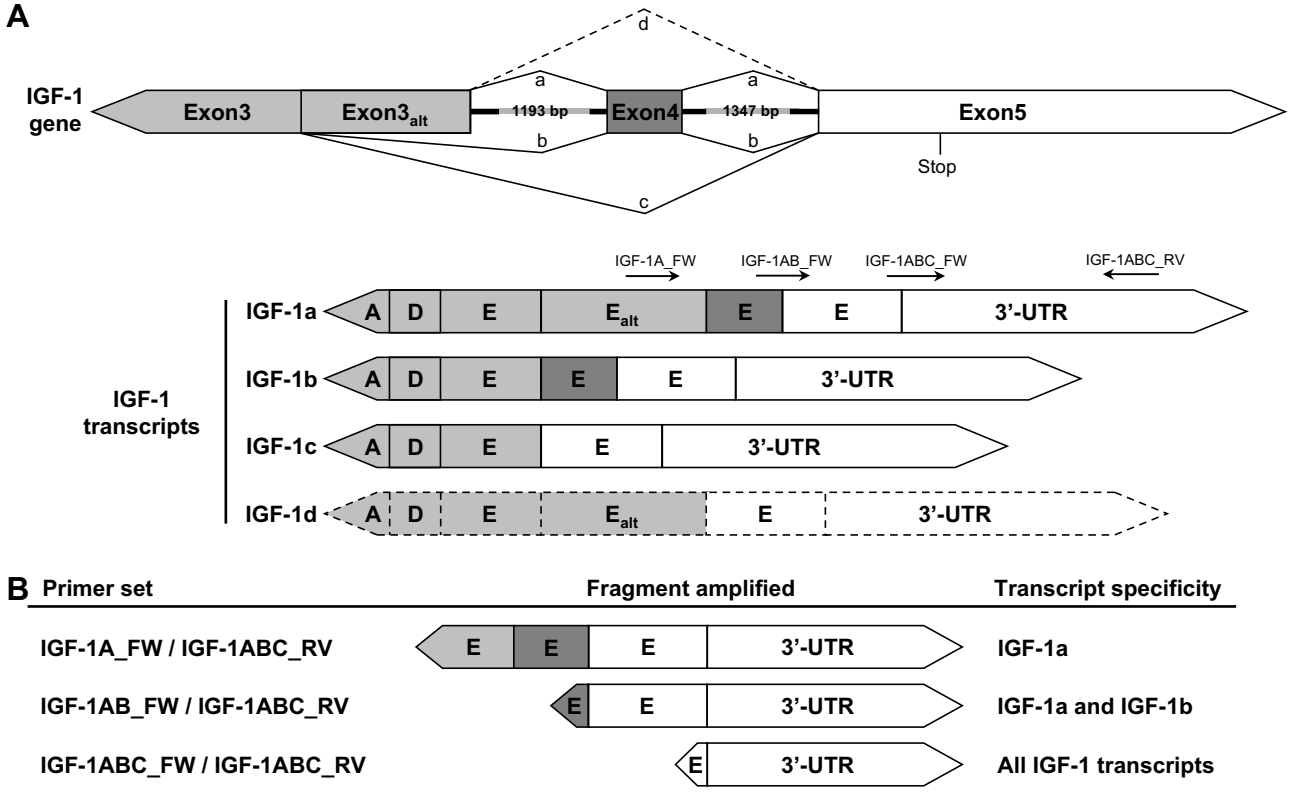

Fig. 3. Schematic representation of *S. aurata* partial IGF-1 gene and related cDNAs. (A) Exons and domains are represented by boxes; introns are represented by solid thick lines; light gray boxes indicate exon 3 and related domains, dark gray boxes indicate exon 4 and related domains and white boxes indicate exon 5 and related domains; boxes with dashed lines indicate putative alternative transcripts; alternative splicing events in exon 3 and exon 4 are represented by solid and dashed lines; primers used for real-time PCR amplification of alternative transcripts are indicated above IGF-1a cDNA. (B) Real-time PCR fragments and primers used to amplify them; first primer set is specific for IGF-1a transcript and amplifies a 258-bp fragment; second primer set is specific for IGF-1a and IGF-1b transcripts and amplifies a 201-bp fragment; third primer set amplifies a 134-bp fragment common to all three transcripts.

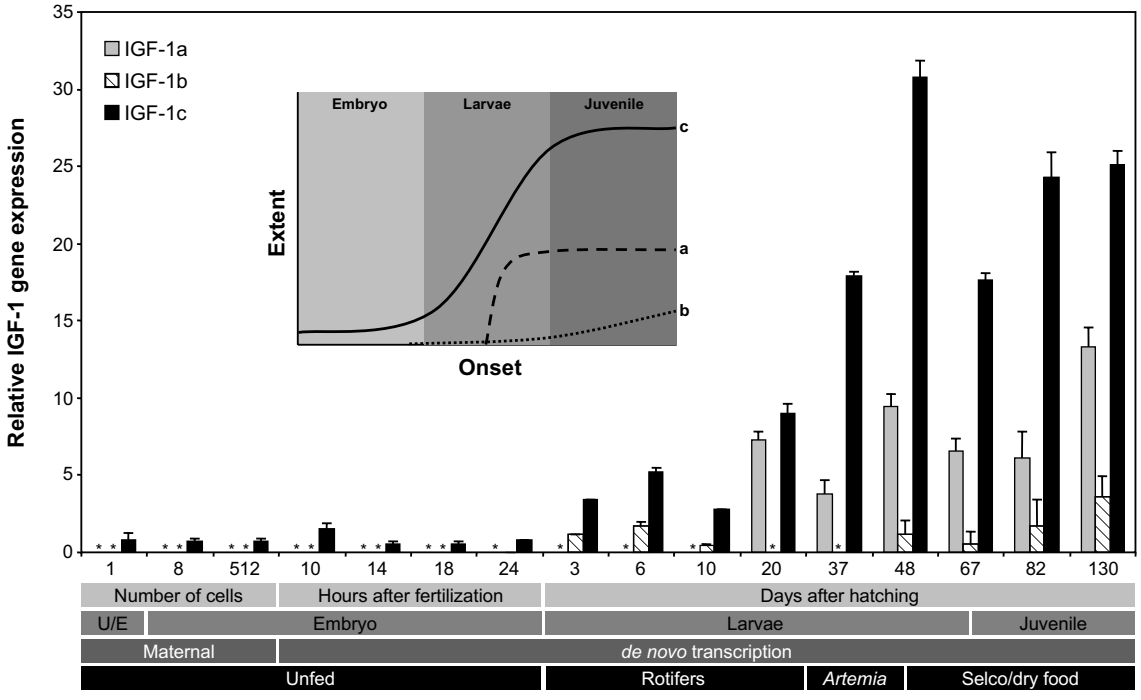

Fig. 4. Relative IGF-1 gene expression during *S. aurata* development measured by real-time PCR. IGF-1 gene expression was normalized using housekeeping gene β-actin; asterisks indicate that transcripts were not detected; U/E means unfertilized eggs; values represent the mean of results obtained in at least three independent real-time PCR experiments; inset illustrates the appearance of different IGF-1 transcripts throughout *S. aurata* development.

Please cite this article in press as: Tiago, D.M. et al., Alternatively spliced transcripts of *Sparus aurata* insulin-like growth factor 1 are differentially expressed in adult tissues and during early development ..., Gen. Comp. Endocrinol. (2008), doi:10.1016/j.ygcen.2008.04.006

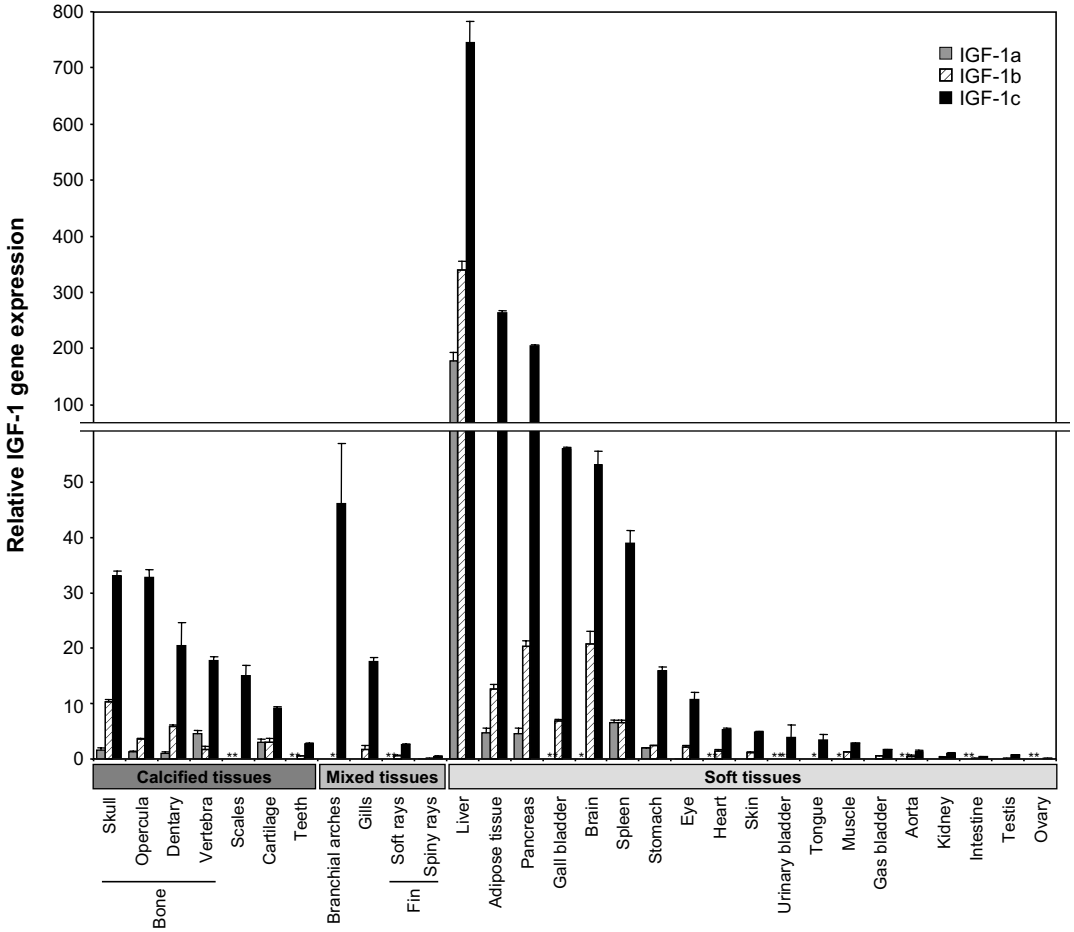

Fig. 5. Relative IGF-1 gene expression in *S. aurata* tissues measured by real-time PCR. IGF-1 gene expression was normalized using housekeeping gene RPL27a; asterisks indicate that transcripts were not detected; values represent the mean of results obtained in at least three independent real-time PCR experiments.

posed mineralogenic role of IGF-1 in mammals (Zhao et al., 2000; Bikle et al., 2001; Zhang et al., 2002) and fish (Suzuki and Hattori, 2003) may be related, in part, to the expression patterns of IGF-1 transcripts during seabream development. Association of IGF-1 with muscle formation (red and white muscle formation at 1 and 35 DAH, respectively (Ayala et al., 1999) is consistent with identification of various spliced transcripts in the muscle of Coho salmon (Duguay et al., 1992) and seabream (this study), and with its role in muscle formation in mammals (Goldspink and Yang, 2004). However, additional experiments (e.g. phenotype analysis of developing larvae or cultured cells where expression of each of the IGF-1 precursors has been altered, or the determination of sites of gene expression by *in situ* hybridization using transcript-specific probes) will need to be performed to confirm the role of IGF-1 in these processes.

4.3. Systemic versus autocrine/paracrine action of IGF-1 spliced variants in seabream

Various physiological mechanisms have been associated with IGF-1 action in mammals. It includes: (i) stem cell differentiation into adipocyte and metabolic mechanisms of fasting and re-feeding in adipose tissue (Bertile and Raclot, 2004; Otto and Lane, 2005); (ii) pancreatic β-cell proliferation (Kulkarni, 2005) and insulin release (Hill et al., 1997); and (iii) regulation of bone mineral density in developing structures (Canalis, 1993). Pattern of IGF-1 expression in adult seabream (i.e. main expression is in liver, adipose tissue and pancreas; relatively high expression in calcified tissues) is in agreement with the reported role of mammalian IGF-1 in these processes. IGF-1c propeptide (or E peptide alone), which transcript is predominant in liver (expression levels are 2–4 times higher than those for variants 1a and 1b), is likely to be involved in important physiological processes upon its release into circulation, a hypothesis consistent with previous observations in mammals, in which a systemic mode of action was demonstrated for IGF-1-Ea, the IGF-1c-like isoform in mammals (Goldspink and Yang, 2004). We propose that IGF-1c isoform assumes a similar role in seabream, and following the same idea, that variants 1a and 1b would assume local functions. Also of interest is our finding of relatively high IGF-1c expression in calcified tissues, which may indicate a role of this variant in bone formation or metabolism.

4.4. Mechanisms of IGF-1 alternative splicing in vertebrates are taxon-specific

In order to understand the occurrence of IGF-1 variants in adult tissues and during seabream development, orthologous sequences have been searched within GenBank sequence data base using Blast facilities at NCBI. Positive search results were considered to be members of the IGF-1 family if they showed significant sequence similarity to any of the previously identified members and if this similarity extended throughout the protein. Our search identified various sequences previously identified as IGF-1 and numerous ESTs (a total of 154 sequences), from which we could identify/reconstruct 52 IGF-1-related cDNAs (see Supplementary data in Fig. S1) from 41 species representing most classes of verte-

Please cite this article in press as: Tiago, D.M. et al., Alternatively spliced transcripts of *Sparus aurata* insulin-like growth factor 1 are differentially expressed in adult tissues and during early development ..., Gen. Comp. Endocrinol. (2008), doi:10.1016/j.ygcen.2008.04.006

brates (i.e. mammals, birds, amphibians and bony fish). An IGF-1-like sequence was also identified in a cartilaginous fish (*Squalus acanthias*) but homology with other IGF-1 sequences, in particular within the E domain, was weak making its identification dubious. Consequently, no sequence from cartilaginous fish was included in our analysis. While all available sequences from bony fish, birds and amphibians were analyzed, only sequences from human and mouse were processed for mammals, since almost nearly complete sets of sequences exist for both species. Four alternatively spliced IGF-1 transcripts were identified in bony fish: IGF-1a, 1b, 1c, and 1d (Fig. 6A). A single transcript, spliced as seabream IGF-1c, was identified in birds and amphibians. Finally, three IGF-1 variants were identified in mammals, one spliced as seabream IGF-1c (IGF-1–Ea), and two variants specific to this taxonomic group: IGF-1–Eb, which includes exons 4 and 5 in the E domain, and IGF-1–Ec, which includes exons 4, partial 5 and 6 (Goldspink and Yang, 2004). Analysis of the distribution of IGF-1 variants in fish taxonomic subgroups revealed that (i) IGF-1a transcript was specific of the Acanthopterygii and Protacanthopterygii, (ii) IGF-1b transcript was mainly found in Ostariophysi (also observed in

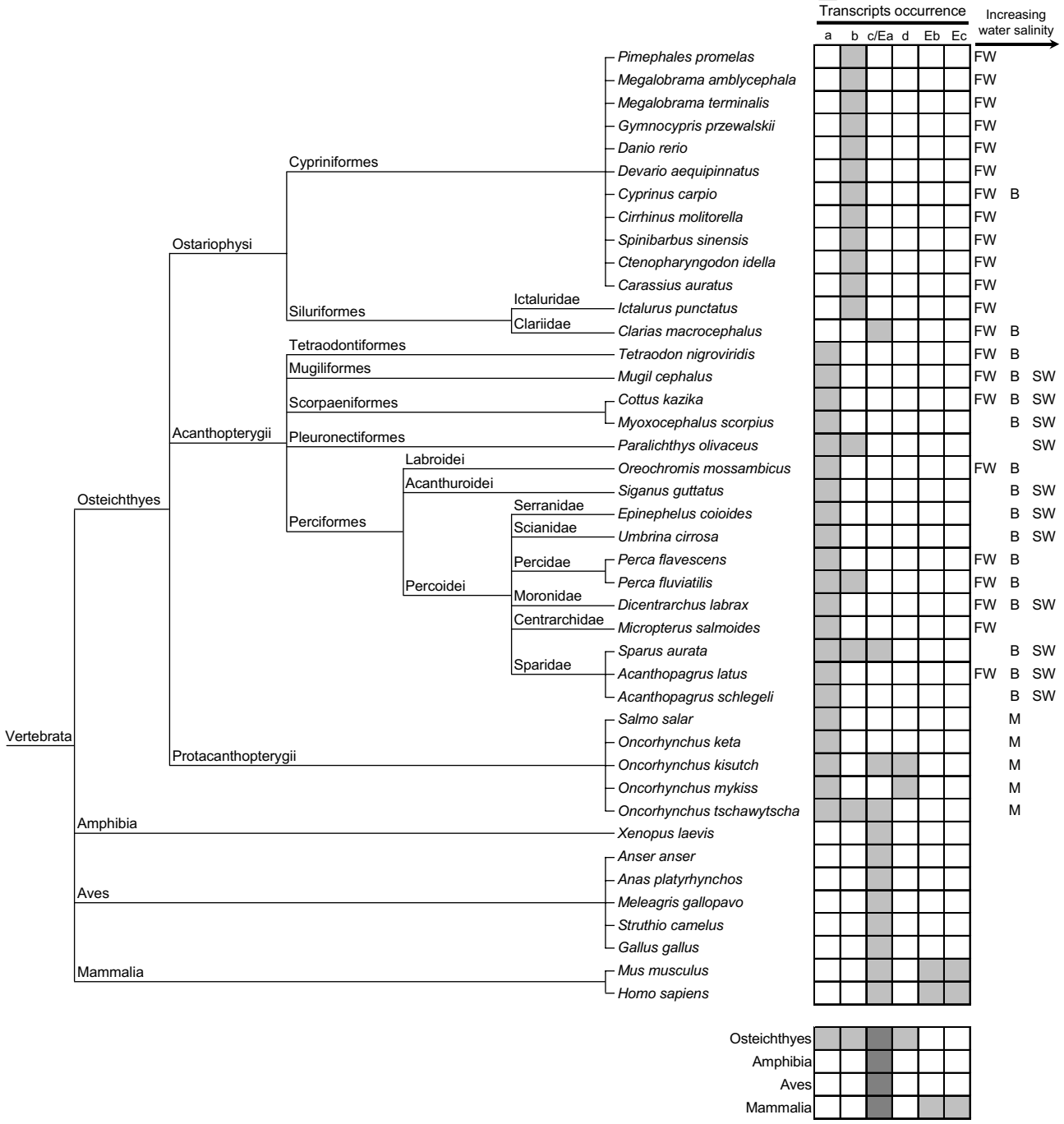

Fig. 6. Species and vertebrate distribution of IGF-1 alternatively spliced transcripts. Taxonomic tree of represented species; taxonomic data were retrieved (10–27–2006) from the Integrated Taxonomic Information System at http://www.itis.usda.gov and fish salinity environment data were retrieved from FishBase website at http://www.fishbase.org; *a*, b, c and d indicate IGF-1a, IGF-1b, IGF-1c, and IGF-1d transcripts, respectively; Eb and Ec indicate the mammalian specific IGF-1 transcripts; FW, B, SW, and M indicate freshwater, brackish, seawater, and migratory species, respectively; gray boxes indicate the presence of a transcript in a species below, table indicates the distribution of IGF-1 transcripts in vertebrates taxons.

Please cite this article in press as: Tiago, D.M. et al., Alternatively spliced transcripts of *Sparus aurata* insulin-like growth factor 1 are differentially expressed in adult tissues and during early development ..., Gen. Comp. Endocrinol. (2008), doi:10.1016/j.ygcen.2008.04.006

few Acanthopterygii and Protacanthopterygii), (iii) IGF-1c was identified only in gilthead seabream and Salmonids, and (iv) IGF-1d, the rarest variant, was exclusively found in Salmonids (*Oncorhynchus kisutch* and *Oncorhynchus mykiss*). However, due to the limited genetic information available in public databases for this taxonomic group, we cannot exclude that IGF-1 isoform distribution presented here may be incomplete. Finally, isoforms 1a, 1b, and 1d were shown to be specific for bony fish, while isoforms Eb and Ec were found exclusively in mammals. On the contrary, IGF-1c/Ea variant was common to all vertebrate taxa and the only one present in amphibians and birds (Fig. 6B). We propose that 1c/Ea propeptide would play a systemic role in fish as shown in mammals (or would have acquired this role throughout evolution), while other propeptides (i.e. 1a, 1b, 1d, Eb, and Ec) would play specific and local roles that remain to be explored in future studies. The strong occurrence of IGF-1a and 1b in fish inhabiting waters of different salinities (Fig. 6A) and the up-regulation of IGF-1 expression in salmon gills during seawater adaptation and smoltification process (Sakamoto et al., 1995) could suggest a role for these variants in osmoregulation. In order to test this hypothesis, additional experiments, such as analysis of IGF-1 expression during adaptation of gilthead seabream, which is euryhaline, to different water salinities should be carried out in studies similar to those described for striped bass (Tipsmark et al., 2007).

4.5. Conclusion

Three seabream IGF-1 alternative transcripts have been identified and extensively analyzed by quantitative real-time PCR in developing and adult specimens. In general, a tight regulation of these transcripts' expression was observed, and we propose that different E domains, associated or not to a mature peptide, assume specific functions. We hypothesize that: (a) IGF-1a and IGF-1b are involved in the regulation of late developmental events (e.g. muscle and bone formation); (b) IGF-1c participates in early developmental events, and in later events in concerted action with IGF-1a and IGF-1b; and (c) IGF-1c isoform is associated to a systemic mode of action. Finally, occurrence of different IGF-1 variants in teleosts could be associated with osmoregulatory processes.

Acknowledgments

D.M.T. was the recipient of a doctoral fellowship (BD/12773/2003) awarded by the Portuguese Science and Technology Foundation (FCT). The authors are grateful to P. Gavaia for his help with *S. aurata* specimens and for expert advices in fish development. We also thank M. Rafael for her collaboration in optimization of qPCR conditions. This work was partially supported by Grant GOCE-CT-2004-505403 (Marine Genomics Europe) from the European Commission under the 6th Framework Program.

Appendix A. Supplementary data

Supplementary data associated with this article can be found, in the online version, at doi:10.1016/j.ygcen.2008.04.006.

References

Ayala, M.D., Lopez-Albors, O., Gil, F., Ramirez-Zarzosa, G., Abellan, E., Moreno, F., 1999. Red muscle development of gilthead sea bream *Sparus aurata* (L.): structural and ultrastructural morphometry. Anat. Histol. Embryol. 28, 17–21.

Bertile, F., Raclot, T., 2004. Differences in mRNA expression of adipocyte-derived factors in response to fasting, refeeding and leptin. Biochim. Biophys. Acta 1683, 101–109.

Bikle, D., Majumdar, S., Laib, A., Powell-Braxton, L., Rosen, C., Beamer, W., Nauman, E., Leary, C., Halloran, B., 2001. The skeletal structure of insulin-like growth factor I-deficient mice. J. Bone Miner. Res. 16, 2320–2329.

Canalis, E., 1993. Insulin like growth factors and the local regulation of bone formation. Bone 14, 273–276.

Canalis, E., Pash, J., Varghese, S., 1993. Skeletal growth factors. Crit. Rev. Eukaryot. Gene Expr. 3, 155–166.

Cao, Q.P., Duguay, S.J., Plisetskaya, E., Steiner, D.F., Chan, S.J., 1989. Nucleotide sequence and growth hormone-regulated expression of salmon insulin-like growth factor I mRNA. Mol. Endocrinol. 3, 2005–2010.

Chen, M.J., Kuo, Y.H., Tian, X.C., Chen, T.T., 2002. Novel biological activities of the fish pro-IGF-I E-peptides: studies on effects of fish pro-IGF-I E-peptide on morphological change, anchorage-dependent cell division, and invasiveness in tumor cells. Gen. Comp. Endocrinol. 126, 342–351.

Chun, C.Z., Tsai, H.J., Chen, T.T., 2006. Trout Ea4- or human Eb-peptide of pro-IGF-I disrupts heart, red blood cell, and vasculature development in zebrafish embryos. Mol. Reprod. Dev. 73, 1112–1121.

D'Ercole, A.J., Ye, P., Gutierrez-Ospina, G., 1996. Use of transgenic mice for understanding the physiology of insulin-like growth factors. Horm. Res. 45 (Suppl. 1), 5–7.

Duguay, S.J., Lai-Zhang, J., Steiner, D.F., Funkenstein, B., Chan, S.J., 1996. Developmental and tissue-regulated expression of IGF-I and IGF-II mRNAs in *Sparus aurata*. J. Mol. Endocrinol. 16, 123–132.

Duguay, S.J., Park, L.K., Samadpour, M., Dickhoff, W.W., 1992. Nucleotide sequence and tissue distribution of three insulin-like growth factor I prohormones in salmon. Mol. Endocrinol. 6, 1202–1210.

Duguay, S.J., Swanson, P., Dickhoff, W.W., 1994. Differential expression and hormonal regulation of alternatively spliced IGF-I mRNA transcripts in salmon. J. Mol. Endocrinol. 12, 25–37.

Dupont, J., Holzenberger, M., 2003. Biology of insulin-like growth factors in development. Birth Defects Res. C Embryo Today 69, 257–271.

Efstratiadis, A., 1998. Genetics of mouse growth. Int. J. Dev. Biol. 42, 955–976.

Falk-Petersen, I.B., 2005. Comparative organ differentiation during early life stages of marine fish. Fish Shellfish Immunol. 19, 397–412.

Funkenstein, B., Cohen, I., 1996. Ontogeny of growth hormone protein and mRNA in the gilthead sea bream *Sparus aurata*. Growth Regul. 6, 16–21.

Goldspink, G., Yang, S.Y., 2004. The splicing of the IGF-I gene to yield different muscle growth factors. Adv. Genet. 52, 23–49.

Hill, D.J., Sedran, R.J., Brenner, S.L., McDonald, T.J., 1997. IGF-I has a dual effect on insulin release from isolated, perifused adult rat islets of Langerhans. J. Endocrinol. 153, 15–25.

Kulkarni, R.N., 2005. New insights into the roles of insulin/IGF-I in the development and maintenance of β-cell mass. Rev. Endocr. Metab. Disord. 6, 199–210.

Kuo, Y.H., Chen, T.T., 2002. Novel activities of pro-IGF-I E peptides: regulation of morphological differentiation and anchorage-independent growth in human neuroblastoma cells. Exp. Cell Res. 280, 75–89.

McCarthy, T.L., Centrella, M., 2001. Local IGF-I expression and bone formation. Growth Horm. IGF Res. 11, 213–219.

Moriyama, S., Ayson, F.G., Kawauchi, H., 2000. Growth regulation by insulin-like growth factor-I in fish. Biosci. Biotechnol. Biochem. 64, 1553–1562.

Ohlsson, C., Bengtsson, B.A., Isaksson, O.G., Andreassen, T.T., Slootweg, M.C., 1998. Growth hormone and bone. Endocr. Rev. 19, 55–79.

Otto, T.C., Lane, M.D., 2005. Adipose development: from stem cell to adipocyte. Crit. Rev. Biochem. Mol. Biol. 40, 229–242.

Patthy, L., 1987. Intron-dependent evolution: preferred types of exons and introns. FEBS Lett. 214, 1–7.

Pinto, J.P., Conceição, N., Gavaia, P.J., Cancela, M.L., 2003. Matrix Gla protein gene expression and protein accumulation colocalize with cartilage distribution during development of the teleost fish *Sparus aurata*. Bone 32, 201–210.

Pinto, J.P., Ohresser, M.C., Cancela, M.L., 2001. Cloning of the bone Gla protein gene from the teleost fish *Sparus aurata*. Evidence for overall conservation in gene organization and bone-specific expression from fish to man. Gene 270, 77–91.

Powell-Braxton, L., Hollingshead, P., Warburton, C., Dowd, M., Pitts-Meek, S., Dalton, D., Gillett, N., Stewart, T.A., 1993. IGF-I is required for normal embryonic growth in mice. Genes Dev. 7, 2609–2617.

Qin, X., Gysin, R., Mohan, S., Baylink, D.J., 2001. Bone growth factors. In: Marcus, R., Feldman, D., Kelsey, J. (Eds.), Osteoporosis. Academic Press, San Diego, pp. 405–431.

Sakamoto, T., Hirano, T., Madsen, S.S., Nishioka, R.S., Bern, H.A., 1995. Insulin-like growth factor-I gene expression during Parr–Smolt transformation of coho salmon. Zool. Sci. 12, 249–252.

Schmid, C., 1995. Insulin-like growth factors. Cell Biol. Int. 19, 445–457.

Shamblott, M.J., Chen, T.T., 1993. Age-related and tissue-specific levels of five forms of insulin-like growth factor mRNA in a teleost. Mol. Marine Biol. Biotechnol. 2, 351–361.

Suzuki, N., Hattori, A., 2003. Bisphenol A suppresses osteoclastic and osteoblastic activities in the cultured scales of goldfish. Life Sci. 73, 2237–2247.

Tanaka, M., Taniguchi, T., Yamamoto, I., Sakaguchi, K., Yoshizato, H., Ohkubo, T., Nakashima, K., 1998. Gene and cDNA structures of flounder insulin-like growth factor-I (IGF-I): multiple mRNA species encode a single short mature IGF-I. DNA Cell Biol. 17, 859–868.

Tian, X.C., Chen, M.J., Pantschenko, A.G., Yang, T.J., Chen, T.T., 1999. Recombinant E-peptides of pro-IGF-I have mitogenic activity. Endocrinology 140, 3387–3390.

UNCORRECTED PROOF

Tipsmark, C.K., Luckenbach, J.A., Madsen, S.S., Borski, R.J., 2007. IGF-I and branchial IGF receptor expression and localization during salinity acclimation in striped bass. Am. J. Physiol. Regul. Integr. Comp. Physiol. 292, R535–R543.

Wallis, A.E., Devlin, R.H., 1993. Duplicate insulin-like growth factor-I genes in salmon display alternative splicing pathways. Mol. Endocrinol. 7, 409–422.

Zhang, M., Xuan, S., Bouxsein, M.L., von Stechow, D., Akeno, N., Faugere, M.C., Malluche, H., Zhao, G., Rosen, C.J., Efstratiadis, A., Clemens, T.L., 2002. Osteoblast-specific knockout of the insulin-like growth factor (IGF) receptor gene reveals an essential role of IGF signaling in bone matrix mineralization. J. Biol. Chem. 277, 44005–44012.

Zhao, G., Monier-Faugere, M.C., Langub, M.C., Geng, Z., Nakayama, T., Pike, J.W., Chernausek, S.D., Rosen, C.J., Donahue, L.R., Malluche, H.H., Fagin, J.A., Clemens, T.L., 2000. Targeted overexpression of insulin-like growth factor I to osteoblasts of transgenic mice: increased trabecular bone volume without increased osteoblast proliferation. Endocrinology 141, 2674–2682.

UNCORRECTED PROOF

Please cite this article in press as: Tiago, D.M. et al., Alternatively spliced transcripts of *Sparus aurata* insulin-like growth factor 1 are differentially expressed in adult tissues and during early development ..., Gen. Comp. Endocrinol. (2008), doi:10.1016/j.ygcen.2008.04.006